The Hashemite Kingdom of Jordan Scientific Research Support Fund The Hashemite University

JJEES

Jordan Journal of Earth and Environmental Sciences

Volume (10) Number (1)

Cover photo © Khaled Moumani

JJEES is an International Peer-Reviewed Research Journal

ISSN 1995-6681 jjees.hu.edu.jo March 2019

Jordan Journal of Earth and Environmental Sciences (JJEES)

JJEES is an International Peer-Reviewed Research Journal, Issued by Deanship of Scientific Research, The Hashemite University, in corporation with, the Jordanian Scientific Research Support Fund, the Ministry of Higher Education and Scientific Research.

EDITORIAL BOARD:

Editor –in-Chief:

- **Prof. Fayez Ahmad**
  The Hashemite University, Jordan

Assistant Editor:

- **Dr. Mohammed Al-Qinna**
  The Hashemite University, Jordan

Editorial Board:

- **Prof. Najib Abou Karaki**
  University of Jordan
- **Prof. Nizar Abu-Jaber**
  German-Jordan University
- **Prof. Anwar Jiries**
  Mu'tah University
- **Prof. Atef Al-Kharabsheh**
  Al Balqa Applied University
- **Prof. Khaled Al Tarawneh**
  Al-Hussein Bin Talal University
- **Prof. Abdullah Al-Diabat**
  Al al-Bayt University
- **Prof. Nezar Al-Hammouri**
  The Hashemite University
- **Prof. Muheeb Awawdeh**
  Yarmouk University

ASSOCIATE EDITORIAL BOARD: (ARRANGED ALPHABETICALLY)

- **Professor Ali Al-Juboury**
  Mosul University, Iraq
- **Professor Bernhard Lucke**
  Friedrich-Alexander University, Germany
- **Professor Dhirendra Pandey**
  University of Rajasthan, India
- **Professor Eduardo García-Meléndez**
  University of León, Spain
- **Professor Franz Fürsich**
  Universität Erlangen-Nürnberg, Germany
- **Professor Olaf Elicki**
  TU Bergakademie Freiberg, Germany

INTERNATIONAL ADVISORY BOARD:

- **Prof. Sayed Abdul Rahman,**
  Cairo University, Egypt
- **Prof. Abdullah Al-Amri,**
  King Saud University, Saudi Arabia
- **Prof. Waleed Al-Zubair,**
  Arabian Gulf University, Bahrain
- **Prof. Ute Austermann-Haun,**
  Fachhochschule und Lipp, Germany
- **Prof. Ibrahim Banat,**
  University of Ulster, UK
- **Prof. Matthias Barjenbruch,**
  Technisch Universitat Berlin, Germany
- **Prof. Mohamed Boukhary,**
  Ain Shams University, Egypt
- **Prof. Mohammad El-Sharkawy,**
  Cairo University, Egypt
- **Prof. Venugopalan Ittekkot,**
  Center for Tropical Marine Ecology, Bremn, Germany
- **Prof. Christopher Kendall,**
  University of North Carolina, U.S.A.
- **Prof. Elias Salameh,**
  University of Jordan, Jordan.
- **Prof. V. Subramanian,**
  Jawaharlal Nehru University, India.
- **Prof. Omar Rimawy,**
  University of Jordan, Jordan.
- **Prof. Hakam Mustafa,**
  Yarmouk University, Jordan.
- **Dr. Michael Crosby,**
  The National Science Board, National Science Foundation, Virginia, U.S.A.
- **Dr. Brian Turner,**
  Durham University, U.K..
- **Dr. Friedhelm Krupp,**
  Senckenberg Research Institute and Natural History Museum, Germany.
- **Dr. Richard Lim,**
  University of Technology, Australia.

Jordan Journal of Earth and Environmental Sciences (JJEES)

SUBMISSION ADDRESS:

Manuscripts should be submitted electronically to the following e-mail:

jjees@hu.edu.jo

For more information and previous issues:

www.jjees.hu.edu.jo

Hashemite Kingdom of Jordan

Scientific Research Support Fund

Hashemite University

Jordan Journal of
Earth and Environmental Sciences

JJEES

An International Peer-Reviewed Scientific Journal

Financed by the Scientific Research Support Fund

Volume 10 Number (1)

http:// jjees.hu.edu.jo/

ISSN 1995-6681

Cover page photo: The Quweira Fault along the Rift margin in Wadi Namala area photographed by the Geologist Khaled Moumani

المجلة الأردنية لعلوم الأرض والبيئة

Jordan Journal of Earth and Environmental Sciences (JJEES)

http://jjees.hu.edu.jo

Hashemite University
Deanship of Scientific Research
TRANSFER OF COPYRIGHT AGREEMENT

Journal publishers and authors share a common interest in the protection of copyright: authors principally because they want their creative works to be protected from plagiarism and other unlawful uses, publishers because they need to protect their work and investment in the production, marketing and distribution of the published version of the article. In order to do so effectively, publishers request a formal written transfer of copyright from the author(s) for each article published. Publishers and authors are also concerned that the integrity of the official record of publication of an article (once refereed and published) be maintained, and in order to protect that reference value and validation process, we ask that authors recognize that distribution (including through the Internet/WWW or other on-line means) of the authoritative version of the article as published is best administered by the Publisher.

To avoid any delay in the publication of your article, please read the terms of this agreement, sign in the space provided and return the complete form to us at the address below as quickly as possible.

Article entitled:--

Corresponding author: ---

To be published in the journal: Jordan Journal of Earth & Environmental Sciences (JJEES)

I hereby assign to the Hashemite University the copyright in the manuscript identified above and any supplemental tables, illustrations or other information submitted therewith (the "article") in all forms and media (whether now known or hereafter developed), throughout the world, in all languages, for the full term of copyright and all extensions and renewals thereof, effective when and if the article is accepted for publication. This transfer includes the right to adapt the presentation of the article for use in conjunction with computer systems and programs, including reproduction or publication in machine-readable form and incorporation in electronic retrieval systems.
Authors retain or are hereby granted (without the need to obtain further permission) rights to use the article for traditional scholarship communications, for teaching, and for distribution within their institution.

☐ I am the sole author of the manuscript

☐ I am signing on behalf of all co-authors of the manuscript

☐ The article is a 'work made for hire' and I am signing as an authorized representative of the employing company/institution

Please mark one or more of the above boxes (as appropriate) and then sign and date the document in black ink.

Signed:____ Name printed: ____
Title and Company (if employer representative) : ____
Date: __________________________________

Data Protection: By submitting this form you are consenting that the personal information provided herein may be used by the Hashemite University and its affiliated institutions worldwide to contact you concerning the publishing of your article.

Please return the completed and signed original of this form by mail or fax, or a scanned copy of the signed original by e-mail, retaining a copy for your files, to:

Deanship of Scientific Research
The Hashemite University P.O. Box 150458, P.C.13115, Zarqa, Jordan
Tel.: 00962 53903333/ Ext. 4235
Fax: 00962 53826823
E-mail: jjees@hu.edu.jo

Subscription

Jordan Journal of Earth & Environmental Sciences (ISSN 1995-6681)
An International Peer- Reviewed Research Journal
Published by the Deanship of Scientific Research - The Hashemite University

Name: .... الاسم:
Specialty:.. التخصص:
Address:.. العنوان:
P.O. Box:... صندوق البريد:
City & Postal Code: .... المدينة: الرمز البريدي:
Country:.. الدولة:
Phone:.. رقم الهاتف:
Fax No:... رقم الفاكس:
E-mail:... البريد الإلكتروني:
Method of payment: .... طريقة الدفع:
Amount Enclosed:.. المبلغ المرفق:
Signature:.. التوقيع:

Cheques should be paid to Deanship of Research - The Hashemite University

I would like to subscribe to the Journal:

For

☐ One year
☐ Two years
☐ Three years

One year Subscription Rates

	Inside Jordan	Outside Jordan
Individuals	10JD	70$
Students	5JD	35$
Institutions	20JD	90$

Correspondence

Subscriptions and sales:

Professor Fayez Ahmad
Deanship of Scientific Research
The Hashemite University P.O. Box 150458, P.C.13115, Zarqa, Jordan
Tel.: 00962 53903333/ Ext. 4235
Fax: 00962 53826823
E-mail: jjees@hu.edu.jo

JJEES
Jordan Journal of Earth and Environmental Sciences

JJEES

JJEES (2019) 10 (1): 1-6
ISSN 1995-6681

Jordan Journal of Earth and Environmental Sciences

Identification of Recharge Sources Using Environmental Isotopes in Piedmont Zone of Himalaya, Hardwar District, India

Mufid Al-Hadithi[1], Mohammad Israil[2], D. Singhal[3], Bhishm Kumar[4]

[1]Middle Technical University, Engineering Technical College, Baghdad, Iraq
[2]Department of Earth Science, Indian Institute of Technology, Roorkee, India
[3]Department of Hydrology, Indian Institute of Technology, Roorkee, India
[4]National Institute of Hydrology, Roorkee, India

Received 28 September, 2018; Accepted 20 November, 2018

Abstract

The environmental tritium contents and chemical composition of twenty-one groundwater samples collected from shallow and deeper aquifers were measured in the present study to identify the recharge sources of various aquifers, and aquifer-aquifer interaction in the Piedmont zone of Himalaya, India. Tritium concentrations in the shallow aquifers varied from 4.2 to 11.24 Tritium Units (TU), whereas in the deeper aquifers, tritium varied from 0.9 to 12 Tritium Units (TU). The tritium concentration map in relation to ground elevation shows that high concentrations of tritium (above 10 TU) are observed at higher altitudes (300-400 m AMSL) in the Bhabhar region (Upper Piedmont), which suggests that the existence of youngest water acts as a groundwater recharge area. The chemical composition of the collected groundwater samples indicates the presence of two water types, which suggests the presence of different sources of recharge to the shallow and deeper aquifers in the region. The Electrical Conductivity (EC) values of the shallow aquifers especially in the Bhabhar zone (Upper Piedmont) were high indicating that the shallow aquifers have a recharge source other than that of the deeper aquifers, and that the interconnection between the shallow and deeper aquifers is poor to moderate.

Keywords: Groundwater, Environmental Isotope, Recharge Source, India.

1. Introduction

Isotope techniques make use of the quality of radioactivity or variations in the isotopic abundance of nuclides in water molecules caused by natural or environmental phenomena as well as monitoring the change in concentration or the movement of artificially-injected isotopes. Stable and radioactive isotopes of different elements in varying concentrations are present in the environment. Several environmental isotopes and tracers can be used to determine the age of groundwater.

Environmental tritium is widely used to differentiate recent from old groundwater by tritium dating as half-life of tritium is 12.43 years. Tritium analysis can be used as a powerful tool to ascertain the groundwater flow rate and its direction in addition to identifying the zones of recharge for deeper aquifers. Tritium analysis may also be used to estimate the time since the recharge to the groundwater system has occurred and the susceptibility of the groundwater system to contamination.

A number of researchers use different applications of environmental isotopes in hydrologic studies, such as the estimation of groundwater quantity, quality and identification of source of recharge. Rao et al. (2000) identified aquifer recharge sources and zones in parts of Ganga- Yamuna Doab using environmental Isotopes. Dassi et al. (2005) identified sources of groundwater recharge in the Merguellil basin (Tunisia) using the isotopic methods of the implication of dam reservoir water accounting. Shivanna et al. (2008) employed environmental isotope techniques to identify the recharge areas of springs in the mountainous region of Gaucher area, Chamoli district, Uttarakhand, India. Choi et al. (2010) evaluated sources and pathways of groundwater recharge for a heterogeneous alluvial aquifer beneath an agricultural field, based on the multi-level monitoring of hydrochemistry and environmental isotopes of a riverside groundwater system in Buyeo, Korea.

2. Research Methodology

2.1 Study Area

In the present study, environmental tritium has been used to identify the recharge sources and the influence of elevation on the recharge characteristics in the piedmont zone of Himalaya, India located between latitudes 29° 50’ 00” to 30° 11’ 21” North and Longitude 77° 54’ 19” to 78° 06’ 21” East covering an area of approximately 430 km^2 (Fig.1).

Geologically, the study area is comprised of Siwalik rocks and alluvial deposits (Pandey et al., 1963). Northwards, the Siwalik sedimentary rocks are composed of indurate to compacted clastic sediments exposed in Haridwar district and represent an over 6000 m thick sequence, consisting of interbedded mudstones, sandstones, conglomerates and subordinate marls (Karanth, 1989).

The formation occurring towards the south of the Siwaliks consists of alluvial fan deposits of a recent age. The alluvial fan deposits are made up of assorted sand and gravel associated with occasional clays (Sharma and Jugran, 1992; Gupta, 1991; and Gupta, 2002). After necessary ground checking and correlation with the existing literature, the

---

* Corresponding author e-mail: mufidalhadithi@yahoo.com

geologic units were mapped using ArcGIS 10.1 software to prepare a thematic map for the geology of the area (Fig.2). Based on hydrogeological characteristics, the area is classified into four geomorphic units. The geomorphic boundaries were digitized on the enhanced image through GIS and generated a hydrogeomorphological map as shown in Figure 3.

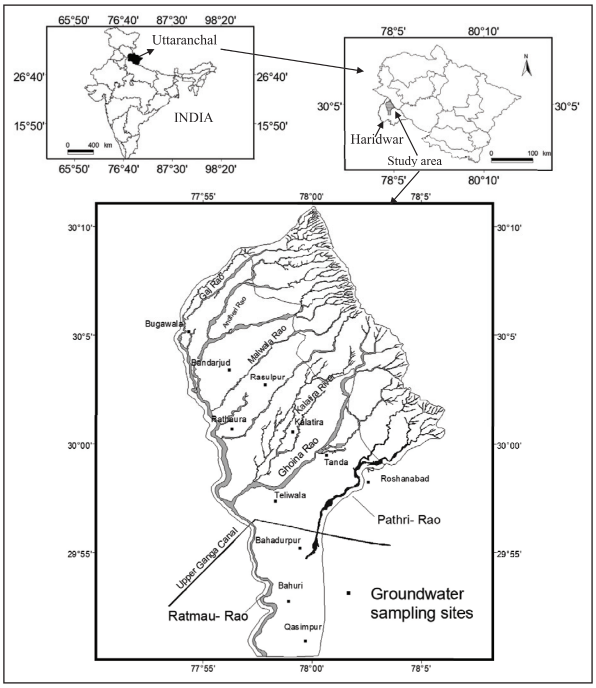

Figure 1. Location map of the study area showing the groundwater sampling sites

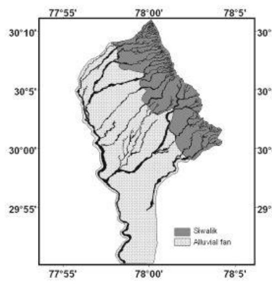

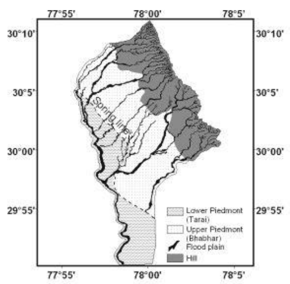

Figure 2. Geological map Figure 3. Hydrogeomorphological map

The Upper Piedmont zone also known as **Bhabhar,** bordering the **Siwalik hill** is comprised of unconsolidated coarse materials. Concerning groundwater, this belt provides an excellent hydrogeological setup for recharge and infiltration. **The Lower Piedmont** (also known as **Tarai**) is separated from the Bhabhar by the spring line along their junction. This zone is composed of coarse-grained sand and clay with gravel. **Flood plains** form the youngest geomorphic unit and include various landforms formed by fluvial action i.e. sandbars, channel bars, and meander scars. These are characterized by a very gentle slope and consist of sub-rounded to rounded fragments of sand, silt and clay.

2.2 Sampling and Analysis

Twenty-one water samples were collected from the shallow and deep aquifers at eleven selected sites during the pre-monsoon season in 2002. These samples represent the geohydrological zones viz., Upper Piedmont (Bhabhar) zone and Lower Piedmont (Tarai) zone. The locations of these samples are shown in Fig.1. The samples were analyzed for the presence of tritium concentration. The measurement of tritium is done by measuring its beta activity through the beta counting using Liquid Scintillation Spectrometer (LSC), 1220 Quantulus model, a complete facility available in Nuclear Hydrology laboratory at the National Institute of Hydrology (NIH). This involves the primary and secondary distillation of water samples, tritium enrichment by electrolytic enrichment of the water samples, subsequent mixing of the water samples with a liquid scintillation cocktail, and Beta counting using a liquid scintillation spectrometer. Commercially available liquid scintillation cocktail viz "Canberra- Packard Pico– flour LLT" (Low Level Tritium) has been used due to its very low background count rate and higher counting efficiency compared to other scintillation solutions. The liquid scintillation counter (LSC) measures the tritium activity in the enriched water samples using the Queue Manager (QM) software. Finally, the environmental tritium contents in the water samples were measured in Tritium Units (TU) as defined in standard literature (IAEA, 1983). The tritium content in all the samples varied ranging from 0.9 to 12 TU as shown in Table 1.

Table 1. Sampling sites and tritium concentrations (TU)

S. No	SiteName	Tritium concentration, EC and error for Shallow aquifers			Tritium concentration, EC and error for deep aquifers		
		TU	Error	Ec (µs/cm)	TU	Error	Ec(µs/cm)
1	Kalatira	11.25	±1.41	788	8.82	±1.79	488
2	Bugawala	8.95	±0.78	522	6.7	±6.07	575
3	Rasulpur	10.74	±1.21	995	7.0	±1.14	465
4	Bandarjud	10.01	±1.44	915	7.01	±1.79	375
5	Roshanabad				12	±1.21	372
6	Tanda	10.12	±0.77	868	7.54	±.98	553
7	Rathaura	4.43	±0.81	1990	0.91	±0.56	353
8	Teliwala	11.24	±1.36	453	8.13	±0.91	352
9	Bahadurpur	7.08	±1.07	503	2.25	±0.23	515
10	Bhauri	7.74	±0.68	693	6.07	±0.66	346
11	Qasimpur	7.8	±0.66	450	5.89	±0.89	360

3. Results and Discussion

3.1. Identification of Recharge Sources

The aquifer recharge sources can be identified on the basis of tritium activity observed in the groundwater samples collected from different locations from shallow and deeper aquifers. The measured tritium activity (TU) has been analyzed in the following sections:

3.1.1. Shallow Aquifers

Ten groundwater samples correspond to the shallow aquifers at depths ranging from 6 m to 11 m. Tritium concentration varies from 4.2 to 11.24 TU and a tritium concentration contour map has been prepared as shown in Fig.4. It is observed that tritium concentration is high in the groundwater samples of wells located in the Bhabhar zone which has a high ground elevation compared with the Tarai Zone. Furthermore, it was noted that tritium concentration is also high (11.24 TU) at the Tialwala site although it has a low elevation of the earth and is located in the Bahabhar region. This can be explained by the possible addition of local recharge from a nearly stream (viz. Ghoina Rao and Kalatira rivers).

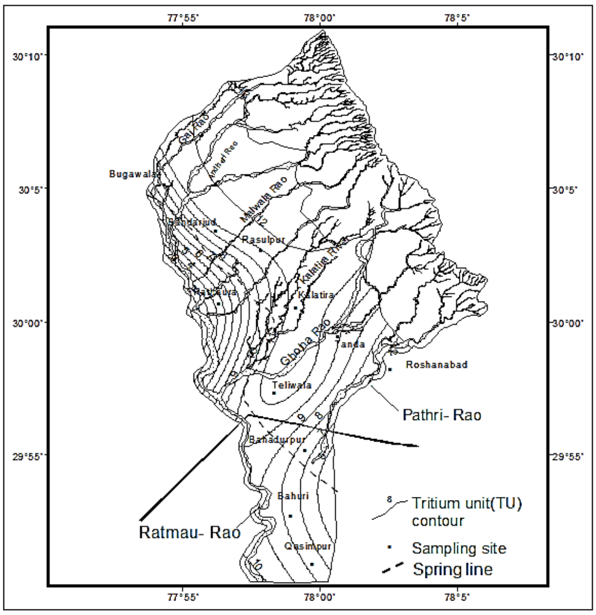

Figure 4. Tritium concentration contour map of a shallow aquifer

3.1.2. Deep Aquifers

Eleven groundwater samples were collected from deep aquifers at depths varying from 50 m to 90 m. Tritium concentration in the deep aquifers varies from 0.9 to 12 TU, and a tritium concentration contour map for the deeper aquifers has been prepared as shown in Fig 5. As in the case of shallow aquifers, it has been observed that tritium concentration is high at high altitudes (Bhabhar zone) gradually declining towards the plain areas (Tarai).

3.2. Influence of Elevation

In order to investigate the possible influence of elevation on the recharge characteristics, the tritium concentration of the samples was plotted with respect to the elevation of sampling sites (Fig. 6). The sampled groundwater sites on the basis of their topographic positioning can be divided into two groups with the Ganga Canal being present in the area separating these two groups:

i- Sites located in the Bhabhar/Tarai region to the north of the Canal: Bugawala, Bandarjud, Rasulpur, Rathaura, Kalatira, Tanda, Teliwala, and Roshanabad villages.

ii- Sites located in the Tarai/Bhabhar region and falling in the south of the Canal: Bahadurpur, Bahuri and Qasimpur.

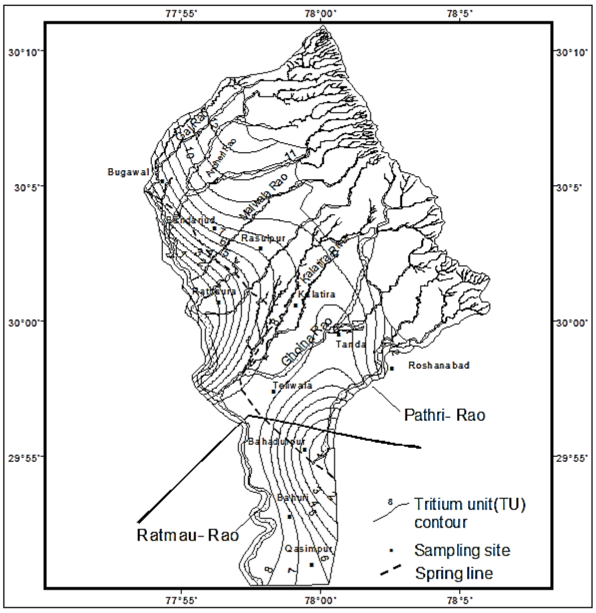

Figure 5. Tritium concentration contour map of a deep aquifer

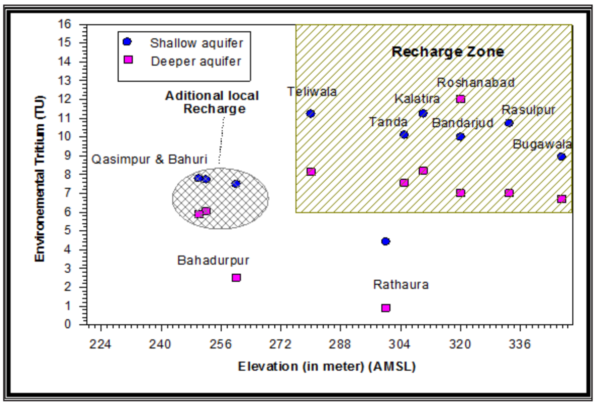

Figure 6. Plot showing variation of environmental tritium with elevations.

It has been observed that the highest tritium observed in the deeper aquifer of Roshanabad sites located within a distance of 1.5 km from the Siwalik range indicates that the youngest water or the highest tritium activity in groundwater is expected to be in the groundwater recharge of the Siwalik Hills. Moreover, the groundwater recharged in the Siwalik Hills region moves down to Bhabhar and down to the rest of the area (Tarai zone).

In the Bhabhar zone, the tritium concentration in the deep aquifers is ~7 TU indicating its probable recharge from Siwalik. The tritium concentration being higher than this in the shallow aquifers can, therefore, be ascribed to the local recharge. The tritium values are comparatively lower in the case of deeper aquifers in Bhabhar zone (7 TU) than those of the shallow aquifers (10 TU). This indicates poor interconnection between shallow and deeper aquifers.

Similarly, the EC (Electrical Conductivity) value are higher in the case of shallow aquifers than in the deeper aquifers which also indicates that deeper aquifers have a different recharge source other than that of the shallow aquifers in this region. Therefore, it can be said that the deeper aquifers have recharge zones located in Siwalik region. In the southern part of Bhabhar at the Bahadurpur village, near the spring line the observed tritium value is 7.01 TU in the shallow aquifers and 2.5 in the deeper aquifers. This also indicates that the interconnection between shallow and deeper aquifers is poor. The increase in the tritium values in the shallow aquifers is possibly due to the canal recharge during the passing of shallow aquifers through it. This assumption is supported by the low EC of 900 µs/ cm in the shallow groundwater in the Bahadurpur village, whereas in the Teliwala well located north of canal the EC is much higher (~ 1990 µs/ cm).

In the northern part of Tarai at the site of Rathaura, groundwater appears to be formed by local recharge and the low tritium could be attributed to the low recharge rate. In the southern part of the Tarai zone at the Qasimpur and Bahuri sites, tritium concentration values show an additional local recharge of the shallow and deeper aquifers probably from the Ganga Canal and Ratmau river. These sites also fall in the discharging zone of the river Pathri Rao and in its palaeo river course. Both sites are therefore expected to receive substantial recharge from these rivers. The interconnection between shallow and deeper aquifers is good at these sites. It has also been observed that tritium values at shallow and deeper levels at Qasimpur and Bahuri villages resemble the tritium values in the deep aquifers in the Bhabhar zone though located away from Bhabhar zone. The EC values are lower than those at the shallow aquifers. This indicates that the aquifers in the Tarai zone receive recharge from the Bhabhar region.

The nearly constant tritium activity about 10 TU obtained above 300m indicates that precipitation is the major source of recharge to the shallow aquifers; the groundwater movement occurs in the direction of the decreasing tritium values in the water samples towards the Tarai zone. It has also been observed that the tritium values of the deep aquifers at Roshanabad located very near to the Siwalik region resemble the tritium values of the shallow aquifers in the Bhabhar zone and the EC values are lower than those at the shallow aquifers. Moreover, its EC values are slightly lower than the other deeper aquifers because the other deeper aquifers are located quite away from the Siwalik region. This observation is in support of the present paper's conclusion that deeper aquifers in the Bhabhar zone receive recharge from the Siwalik region.

4. Groundwater Quality

In the present work, water chemistry is used as supportive evidence in the study of recharge rather than to make a detailed investigation. Cations and anions in addition to the other physical parameters such as pH, TDS and EC have been measured in all the collected water samples. Cations (Ca^{++}, Na^{+}, and K^{+}) have been analyzed by flame photometer, Mg^{++} in EDTA titration method, HCO_3^{--} and Cl^- analyzed by H_2SO_4 and $AgNO_3$ titration method, respectively. The measured values are summarized in table 2.

Table 2. Major cation, anion concentrations and Physical parameters. [S-Shallow, D- Deeper aquifer]

S. No	Depth	pH	EC	TDS	Ca^{++}	Mg^{++}	Na^+	K^+	Cl^-	SO_4^{--}	CO_3^-	HCO_3^-
1	D	8.3	488	320	40.05	31.58	17.10	1.60	5.00	67.90	33.00	192.17
2	S	9.1	788	520	67.08	37.66	41.70	9.80	24.99	69.95	63.01	268.42
3	D	8.7	575	380	28.03	38.87	35.60	3.40	3.75	67.90	39.01	256.22
4	S	8.2	522	346	55.07	21.87	10.50	3.20	12.50	74.07	24.00	170.81
5	D	8.5	465	350	40.05	28.55	13.50	2.00	5.00	67.90	24.00	179.96
6	S	8.2	995	658	100.12	18.83	45.10	3.30	81.22	189.29	36.00	125.06
7	D	8.3	915	602	96.12	27.33	19.80	2.00	106.22	205.75	12.00	164.71
8	S	8.8	375	248	29.03	12.76	9.90	22.70	12.50	65.84	18.00	94.56
9	D	8.5	372	245	47.06	11.54	6.90	1.30	3.75	43.21	39.01	100.66
10	S	8.2	868	573	85.00	27.33	35.40	1.80	44.99	96.70	18.00	280.62
11	D	9.1	553	365	33.04	25.51	33.00	2.90	29.99	88.47	27.00	161.66
12	S	8.3	1990	1320	137.16	35.23	86.90	78.50	231.18	316.85	9.00	103.71
13	D	8.8	453	298	53.06	12.76	10.20	1.10	16.24	63.78	33.00	137.26
14	S	9.4	353	233	29.03	15.18	17.70	3.00	10.00	61.73	30.00	125.06
15	D	9.3	352	232	25.03	17.61	15.30	2.90	6.25	69.95	27.00	149.46
16	S	8.8	503	335	62.07	9.72	4.40	1.50	6.25	98.76	33.00	167.76
17	D	8.7	418	276	46.06	14.58	6.10	1.20	8.75	57.61	21.00	134.21
18	S	8.6	515	339	36.04	10.93	10.70	48.80	21.24	49.38	18.00	118.11
19	D	9.3	693	458	71.09	19.44	10.70	12.90	37.49	67.90	36.00	128.11
20	D	8.7	346	227	40.07	8.50	11.00	1.10	7.50	59.67	15.00	152.51
21	D	8.8	450	299	53.16	12.78	10.28	1.11	16.25	63.79	33.01	137.27

Hydrochemical facies or hydrochemicla zoneation for the present investigation has been carried out by plotting the percentage of reacting values of major ions in Pipers (1944) trillnear diagrams (Fig. 7). This diagram shows that 90 % of groundwater in the study area belongs to Ca^{2+} – HCO_3^- type with a significant portion of Mg^{2+}. At few places which receive additional recharge, the groundwater belongs to SO_4^{-} ^{2}- Cl^{-}. The expected EC in the resultant groundwater can be estimated from the EC data of the recharge sources and the present recharge from these sources. Any differences between the estimated and the observed EC of groundwater at the same site provides information on salt concentrations separated or added to the groundwater during the infiltration or flow processes and also on errors in the estimated recharge percentages.

As observed from the data of the environmental tritium, the deep aquifers of Bhabhar zone receive recharge from high altitude regions (Siwalik region); therefore, as expected, these aquifers show EC in the range of 370-420 µS/ cm as shown in Figures 8 and 9. The increase in EC of the shallow aquifers at the Bhabhar zone provides a measure of the EC of the local recharge groundwater in this zone and shows that the interconnection between the shallow and deeper aquifers is poor.

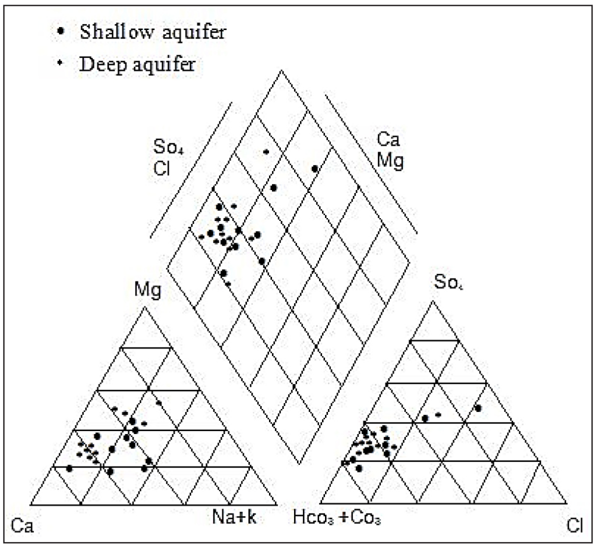

Figure 7. Pieper diagram showing the chemical composition of Groundwater from shallow and deeper aquifers in the study area

In the northern part of the Tarai zone, the local recharge and the marginal evaporation enrichment of the salt content increased the EC of its shallow aquifers above the background 600 µS/ cm (788 µS/ cm); the value is close to this (575 µS/ cm) in its deep aquifers . In the southern part of the Bhabhar/ Tarai zone when passing through the Canal Zone, the recharge is expected to reduce the EC at these sites. This is close to the observed value of 995 µS/ cm at the Bahadurpur village. Similarly, a respective recharge from the rivers Ratmau and Pathri Rao refreshes the shallow and deeper aquifers as observed at the Bhauri and Qasimpur sites. This indicates that the interconnection between the shallow and deeper aquifers in this region is moderate to good. The close resemblance between water chemistry and tritium data explains the source and recharge from these sources to the groundwater system of the study area.

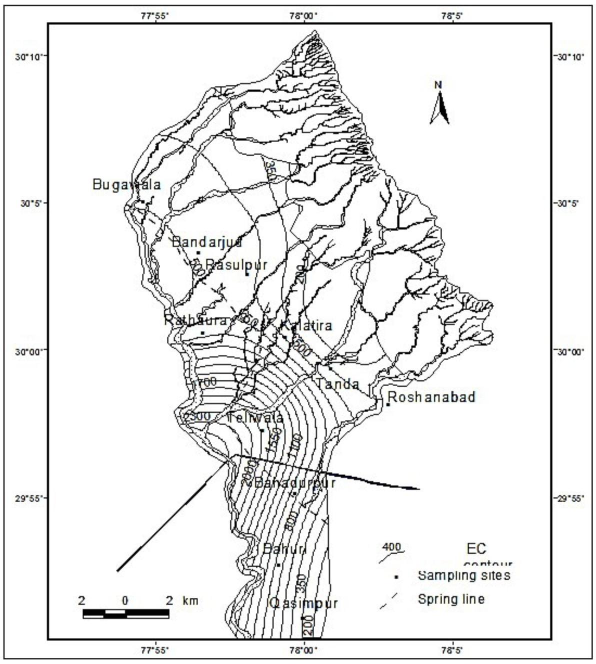

Figure 8. contour map of a shallow aquifer

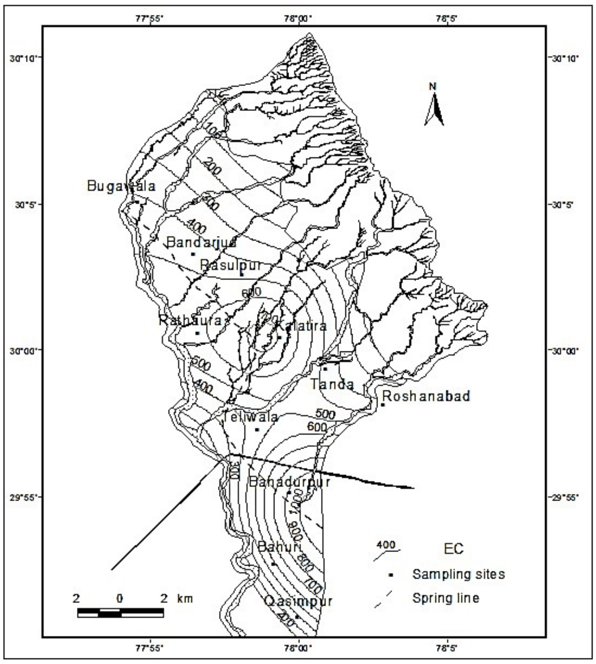

Figure 9. EC contour map of the deeper aquifer

5. Conclusions

The evaluation of groundwater quality has been carried out to explain the recharge sources of various aquifers, and aquifer-aquifer interaction in the Piedmont zones of the Haridwar District, India. The current study shows that precipitation is the major source of recharge and that groundwater recharge takes place mainly at higher altitudes (300-400 m AMSL) in the Bhabhar region where the shallow and deeper aquifers have good interconnections. The piper diagram shows that there are different water types in the study area which indicate that there are different recharge sources. These findings are supported by the Electrical Conductivity (EC) data of groundwater which show an increase in the shallow aquifers. The increase in the EC indicates that the shallow aquifers have different recharge sources from those of the deeper aquifers, and that the interconnection between the shallow and deeper aquifers is poor to moderate in this region.

References

Choi, B.Y., Yun, S.T., Mayer, B., Chae, G.T., Kim, K.H., Kim, K. Koh, Y.K. (2010). Identification of groundwater recharges sources and processes in a heterogeneous alluvial aquifer: results from multi-level monitoring of hydrochemistry and environmental isotopes in a riverside agricultural area in Korea. Hydrol. Process, 24: 317–330. doi:10.1002/hyp.

Dassi, L., Zouari, K., Faye, S. (2005). Identifying sources of groundwater recharge in the Merguellil basin (Tunisia) using isotopic methods: implication of dam reservoir water accounting, Environ. Geol., 49: 114-123.

Gupta R.P., (1991). Remote Sensing Geology, (1st edition), Springer-Verlag Berlin Heidelberg New York.

Gupta, R.P. (2002). Remote Sensing Geology, (1st edition), Springer-Verlag Berlin Heidelberg New York, 2002.

Karanth, K.R. (1989). Hydrogeology, Tata McGraw- Hill Publishing Company Limited, New Delhi.

Pandey, M.P., Raghava Rao, K.V., Raju, T.S. (1963). Groundwater resources of Tarai-Bhabhar belts and intermountain Doon Valley of Western UTTAR PRADESH. Report Prepared for MFAA, 253 p.

Rao, M.S., Kumar, B., Nachiappan, R., Jagmohan, P. (2000). Identification of aquifer recharge sources and zones in parts of Ganga-Yamuna Doab using environmental isotopes. In Mehrotra, R.; Soni, B., Bhatia, K. K. S. (Eds.), Integrated water resources management for sustainable development - Volume 1. Roorkee, India: National Institute of Hydrology. pp.271-281.

Sharma, D., and Jugran, D.K. (1992). Hydromorphogeological studies around Pinjaur-Kala Amb area, Ambala District (Haryana), and Sirmur district (Himachal Pradesh). Journal of the Indian Society of Remote Sensing, 20(4): 281-286.

Shivanna, K., Tirumalesh, K., Noble, J., Joseph, T.B., Singh, G., Joshi, A.P., Khati, V.S. (2008). Isotope techniques to identify recharge areas of springs for rainwater harvesting in the mountainous region of Gaucher area, Chamoli District, Uttarakhand, Current Science, 94(8): 1003-1011.

JJEES

Jordan Journal of Earth and Environmental Sciences

JJEES (2019) 10 (1): 7-14
ISSN 1995-6681

Temporal Variations of Submicron Particle Number Concentrations at an Urban Background Site in Amman-Jordan

Shatha Ali-Saleh[1], Zain Shilbayeh[1], Hamza Alkattan[1], Mohammad Al-Refie[1],
Omar Jaghbeir[1], Tareq Hussein[1,2]

[1]*The University of Jordan, Department of Physics, Amman 11942, Jordan*
[2]*University of Helsinki, Institute for Atmospheric and Earth System Research (INAR), PL 64, FI-00014 UHEL, Helsinki, Finland*

Received 15 October, 2018; Accepted 20 December, 2018

Abstract

This paper presents the temporal variation of fine particle number concentrations and their dependence on some weather parameters (T, P, and RH) during August 2016 – May 2017 at an urban background site in Amman. The measurement was conducted with a condensation particle counter with one-minute time resolution. The daily mean concentrations showed a clear annual cycle (annual average of ~8×10^3 cm^{-3}) with high concentrations (~2.8×10^4 cm^{-3}) during winter and low concentrations (~1.2×10^4 cm^{-3}) during summer. This annual cycle was inversely correlated with the daily mean temperature (T), but was proportional with the daily mean relative humidity (RH); however, the concentration cycle had about a twenty-two day shift with respect to T and RH cycles. Further analysis based on the hourly mean aerosol database revealed a weekly cycle and distinguished daily patterns for three types of days: (1) Sunday–Wednesday, (2) Thursday, and (3) Friday–Saturday. The workdays had the highest daily mean concentrations, and their daily pattern had the highest concentrations during morning rush hours. The weekend type daily pattern had the highest concentrations during midday and late night. Both pattern types had the lowest concentrations between the times 03:00 – 06:00. These temporal variations (annual, weekly, and daily) reflect the anthropogenic emissions, especially those emitted from combustion traffic-related activities in the city. The aerosol database was of a long-term type (about eight months in total), which encourages the researchers to perform more extensive measurements for a longer term to fill in the missing gaps and reveal more accurate temporal characteristics of the fine particle number concentrations.

Keywords: seasonal, diurnal Pattern, meteorological dependence, traffic emissions.

1. Introduction

Aerosol particles play an important role in the climate via their direct effect, which is represented by the ability to absorb and reflect radiation, or via the indirect effect acting as Cloud Condensation Nuclei (CCN) or Ice Nuclei (IN) (e.g. Myhre et al., 2013; Haywood and Boucher, 2000; Lohmann and Feicher, 2005). Aerosols might also affect human health because some types of aerosols have been classified as toxic and carcinogenic causing mortality and morbidity (Pop et al., 2002; Vinzents et al., 2005; Krewski, 2009; Lepeule et al., 2012; Burnett et al., 2012).

Urban areas are major sources of aerosols as a result of activities associated with large population densities and their anthropogenic activities (Fenger, 1999). Among the major sources are combustion emissions that are mainly accompanied with traffic and industrial activities. Urban aerosols have a complex mixture of those that are locally emitted and those from long- range transport (e.g. Hussein et al., 2014). Therefore, the physical and chemical properties of urban aerosols often have a complex trend in time and space. Meteorological conditions remarkably affect aerosols properties and concentrations (e.g. Wehner and Wiedensohler, 2003; Wu, et al., 2008; Zhao et al., 2015; Vakeva et al., 2000; Hussein et al., 2006).

An important feature of aerosol concentrations is their temporal variation with different time scales: daily, weekly, and seasonal (e.g. Rahman et al., 2017; Hussein et al., 2016; Hussein et al., 2004; Jin et al., 2005; Wehner and Wiedensohler (2003). Jin et al., (2005) indicated that seasonality is evident in aerosol optical thickness measurements, with a minimum in January and a maximum in April to July, and demonstrated the diurnal variations of aerosols which were detectable but largely affected by local and regional weather conditions, such as surface and upper-level winds, also he reported that for calm clear days, aerosols peak during the two rush hours in the morning and evening. Wehner and Wiedensohler (2003) showed the weekly and daily aerosol concentration variations in an urban area of Leizpzig (Germany), and concluded that Meteorological conditions remarkably affect the particle concentrations. Rahman, et al. (2017) investigated the diurnal trend of the particle number concentrations, and they showed that vehicular emissions and new particle formation events increased the total particle number concentrations. Understanding urban aerosol temporal variations can help in developing climate models to calculate the climate forcing of aerosol particles, in addition to the possibility of using the long-term aerosol concentration data for correlation with epidemiological data; such a study can reveal the effects of these concentrations on respiratory diseases in urban areas.

There have been many studies in the eastern

---

* Corresponding author e-mail: t.hussein@ju.edu.jo

Mediterranean region interested in aerosols. They focus on the PM and some chemical characterization and aerosol transport (e.g. Abdeen et al., 2014; Alghamdi et al., 2014a, 2014b, 2015; Boman et al., 2013; Daher et al. 2013; El-Araby et al., 2011; Engelbrecht and Jayanty, 2013; Gherboudj and Ghedira, 2014; Hamad et al., 2015; Hussein et al., 2014; Hussein et al., 2011; Hassan et al., 2013; Habeebullah, 2013; Khodeir et al., 2012; Kouyoumdjian and Saliba, 2006; Rushdi et al., 2013; Shaltout et al., 2013; Waked et al., 2013; Saliba et al., 2010; Al Dousari et al., 2017; Basha et al., 2015; Doronzo et al., 2015; Alam et al., 2014; Jaafar et al., 2014; Saeed et al., 2014; Dada et al., 2013; El-Askary et al., 2009; El-Askary and Kafatos, 2008; Reid et al., 2008; Saliba et al., 2007; Satheesh et al., 2006). However, those researches didn't shed the light on the particle number concentrations, long-term database, and particle number size distribution. In Jordan, which is considered to be at a central location in the eastern Mediterranean region, there have been several aerosol studies concerning particle number concentrations. For example, Hussein et al. (2011) investigated the number concentration of submicron particles in urban and suburban atmospheres of Amman during a short-term measurement aiming to compare the concentrations before and after a dust episode.

In a recent study, Hussein et al. (2016) have measured the fine number concentrations and deduced their spatial and diurnal variation in the two most populated cities (Amman and Zarqa). However, the measurement campaigns were too short to predict the seasonal pattern. The research was extended by Hussein and Betar (2017) to present the size-fractionated particle number and mass concentrations in Amman during short-term investigations and deduce an estimate for the urban particle number size distribution. Most recently, Hussein et al. (2017) developed a simple mobile setup and measured the spatial variation of aerosol concentrations across cities and highways in Jordan. Although their study covered a large geographical area of Jordan, it was very short.

In this study, the main objective is to investigate the temporal variation of submicron particle number concentrations at an urban background site in Amman, Jordan. The researchers focused on three temporal scales: seasonal, weekly, and daily. This is very important to further understand the temporal characteristics of the emission of submicron aerosols in Amman, and will provide useful information (e.g. relationship with some meteorological parameters) which is also important for modeling the urban air quality based on proxies.

2. Materials and Methods

2.1. Aerosol Measurements

The researchers measured the particle number concentrations of submicron aerosols at an urban background site in Amman, Jordan. The site is located on the third floor of the Department of Physics in the middle of the University of Jordan campus. The aerosol measurement was performed over the period from August 1, 2016 to June 22, 2017.

The aerosol instrument was a portable condensation particle counter (CPC 3007-2, TSI). The cutoff size of this CPC was 10 nm, and it was capable of measuring submicron particle number concentration for aerosols with diameters up to 1 µm. According to the specifications provided by the manufacturer, the maximum detectable concentration was 10^5 cm^{-3} with a 20 % accuracy. The sampling flow rate was 0.1 lpm (inlet flow rate 0.7 lpm). The aerosol inlet consisted of short Tygon tubes (4 mm inner diameter) connected to a diffusion drier (TSI model 3062-NC). The diffusion drier is used to remove the excess of moisture from the aerosol sample. Since the aerosol never comes in contact with the desiccant material, there is a minimal aerosol loss. The main inlet (~1-meter-long and 8 mm inner diameter) was led through the wall to sample the outdoor aerosols. The aerosol transport efficiency through the aerosol inlet was estimated experimentally, and the aerosol data were corrected accordingly.

The measurement time-resolution was set to one-minute average scans. After correcting the raw data for aerosol losses in the experimental setup, the processed aerosol data were then converted to statistical analysis. This hourly averaged database was then used to calculate the daily and monthly statistical values. The statistical analysis included average, standard deviation, standard error, minimum, 5 %, 25 %, median, 75 %, 95 %, max, valid number of data points, and percentage of valid data points.

The hourly averaged database was also used to generate the daily pattern of the particle number concentrations. The daily pattern is usually calculated by taking the average (or any statistical parameter) separately for every hour of a certain weekday (Mondays, for instance). Then workdays and weekends/holidays are considered separately as two distinct groups.

2.2. Weather Conditions

The weather conditions were measured continuously on the roof top of the Department of Physics since February 2015. The measurement was conducted with a weather station (Weather Station WH-1080, Clas Ohlson: Art.no. 36-3242). The time resolution of the measurement was five minutes. The weather station consists of an automatic data logger, which is controlled by its own software installed on a personal computer, and sensors connected wirelessly with the data logger. The sensors measure ambient temperature, absolute pressure, relative humidity, wind speed and direction, and precipitation.

For the purpose of the analysis made for this study, the researchers only included the temperature and the relative humidity from July 1, 2016 to June 30, 2017. The daily average temperature varied between 1.3 °C and 30.5 °C with an overall average of 17.3±7.4 °C, and the relative humidity was in the range of 16 % – 100 % (median 59 %). The daily average wind speed was 4.9±2.4 km/h.

3. Results and Discussion

3.1. Seasonal Variation of the Submicron Aerosol Concentrations

Throughout the measurement period, the daily average concentration of the submicron aerosols was in the range of 6.9×10^3 – 4.1×10^4 cm^{-3} with a yearly average of 1.94×10^4 cm^{-3}, and a yearly median of 1.8×10^4 cm^{-3}. These concentrations were higher than what was reported in some cities. For example, Salma, et al. (2011) measured the particle number concentrations in the range (0.006 to 1 µm) near central Budapest for a year, and found that the daily median number concentrations of particles varied from 3.8 × 10^3 to 2.9 ×10^3 cm^{-1} with a yearly median of 1.18 ×10^4 cm^{-3}, this is 42 % lower than the results in this study. Birmili, et al. (2009) measured the particle number concentrations that are less than 0.5 µm at sites 80m and 400m far away from a main road in Berlin, Germany, and their results were 1.1×10^4 cm^{-3}, 9 ×10^3 cm^{-3} respectively, which are, also, lower than the results of the current study. However, the results of this study are in line with many other results reported for various locations in Europe. For example, Reche, et al. (2011) reported the average particle concentrations in the urban background of Barcelona (Spain), North Kensington (UK), and Lugano (Italy) as 1.7×10^4 cm^{-3}, 1.2×10^4 cm^{-3}, and 1.5×10^4 cm^{-3}, respectively. The results of the current study are also in agreement with a similar study at an urban background site (North- Eastern Iberian Peninsula) which had a daily average of particle number concentrations in the range of 7.0×10^3 cm^{-3} - 3.1×10^4 cm^{-3} with an annual average of 2.5 ×10^4 cm^{-3} (Perez et al., 2010).

The average concentration of the submicron aerosols was the highest during winter and the lowest was during summer. The lowest monthly average (~1.3×10^4 cm^{-3}) was observed during June–August, whereas the highest concentrations (~2.6×10^4 cm^{-3}) were observed during December–February (Table 1 and Figure 1). The average number concentration in winter was two times higher than that in summer. This result could be attributed to the increased particle emissions in winter (e.g. from heating processes). Also, these high concentrations in winter are related to the boundary layer height, which is proportional to the ambient temperature. Therefore, during winter, particle number concentrations are accumulated in a smaller volume (below boundary layer) giving higher concentrations than winter.

Table 1. Monthly statistical values for the submicron particle number concentrations. The last two columns are the number of valid data points and the corresponding percentage in each month. This table was generated from the hourly averages.

Year	Month	Mean	Stdev	Min	5%	25%	Median	75%	95%	Max	N	%
2016	July	--	--	--	--	--	--	--	--	--	--	--
2016	Aug	12907	6224	3398	5436	8585	11220	15583	25517	34669	297	40
2016	Sep	16491	8013	3334	6248	10826	15475	20634	31988	47040	298	41
2016	Oct	21342	9892	3552	6794	14640	20119	26975	39831	64945	569	76
2016	Nov	23935	14491	3692	5925	12951	22163	30332	54361	82004	358	50
2016	Dec	--	--	--	--	--	--	--	--	--	--	--
2017	Jan	--	--	--	--	--	--	--	--	--	--	--
2017	Feb	26320	13303	4047	6710	16668	25453	35159	48769	82791	438	65
2017	Mar	21306	10486	3449	5835	13972	20299	27340	41091	61939	530	71
2017	Apr	19152	9867	3504	6278	13111	17918	23803	36604	88080	220	31
2017	May	--	--	--	--	--	--	--	--	--	--	--
2017	Jun	13394	7172	4173	6127	8254	11570	16105	27775	40069	229	32

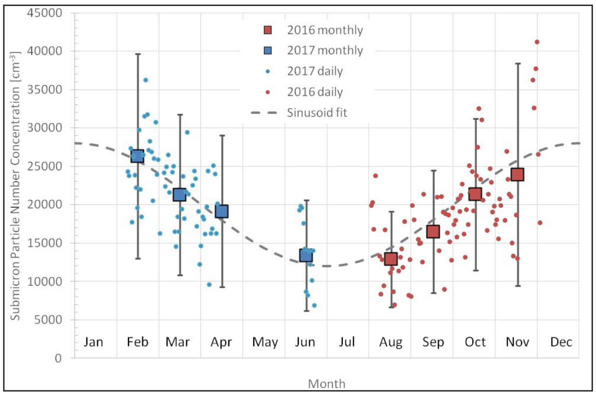

Figure 1. Seasonal variation of the submicron particle number concentrations fitted to a sinusoidal function of the form PN = 8×10^3 COS (360 t / 365) + 2×10^4, where PN is the particle number concentration [cm^{-3}], and t is the day of year starting from January 1st.

This result is consistent with several previous studies in other urban areas (e.g. Wehner and Wiedensohler, 2003; Olivares et al., 2007; Wu, et al., 2008). For example, Wehner and Wiedensohler (2003) showed the seasonal trend in the particle number concentrations at a moderately polluted site in Leipzig (Germany) with lowest average concentration (~1.1×10^4 cm^{-3}) in summer and highest average concentration (~2.1 ×10^4 cm^{-3}) in winter. However, the findings of the current study are not in line with the results of Singh, et al. (2000), who studied the variation of aerosol concentration in view of some meteorological parameters in Roorkee, north India during monsoon (June–Sep / 1996) and winter (November – Feb/1997), and found that aerosol concentrations were minimum in August, September, and November, 1996, but remained around the maximum concentrations in (June–July), 1996 and (January–February), 1997.

The annual cycle of the concentrations is revealed by looking closely at the monthly analysis (Table 1 and Figure 1). The annual cycle of the daily mean concentration can be fitted with a periodic function in the form

$$PN = 8(\cos(t/365 * ('' 360^{\circ}) + 20 \quad \text{.................................(1)}$$

where *PN* is the daily average aerosol number concentration [×10^3 cm^{-3}], and *t* is the number of days starting from January 1st (Figure 1). According to this fitting, the lowest concentrations seem to be also observed in July (summer), whereas higher concentrations are expected in January or December (winter).

Based on the monthly analysis of the submicron aerosol concentration against the relative humidity and the temperature, the monthly mean of the concentrations was proportional to the monthly mean of the relative humidity, but was inversely proportional to the monthly mean of the temperature (with a lag of less than a month). For example, the annual cycle of the daily mean relative humidity was also fitted to a periodic function

$$RH = 23(\cos(t/365 \cdot ('' 360^\circ) + 55 \qquad \text{(2)}$$

where *RH* is the daily average relative humidity [%], and *t* is again the number of days since January 1st (Figure 2a). This means that the annual cycle of the daily mean relative humidity is in phase with the daily mean submicron aerosol concentration.

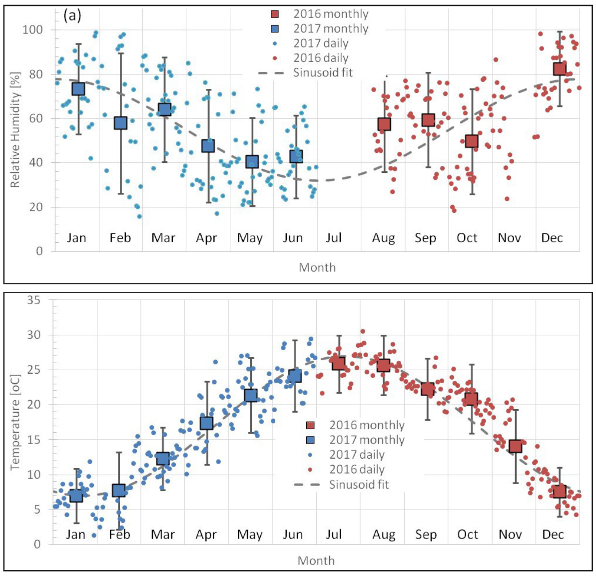

Figure 2. Seasonal variation of **(a)** relative humidity fitted to a sinusoidal function (RH = 23 COS (360 t / 365) + 55, where RH is the relative humidity [%] and t is the day of year starting from January 1st) and **(b)** temperature fitted to a sinusoidal function (T = 10 SIN (360 (t – 112)/ 365) + 17, where T is the Temperature [°C] and t is again the day of year).

Similarly, the annual cycle of the daily mean temperature was fitted to a periodic function

$$T = 10(\cos(t/365 \cdot ('' 360^\circ - 200^\circ) + 17 \qquad \text{(3)}$$

where *T* is the daily average temperature [°C], and *t* is again the number of days since January 1st (Figure 2b). However, this annual cycle of the temperature was shifted by about six months and twenty-two days. In other words, the annual cycle of the temperature is inversely proportional (with ~22 days lag) to both the relative humidity and the submicron aerosol concentration. So, a satisfactory relation between number concentrations and (temperature and RH) is deduced. This is not in agreement with Wu, et al. (2008) who reported that the number concentration in their study didn't show a clear dependency on ambient relative humidity and temperature, and that a complex relation connected them, although their measurements lasted for two years.

Based on the hourly means, the submicron aerosol concentration was inversely proportional to the temperature (T), relative humidity (RH), and the wind speed (WS) (Figure 3). The relationship between the concentration and these three weather parameters is best described by an exponential function, where the concentration decreases with the increase of T, RH, or WS. Interestingly, at zero T, RH, and WS, the concentration approaches 2.5×10^4 cm^{-3}, which is close to the monthly average during winter (e.g. Figure 1). On the other end of the curves; i.e. high T, RH, and WS, the concentration approaches 1.5×10^4 cm^{-3}, which is close to the monthly average during summer (e.g. Figure 1).

This dependence on some weather conditions is very close to the outcome reflected by Hussein et al. (2006). They studied the dependency of aerosol particle number concentrations on the meteorological variables in Helsinki, and showed that the particle number concentrations can be expressed as a function of temperature and wind speed only, but are not dependent on relative humidity; in fact relative humidity dependency was not clear in their study. However, the results of the present study seem to be inconsistent with Singh, et al. (2000), who found that aerosol concentrations increased with relative humidity during the winter season and decreased with temperature. Also, Olivares et al. (2007) reported that the increase in particle number concentrations with the decline of temperature is different for different particle sizes They also showed a distinct correlation between number concentration and (temperature and relative humidity) higher concentrations during periods with low temperatures or a high relative humidity.

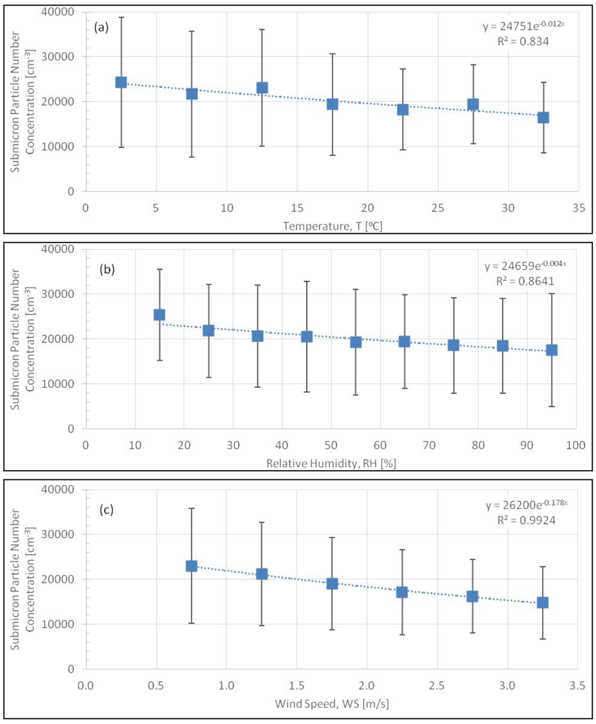

Figure 3. Submicron aerosol concentration versus the **(a)** temperature, **(b)** relative humidity, and **(c)** wind speed. These figures (average and standard deviation) were generated from the hourly average of the submicron particle number concentrations, and the trends were fitted to an exponential function.

In this research, two separate relations were deduced connecting temperature and relative humidity to number concentrations depending on monthly and hourly means. The hourly dependence relation falls under the control of the monthly dependence relation, which can be imagined as wave containing group and phase velocity.

The relationship between the submicron aerosol concentration and meteorological conditions is very important for modeling the urban air quality based on proxies (e.g. Hussein et al., 2006). These models can help predict particle number concentrations on any day, depending on the meteorological parameters of that day. For example, a statistical forecast model was developed to predict the urban particle number concentration based on long-term aerosol database (Mølgaard et al., 2012 and 2013).

3.2. Weekly and Daily Patterns

The submicron aerosol concentration showed a clear weekly pattern with high daytime concentrations during workdays (Figure 4). Similar to many other urban environments, this reflects the combustion emissions from traffic activity, which are more during workdays (e.g. Hussein et al., 2002 and 2004). The researchers anticipated this weekly pattern previously, but the analysis was based on a short-term database limited to less than two months only (March and April 2014) (Hussein et al., 2016).

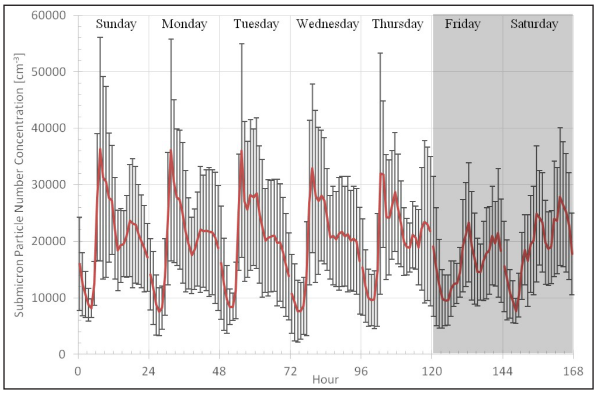

Figure 4. Weekly pattern of the submicron particle number concentrations.

In Jordan, workdays are Sunday through Thursday whereas the weekend days are Friday and Saturday. From the detailed analysis of the daily patterns of the submicron aerosol concentration, three distinguished types of daily patterns were detected (Figure 5): (1) TYPE-I for Sunday – Wednesday, (2) TYPE-II for Thursday, and (3) TYPE-III for weekend days (Friday – Saturday).

TYPE-I (i.e. Sunday – Wednesday) was characterized by the highest concentrations (in the range of 2×10^4 – 3.5×10^4 cm^{-3}) during morning traffic rush hours (06:00 – 12:00). This first peak was also observed by Hussein et al. (2016), but with a higher concentration amounting to 45000 cm^{-3}. A second peak with intermediate concentrations (2×10^4 – 2.2×10^4 cm^{-3}) was spanned between the times15:00 - 21:00. The concentration decreased after 21:00 reaching a background level of (8×10^3 cm^{-3}) between the times 03:00 - 04:00. These two peaks are relevant for the morning and afternoon traffic rush hours, which are similar to those noticed in most cities in developed countries (e.g. Wehner and Wiedensohler, 2003; Olivares et al., 2007; Wehner et al., 2004).

Since ***TYPE-II*** represents the daily pattern for Thursdays, which is a workday, it had characteristics similar to those of TYPE-I, but with a difference in the afternoon peak. The second peak of TYPE-II had slightly higher concentrations (2×10^4 – 2.4×10^4 cm^{-3}) than those observed for TYPE-I extending to after midnight. This little difference can be attributed to late night traffic activities in the city, where people spend their leisure time at coffee shops and restaurants because Thursday is the last workday. It is worth mentioning here that this pattern wasn't clear in the study of Hussein et al. (2016), because their measurements were restricted only to few months.

TYPE-III (Friday – Saturday) was different than the other two types in terms of daytime concentrations. The first peak (i.e. morning peak) started gradually around 06:00 and reached its maximum (~2.4×10^4 cm^{-3}) around midday. The concentrations decreased to ~1.7×10^4 cm^{-3} around 15:00. The second peak also had intermediate concentrations (as high as ~2.4×10^4 cm^{-3}) lasting until midnight, which is another difference between this type of pattern and the other two types. In general, the concentrations in this pattern were lower than those observed during workdays. This result agrees with what was reported by (Hussein et al., 2016). However, their short-term measurements couldn't reveal the duration differences between workdays and weekends.

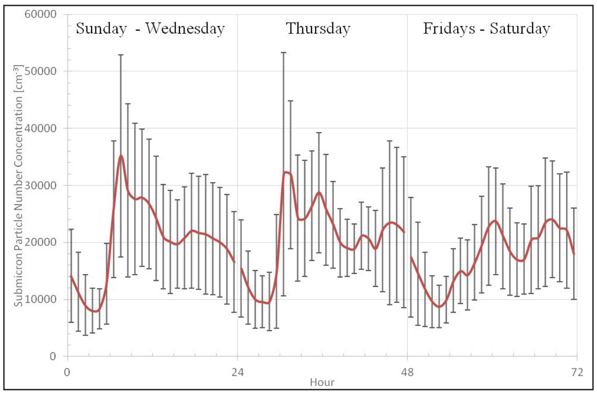

Figure 5. Daily patterns of the submicron particle number concentrations on three weekdays groups: (a) Sunday – Wednesday, (b) Thursday, and (c) Friday – Saturday.

4. Conclusions

The researchers measured the fine particle number concentrations with a condensation particle counter over the period from August 2016 to May 2017 at an urban background site in Amman, Jordan. On-site measurements for weather conditions were also conducted for this study. Both the aerosol database and the weather data-base were converted to an hourly statistical database that was used in further analysis. the main objective was to investigate the temporal variation of urban submicron particle number concentrations.

The results of this study confirmed three temporal cycles for the submicron particle number concentrations: (1) annual cycle, (2) weekly cycle, and (3) diurnal cycle. These temporal variations (annual, weekly, and daily) reflect the anthropogenic emissions, especially those emitted from combustion traffic-related activities in the city.

The annual cycle was clearly observed based on the daily mean of the fine particle number concentration with high concentrations (~2.8×10^4 cm^{-3}) during winter and low concentrations (~1.2×10^4 cm^{-3}) during summer with an annual average of about 8×10^3 cm^{-3}. This annual cycle was inversely correlated with the daily mean T cycle, but was proportional with the daily mean RH including a shift ~22 days.

The submicron particle number concentrations also showed a weekly cycle with the highest concentrations during workdays (Sunday–Thursday). As such, the concentrations had three distinguished types of diurnal patterns: (1) the first four workdays (Sunday–Wednesday), (2) Thursday, and (3) weekend days (Friday–Saturday). The workdays had the highest concentrations during the morning rush hours. The weekend type daily pattern had the highest concentrations during midday and late night. Both pattern types had the lowest concentrations between the times 03:00 – 06:00.

The results presented in this paper are based on a long-term database, which encourages the researchers to perform more extensive measurements for a longer term and fill in the missing gaps in order to reveal more accurate temporal characteristics of the fine particle number concentrations.

Acknowledgments

This study was supported by the Deanship of Academic Research (DAR, project number 1516) at the University of Jordan and the Scientific Research Support Fund (SRF, project number BAS-1-2-2015), Ministry of Higher Education, Amman, Jordan. This work was a part of a close collaboration between the University of Jordan and the Institute for Atmospheric and Earth System Research (INAR) at the University of Helsinki via ERA-PLANET (www.era-planet.eu), trans-national project SMURBS (www.smurbs.eu) (Grant Agreement n. 689443), funded under the EU Horizon 2020 Framework Programme and Academy of Finland via Center of Excellence in Atmospheric sciences and NanoBioMass (project number 1307537). This study and other urban research by the Aerosol Laboratory of the University of Jordan have been encouraged by the World Health Organization regional office in Amman.

References

Abdeen, Z., Qasrawi, R., Heo, J., Wu, B., Shpund, J., Vanger, A., Sharf, G., Moise, T., Brenner, S., Nassar, K., Saleh, R., Al-Mahasneh, Q., Sarnat, J., Schauer, J. (2014). Spatial and temporal variation in fine particulate matter mass and chemical composition: MECARS., ID 878704: 1–16.

Alam, K., Trautmann, T., Blaschke, T., Subhan, F. (2014). Changes in aerosol optical properties due to dust storms in the Middle East and Southwest Asia. Remote Sens. Environ., 143: 216–227.

Al-Dousari, A., Doronzo, D., Ahmed, M. (2017). Types, Indications and Impact Evaluation of Sand and Dust Storms Trajectories in the Arabian Gulf. Sustainability, 9(9): 1–14.

Alghamdi, M.A., Almazroui, M., Shamy, M., Redal, M.A., Alkhalaf, A.K., Hussein, M.A., Khoder M.I. (2015). Characterization and elemental composition of atmospheric aerosol loads during springtime dust storm in western Saudi Arabia. Aerosol Air Qual. Res., 15: 440–453.

Alghamdi, M.A., Khoder, M., Abdelmaksoud, A.S., Harrison, R.M., Hussein, T., Lihavainen, H., Al-Jeelani, H., Goknil, M.H., Shabbaj, I.I., Almehmadi, F.M., Hyvärinen, A.-P., Hämeri, K. (2014a). Seasonal and diurnal variations of BTEX and their potential for ozone formation in the urban background atmosphere of the coastal city Jeddah, Saudi Arabia. Air Qual. Atmos. Health, 7: 467–480.

Alghamdi, M.A., Khoder, M., Harrison, R.M., Hyvärinen, A.-P., Hussein, T., Al-Jeelani, H., Abdelmaksoud, A.S., Goknil, M.H., Shabbaj, I.I., Almehmadi, F.M., Lihavainen, H., Hämeri, K. (2014b). Temporal variations of O3 and NOx in the urban background atmosphere of the coastal city Jeddah, Saudi Arabia. Atmos. Environ., 48: 409–417.

Basha, G., Phanikumar, D.V., Kumar, K.N., Ouarda, T.B.M.J., Marpu, P.R. (2015). Investigation of aerosol optical, physical, and radiative characteristics of a severe dust storm observed over UAE. Remote Sens. Environ., 169: 404–417.

Birmili W., Alaviippola, B., Hinneburg, D., Knoth1, O.,Touch, T., Borken-Kleefeld, J., Schacht, A. (2009). Dispersion of traffic-related exhaust particles near the Berlin urban motorway – estimation of fleet emission factors. Atmos. Chem. Phys., 9: 2355–2374.

Boman, J., Shaltout, A.A., Abozied, A.M., Hassan, S.K. (2013). On the elemental composition of PM2.5 in central Cairo, Egypt. X-Ray Spectrom., 42: 276–283.

Burnett, R.T., Pop III, C.A., Ezzati, M., Olives, C., Lim, S.S., Mehta, S., Shin, H.H., Singh, G., Hubbell, B., Brauer, M., Anderson, H.R., Smith, K.R., Balmes, J.R., Bruce, N.G., Kan, H., Laden, F., Ustün, A.P., Turner, M.C., Gapstur, S.M., Diver, W.R., Cohen, A. (2012). An integrate risk Function for estimating the global burden of disease attribute to ambient fine particulate matter exposure. EHP., 122(4): 397–403.

Dada, L., Mrad, R., Siffert, S., Saliba N.A. (2013). Atmospheric markers of African and Arabian dust in an urban Eastern Mediterranean environment, Beirut, Lebanon. J. Aerosol Sci., 66: 187–192.

Daher, N., Saliba, N. A., Shihadeh, A. I., Jaafar, M., Baalbaki, R., Sioutas, C. (2013). Chemical composition of size-resolved particulate matter at near-freeway and urban background sites in the greater Beirut area. Atmos. Environ., 80: 96–106.

Doronzo, D.M., Khalaf, E.A., Dellino, P., de Tullio, M.D., Dioguardi, F., Gurioli, L., Mele, D., Pascazio, G., Sulpizio, R. (2015). Local impact of dust storms around a suburban building in arid and semi-arid regions: numerical simulation examples from Dubai and Riyadh, Arabian Peninsula. Arab J. Geosci., 8(9):7359–7369.

El-Araby, E.H., Abd El-Wahab, M., Diab, H.M., El-Desouky, T.M., Mohsen, M. (2011). Assessment of atmospheric heavy metal deposition in North Egypt aerosols using neutron activation analysis and optical emission inductively coupled plasma. Appl. Radiat. Isotopes, 69: 1506–1511.

El-Askary, H., and Kafatos, M. (2008). Dust storm and black cloud influence on aerosol optical properties over Cairo and the Greater Delta region, Egypt. Int. J. Remote Sens., 29: 7199–7211.

El-Askary, H., Farouk, R., Ichoku, C., Kafatos, M. (2009). Transport of dust and anthropogenic aerosols across Alexandria, Egypt. Ann. Geophys., 27: 2869–2879.

Engelbrecht, J.P., and Jayanty, R.K.M. (2013). Assessing sources of airborne mineral dust and other aerosols, in Iraq. Aeolian Res., 9: 153–160.

Fenger, J. (1999). Urban air quality. Atmos Environ., 33(29): 4877–4900.

Gherboudj, I., and Ghedira, H. (2014). Spatiotemporal assessment of dust loading over the United Arab Emirates. Int. J. Climatol., 34: 3321–3335.

Habeebullah, T.M. (2013). An analysis of air pollution in Makkah - a view point of source identification. Environ. Asia, 2: 11–17.

Hamad, A.H., Schauer, J.J., Heo, J., Kadhimd, A.K.H. (2015). Source apportionment of PM2.5 carbonaceous aerosol in Baghdad, Iraq. Atmos. Res., 156: 80–90.

Hassan, S.K., El-Abssawy, A.A., Abd El-Maksoud, A.S., Abdou, M.H., Khoder, M.I. (2013). Seasonal behaviours and weekdays/weekends differences in elemental composition of atmospheric aerosols in Cairo, Egypt. Aerosol Air Qual. Res., 13: 1552–1562.

Haywood, J.M., and Boucher, O. (2000). Estimates of the direct and indirect radiative forcing due to tropospheric aerosols: A review. Reviews of Geophysics, 38(4): 513–543.

Hussein, T., and Betar, A. (2017). Size-Fractionated number and mass concentrations in the urban background atmosphere during spring 2014 in Amman-Jordan. JJP., 10(1): 51–60.

Hussein, T., Karppinen, A., Kukkonen, J., Härkonen, J., Aalto, P.P., Hämeri, K., Kerminen, V.M., Kulmala, M. (2006). Meteorological dependence of size fractionated number concentrations of urban aerosol particles. Atmos Environ., 40(8): 1427–1440.

Hussein, T., Abu AlRuz, R., Petäjä, T., Junnienen, H., Arafa, D., Hämeri, K., Kumala, M. (2011). Local air pollution versus short- range transported dust episodes: A comparative study for submicron particle number concentration. Aerosol Air Qual. Res., 11: 109–119.

Hussein, T., Boor, B.E., Santos, V.N., Kangasluoma, J., Petäjä, T., Lihavainen, H. (2017). Mobile aerosol measurement in the eastern Mediterranean – A utilization of portable instruments. Aerosol Air Qual. Res., 17: 1875–1886.

Hussein, T., Halayka, M., Abu Al-Ruz, R., Abdullah, H., Mølgaard, B., Petäjä, T. (2016). Fine Particle Number Concentrations in Amman and Zarqa during Spring 2014. JJP., 9(1): 31–46.

Hussein, T., Hämeri, K., Kulmala M. (2002). Long-term indoor-outdoor aerosol measurement in Helsinki, Finland. Boreal Environ Res., 7: 141–150.

Hussein, T., Mølgaard, B., Hannuniemi, H., Martikainen, J., Järvi, L., Wegner, T., Ripamonti, G., Weber, S., Vesala, T., Hämeri, K. (2014). Fingerprints of the urban particle number size distribution in Helsinki, Finland: Local versus regional characteristics. Boreal Env. Res., 19: 1–20.

Hussein, T., Puustinen, A., Aalto, P. P., Mäkelä, J. M., Hämeri, K., Kulmala, M (2004). Urban aerosol number size distributions. Atoms. Chem. Phys., 4: 391–411.

Jaafar, M., Baalbaki, R., Mrad, R., Daher, N., Shihadeh, A., Sioutas, C., Saliba, N.A. (2014). Dust episodes in Beirut and their effect on the chemical composition of coarse and fine particulate matter. Sci. Tot. Environ., 496: 75–83.

Jin, M., Sheferd, J.M., King, M.D. (2005). Urban aerosols and their variations with clouds and rainfall: A case study for New York and Houston. JGES., 110(D10S20): 1–12.

Khodeir, M., Shamy, M., Alghamdi, M., Zhong, M., Sun, H., Costa, M., Chen, L.-C., Maciejczyk, P. (2012). Source apportionment and elemental composition of PM2.5 and PM10 in Jeddah City, Saudi Arabia. Atmos. Pollut. Res., 3: 331–340.

Kouyoumdjian, H., and Saliba, N.A. (2006). Mass concentration and ion composition of coarse and fine particles in an urban area in Beirut: effect of calcium carbonate on the absorption of nitric and sulfuric acids and the depletion of chloride. Atmos. Chem. Phys., 6: 1865–1877.

Krewski, D. (2009). Evaluating the effects of ambient air pollution on life expectancy. NEJM., 360(4): 413 – 415.

Lepeule, J., Laden, F., Dockery, D., Schwartz, J. (2012). Chronic exposure to fine particles and mortality: An extended follow-up of the Harvard six cities study from 1974 to 2009. 2012. EHP., 120(7): 965–970.

Lohmann, U., and Feichter, J. (2005). Global indirect aerosol effects: a review, Atmos. Chem. Phys., 5(3): 715-737.

Mølgaard, B., Hussein, T., Corander, J., Hämeri, K. (2012). Forecasting Size-Fractionated Particle Number Concentrations in the Urban Atmosphere. Atmos Environ., 46: 155–163.

Mølgaard, B., Birmili, W., Clifford, S., Massling, A., Eleftheriadis, K., Norman, M., Vratolis, S., Wehner, B., Corander, J., Hämeri, K., Hussein, T. (2013). Evaluation of a statistical forecast model for size-fractionated urban particle number concentrations using data from five European cities. J Aerosol Sci., 66: 96–110.

Myhre, G., Myhre, C.E.L., Samset, B.H., Storelvomo, T. (2013). Aerosols and their relation to Global climate and climate sensitivity. Nature Education Knowledge Project, 4(5):1–7.

Olivares, G., Johansson, C., Ström, J., Hansson, H.C. (2007). The role of ambient temperature of particle number concentrations in a street canyon. Atmos Environ., 41: 2145–2166.

Pérez, N., Pey, J., Cusack, M., Reche, C., Querol, X., Alastuey, A., Viana, M. (2010). Variability of Particle Number, Black Carbon, and PM10, PM2.5, and PM1 Levels and Speciation: Influence of Road Traffic Emissions on Urban Air Quality. Aerosol Science and Technology., 44(7): 487-499.

Pope, C.A. III, Burnett, R.T., Thun, M.J., Calle, E.E., Krewski, D., Ito, K., Thurnston, G.D. (2002). Lung Cancer, Cardiopulmonary Mortality, and Long-term Exposure to Fine Particulate Air Pollution. J. Am. Med. Assoc., 287(9): 1132–1140.

Rahman, M.M., Mazaheri, M., Cillford, S., Morawska, L. (2017). Estimate of main local sources to ambient ultrafine particle number concentrations in an urban area. Atmos. Res., 194: 178–189.

Reche, C., Querol, X., Alastuey, A., Viana, M., Pey, J., Moreno, T., Rodr´ıguez, S., Gonz´alez, Y., Fern´andez-Camacho, R., S´anchez de la Campa, A.M., de la Rosa, J., Dall’Osto, M., Pr´evˆ, A.S.H., Hueglin, C., Harrison, R.M., Quincey, P. (2011). New considerations for PM, Black Carbon and particle number concentration for air quality monitoring across different European cities. Atmos. Chem. Phys., 11: 6207–6227.

Reid, J.S., Reid, E.A., Walker, A., Piketh, S., Cliff, S., Al Mandoos, A., Tsay, S.-C., Eck, T.F. (2008). Dynamics of southwest Asian dust particle size characteristics with implications for global dust research. J. Geophys. Res., 113, D14212.

Rushdi, A.I., Al-Mutlaq, K.F., Al-Otaibi, M., El-Mubarak, A.H., Simoneit, B.R.T. (2013). Air quality and elemental enrichment factors of aerosol particulate matter in Riyadh City, Saudi Arabia. Arab. J. Geosci., 6: 585–599.

Saeed, T.M., Al-Dashti, H., Spyrou, C. (2014). Aerosol's optical and physical characteristics and direct radiative forcing during a shamal dust storm, a case study. Atmos. Chem. Phys., 14: 3751–3769.

Saliba, N.A., El Jam, F., El Tayar, G., Obeid, W., Roumie, M. (2010). Origin and variability of particulate matter (PM10 and PM2.5) mass concentrations over an Eastern Mediterranean city. Atmos. Res., 97: 106–114.

Saliba, N.A., Kouyoumdjian, H., Roumie´, M. (2007). Effect of local and long-range transport emissions on the elemental composition of PM10–2.5 and PM2.5 in Beirut. Atmos. Environ., 41: 6497–6509.

Salma, I., Borsos, T., Weidinger, T., Alato, P., Hussein, T., Dal Maso, M., Kulmala, M. (2011). Production, growth and properties of ultrafine atmospheric aerosol particles in an urban environment. Atmos. Chem. Phys., 11: 1339–1353.

Satheesh, S.K., Deepshikha, S., Srinivasan, J. (2006). Impact of dust aerosols on Earth–atmosphere clear-sky albedo and its short-wave radiative forcing over African and Arabian regions. Int. J. Remote Sens., 27: 1691–1706.

Shaltout, A.A., Boman, J., Al-Malawi, D.-A.R., Shehadeh, Z.F. (2013). Elemental Composition of PM2.5 Particles Sampled in Industrial and Residential Areas of Taif, Saudi Arabia. Aerosol Air Qual. Res., 13: 1356–1364.

Singh, A.K., Rai, J., Niwas, S. (2000). Variations of aerosols in relation to some meteorological parameters during different weather conditions. Atmosphera, 13(3): 177-184.

Väkevä, M., Hämeri, K., Puhakka, T., Nilsson, E.D., Hohti, H., Mäkelä, J.M. (2000). Effects of meteorological processes on aerosol particle size distribution in an urban background area.

J. Geophys. Res., 105: 9807-9821.

Vinzents, P.S., Moller, P., Sorensen, M., Knudsen, L.E., Hertel, O., Jensen, F.P., Schibye, B., Loft, S. (2005). Personal exposure to ultrafine particles and oxidative DNA damage. EHP., 113(11): 1485–90.

Waked, A., Afif, C., Brioude, J., Formenti, P., Chevaillier, S., El Haddad, I., Doussin, J.-F., Borbon, A., Seigneur, C. (2013). Composition and source apportionment of organic aerosol in Beirut, Lebanon, during winter 2012. Aerosol Sci. Technol., 47:1258–1266.

Wehner, B., and Wiedensohler, B. (2003). Long term measurements of submicrometer urban aerosols: statistical analysis for correlations with meteorological conditions and trace Gases. Atoms. Chem. Phys., 3: 867–879.

Wehner, B., Wiedensohler, A., Tuch, T.M., Wu, Z.J., Hu, M., Slanina, J., Kiang, C.S. (2004). Variability of the Aerosol Number Size Distribution in Beijing, China: New Particle Formation, Dust Storms, and High continental Background. Geophys. Res., 31(L22108): 1–4.

Wu, Z., Hu, M., Lin, P., Liu, S., Wehner, B., Widensohler, A. (2008). Particle number size distribution in the urban atmosphere of Beijing, China. Atmos Environ., 42: 7967–7980.

Zhao, S., Yu, Y., Yin, D., He, J. (2015). Meteorological dependence of particle number concentrations in an urban area of complex terrain, North-western China. Atmos. Res., 164(165): 304–317.

JJEES

Jordan Journal of Earth and Environmental Sciences

JJEES (2019) 10 (1): 15-20
ISSN 1995-6681

Groundwater Quality Assessment Using Irrigation Water Quality Index and GIS in Baghdad, Iraq

Mufid Al-Hadithi[1], Karima Hasan[2], Amer Algburi[3], Kamal Al-Paruany[4]

[1]Middle Technical University, Engineering Technical College, Baghdad, Iraq
[2]Middle Technical University, Institute of Technology, Baghdad, Iraq
[3]University of Anbar, College of Science, Iraq
[4]Ministry of Science and Technology, Iraq

Received 25 August, 2018; Accepted 17 January, 2019

Abstract

Twelve water samples were collected to evaluate groundwater quality in Baghdad city, Iraq using the irrigation water quality index (IWQI) method with the help of the Geographical Information System (GIS) technique. Five chemical parameters were used including Electrical Conductivity (EC), Cl^-, HCO_3^{-1}, Na % and Sodium Absorption Ratio (SAR) to create the database of water quality. These parameters have been inputted to the GIS platform to produce a spatial distribution map for each parameter using the inverse interpolation technique (IDW).These parameters were used to calculate water quality index values which were also reassigned to the GIS environment to generate the IWQI maps. The map results showed that only 25 % of the studied samples fall in Low Restriction (LR) categories indicating that this water can be used for irrigation purposes without reservation. 94 % of the groundwater was found to be moderate to highly restricted for use in irrigation and can be used only in soils with a high permeability without compact layers, requiring moderate leaching of salts. The map results also showed that 26 % of the studied water samples should be avoided and not used for irrigation under normal conditions because they fall within the Severe Restriction (SR) categories. The former type can be used only if the soil permeability is high, and the excess of water is applied to avoid the accumulation of salt.

Keywords: Irrigation Water Quality Index (IWQI), GIS, Baghdad, Iraq

1. Introduction

The entire city of Baghdad uses the waters of the Tigris River for drinking, agriculture and other purposes. In the recent years, however, the river has suffered from many problems, including scarcity of resources, construction of dams by the neighboring countries, as well as the inflow of industrial and agricultural waste water and local waste. These problems have created an urgent need to search for other water sources and assess the groundwater of the wells that are already in the area to meet the people's water needs, especially in areas located far from the river. This study is conducted to evaluate the quality of well water in Baghdad city for irrigation purposes using the irrigation water quality index (IWQI) method as well as the technology of the Geographic Information System (GIS). This approach has been successfully used in recent years and on a large scale. It provides an excellent overview of the condition of groundwater through the integration of composite data. Previously and prior to this approach, researchers used to rely on irrigation water standards set by the United States Salinity Laboratory (USSL, 1954) and Wilcox (1955) diagrams to assess water for irrigation purposes. In 2010, Meireles et al. developed an IWQI model to assess water to be used for irrigation purposes using Electrical Conductivities (EC), Magnesium (Mg^{2+}), Sodium (Na^+), Potassium (K^+), Chloride (Cl^-) and Bicarbonate (HCO_3^-) parameters, which reflect soil salinity, sodicity hazards, and water toxicity to plants. This model has been used successfully and on a large scale to assess the quality of water used for irrigation purposes by many researchers e.g. (Omran and Marwa, 2015; Al-Musawi, 2014; Rasul and Waqed, 2015; Rokbani et al., 2011; Jerome and Pius, 2010). Those researchers proved that this method is an excellent way to give an overview of the state of groundwater through the integration of composite data by summarizing the monitored data or showing the spatial distribution of quality as index allowing the best use of this water in the future. The current study is carried out with the aim of using the GIS integrated with the IWQI method which has been established by (Meireles et al., 2010) to assess the quality of groundwater, and to determine its suitability for irrigation purposes in Baghdad city.

2. Area of study

The study area lies between latitude 33° 10' to 33° 29' N, longitudes 44° 09' to 44° 33' E, the elevation of catchment area ranges from 33m to 37m above sea level covering area about 5159 km^2 (Figure 1).

The city of Baghdad is characterized by a warm and dry climate in summer and cool humidity in winter with the annual precipitation rates ranging from 0.05 mm to 24.66 mm. The monthly temperature ranges between 9.64 and 35.39 C°, while

---

* Corresponding author e-mail: mufidalhadithi@yahoo.com

evaporation ranges from 66.85 to 530 mm. Relative humidity has a direction compared to temperature and evaporation. Geologically, the study area is relatively simple represented by the Quaternary deposits (Pleistocene), and is covered mainly by the Holocene deposits (Jassim and Goff, 2006). Hydrogeologically, good sand aquifer has been observed underground at the depths of 8-20 m in the studied area.

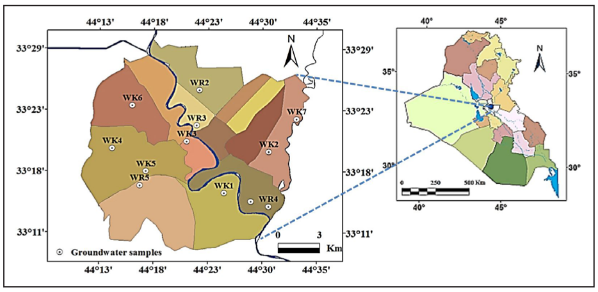

Figure 1. Location map of the study area showing sampling site

3. Methodology

3.1. Water Samples and Analysis

Twelve water samples were collected from twelve wells covering the whole area of the study analyzed by the Ministry of Science and Technology (MOST). Table 1 shows the details of the sampling locations along with their latitude and longitude. The collected samples were analyzed chemically concerning different elements including EC, Na^+, Cl, HCO_3^- ,and SAR which affect the quality of water used for irrigation purposes. These parameters have been used to calculate IWQI. EC has been measured in the field using a conductivity meter. Sodium (Na^+) has been analyzed by a flame photometer, HCO_3^{-1} and Cl^- were analyzed by H_2SO_4 and $AgNO_3$ titration methods, respectively (Jackson, 1976). All the results of the chemical analysis were summarized in Table 2.

Table 1. Sampling locations

Location	Well code	Latitude	Longitude	Elevation (m)	Depth (m)	Water level (m)
Al-Dora	WK1	33 16 58.9	44 26 37.6	35	14	20
Saidia	WK2	33 16 12.4	44 27 43.7	34	27	28
Karadha M.	WK3	33 18 50.1	44 22 20.2	32	26	28
Al-Mansour	WK4	33 19 12.4	44 24 52	33	11	12
Yarmouk	WK5	33 16 11.9	44 21 11.4	35	13	13
Shulah	WK6	33 22 17	44 17 27.0	38	22	22
Rahmania	WK7	33 21 11.1	44 21 15.1	36	20	20
Zafrania	WR1	33 14 9.7	44 28 07.7	33	15	15
Shabe	WR2	33 23 34	44 25 7.2	34	13	13
Adamia	WR3	33 21 40	44 23 18.6	34	14	14
Dyala	WR4	33 12 17	44 30 52	33	21	21
MOST	WR5	33 16 43.6	44 24 09.3	34.5	18	18

Table 2. Chemical analysis of groundwater samples in the study area (Units in meq. l-1 except EC in (µs/cm) and TDS in ppm)

Well code	pH	TDS	EC	Ca^{+2}	Mg^{+2}	K^+	Na^{+2}	HCO_3^-	Cl^-	SO_4^{-2}	Na%	SAR
WK1	7.3	2298	3800	12.97	8.22	0.11	16.30	3.33	24.8	9.9	43.6	5.01
WK2	6.9	2573	5320	16.72	14.47	0.11	13.04	6.07	30.1	6.6	29.6	3.30
WK3	7.4	1578	3100	5.49	10.20	0.08	8.61	9.84	7.8	5.5	35.6	3.07
WK4	7.2	2877	11000	17.12	15.38	0.15	12.17	3.20	18.5	25.2	27.5	3.02
WK5	7.3	970	1840	6.64	4.52	0.13	4.26	4.10	3.4	6.4	28.2	1.80
WK6	7.3	2042	2300	9.38	8.39	0.13	13.26	5.25	9.0	16.6	43.9	4.45
WK7	7.8	561	1210	2.59	2.71	0.08	2.74	2.89	2.5	3.0	34.6	1.68
WR1	7.7	786	1000	4.54	2.88	0.12	4.26	4.93	2.5	3.5	37.1	2.21
WR2	7.2	1210	1990	7.68	6.17	0.19	5.00	5.74	4.8	7.1	27.3	1.90
WR3	7.4	2228	4260	22.95	6.91	0.18	4.65	2.30	3.0	27.5	13.9	1.20
WR4	7.3	1528	2420	8.53	6.41	0.19	7.65	3.80	6.0	13.5	34.4	2.80
WR5	6.8	1901	3210	8.68	4.93	0.16	13.96	5.84	6.0	16.0	50.9	5.35

3.2. Calculation of the Irrigation Water Quality Index (IWQI)

The EC, Na^+, Cl^-, $HCO_3^-$and SAR parameters suggested by (Meireles et al., 2010) have been used to calculate the IWQI. EC, Na^+, Cl^- and HCO_3^- parameters were measured in the laboratory and (SAR) was calculated as the ratio of sodium absorption using the following equation:

$$SAR = Na^+ / \sqrt{(Ca^{2+} + Mg^{2+})/2} \quad \text{..(1)}$$

In the first step, values of the accumulation weights (w_i) suggested by (Meireles et al., 2010) have been defined based on their relative significance to the irrigation water quality. Its normalized values and their total are equal one as shown in Table 3. Based on different parameters recommended by (Ayers and Westcot, 1994), Qi value was estimated in the second step as shown in Table 4. It represents non-dimensional number with the higher value indicating a better water quality and vice versa. Qi value was calculated using the following equation:

$$Q_i = q_{imax} - \left\{ \frac{[(x_{ij} - x_{inf}) * q_{iamp}]}{x_{amp}} \right\} \text{....................................} (2)$$

where q_{imax} is a maximal value of qi for the class, x_{ij} is the observed value of chemical parameters, x_{inf} is the minimal limit of the class to each parameter belongs; q_{iamp} is class amplitude; and x_{amp} is upper limit of the last class of each parameter. Finley Irrigation water quality index (IWQI) has been calculated according to the following equation:

$$IWQI = \sum_{i=1}^{n} Qi * wi \text{ ....} (3)$$

where IWQI is the non-dimensional irrigation water quality index ranging from 0 to 100; Qi is the quality measurement of the parameter, (i_{th}) a number from (0 to 100) is a function of its concentration; and wi is the normalized weight of the i_{th} parameter.”(Meireles et al. 2010) have divided the values of IWQI for the suitability of the irrigation water class into five dimensionless parameter classes based on the proposed groundwater quality index determined by the existing groundwater quality index as shown in Table 5. The classes were defined based on salinity hazard problems, soil water infiltration reduction, and toxicity to plants as suggested by (Bernardo, 1995). The method of calculating the irrigation water quality index was explained in details as an example of well number one (WK1) in Table 6.

Table 3. Weights for the IWQI parameters according to Meireles et al., 2010

Parameter	Weight (wi)
EC	0.211
Na^{+2}	0.204
HCO_3^-	0.202
Cl^-	0.194
SAR	0.189
Total	**1.0**

Table 4. Limiting values of (qi) calculations (Ayers and Westcot, 1994).

HCO_3^{-1}	Cl^-	Na^+	SAR $(meq/l)^{1/2}$	EC (µS/cm)	Q_i
(meq/l)					
$1 \leq HCO_3 < 1.5$	$1 \leq Cl < 4$	$2 \leq Na < 3$	$2 \leq SAR < 3$	$200 \leq EC < 750$	85-100
$1.5 \leq HCO_3 < 4.5$	$4 \leq Cl < 7$	$3 \leq Na < 6$	$3 \leq SAR < 6$	$750 \leq EC < 1500$	60-85
$4.5 \leq HCO_3 < 8.5$	$7 \leq Cl < 10$	$6 \leq Na < 9$	$6 \leq SAR < 12$	$1500 \leq EC < 3000$	35-60
$HCO_3 < 1$ or $HCO_3 \geq 8.5$	$1 < Cl \geq 10$	$Na < 2$ or $Na \geq 9$	$2 \leq SAR$ ≥ 12	$EC < 200$ or $EC \geq 3000$	0-35

Table 5. Irrigation Water Quality Index Characteristics (Meireles et al. 2010).

Recommendation		Water use restrictions	IWQI
Plant	Soil		
No toxicity risk for most plants	May be used for the majority of soils with low probability of causing salinity and sodicity problems. Leaching recommended within irrigation practices, except for in soils with extremely low permeability”	No restriction (NR)	85-100
Avoid salt sensitive plants”	Recommended for use in irrigated soils with light texture or moderate permeability. Salt leaching recommended. Soil sodicity in heavy texture soils may occur, being recommended to avoid its use in soils with high clay	Low restriction (LR)	70- 85
Plants with moderate tolerance to salts may be grown	May be used in soils with moderate to high permeability values, moderate leaching of salts suggested.	Moderate restriction (MR)	55- 70
Should be used for the irrigation of plants with moderate to high tolerance to salts with special salinity control practices, except water with low Na, Cl and HCO_3 values”	May be used in soils with high permeability without compact layers. High frequency irrigation schedule should be adopted for water with EC above 2000 µS cm^{-1} and SAR above 7.0	High restriction (HR)	40 -55
Only plants with high salt tolerance, except for waters with extremely low values of Na^+, Cl^- and HCO_3^-	Should be avoided for irrigation under normal conditions. May be used occasionally in special cases,. Water with low salt levels and high SAR require gypsum application. In high saline water, soils must have high permeability, and excessive water should be applied to avoid salt accumulation	Severe restriction (SR)	0-40

Table 6. Calculating of the irrigation water quality index (IWQI) of the well No. 1

Chemical parameter	Xij	Class	Q_{imax}	Q_{iamp}	X_{inf}	X_{amp}	Qi	Wi	IWQI
EC	3800	4	35	35	200	10800	23.33	0.211	4.92
Na+	16.30	4	35	35	2	14.3	-0.01	0.204	0.00
HCO_3-	3.33	2	85	25	1.5	3	69.77	0.202	14.09
Cl-	24.79	4	35	35	1	29	6.29	0.194	1.22
SAR	5.01	2	85	25	3	3	68.27	0.189	12.90
								1	**33.14**

3.3. GIS Database Generation and Analysis

The results of the chemical analysis of the water samples were transferred to the GIS environment to create a water quality database in the study area, and the spatial distribution map for each parameter has been generated using the ArcGIS 10.1 software, spatial analyst extension, and inverse distance weight (IDW) interpolation methods as shown in Figures 2 to 8.

4. Results and Discussion

4.1. Salinity Hazard

Electrical Conductivity (EC) of the water samples collected from the study area has been measured, and the spatial distribution map was prepared using GIS as shown in Figure 2. In general, it could be concluded that the large variation in EC ranges from 100 µmhos/cm to 11000 µmhos/cm. This is mostly due to the dominant human activities in this area. According to Rao (1986), the high values of EC may be attributed to the reduction of the osmotic activity of the plants which interferes with the absorption of water and nutrients from the soil.

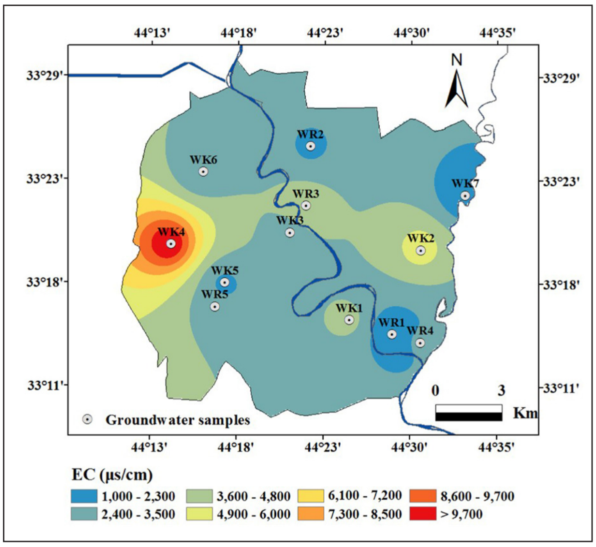

Figure 2. EC Spatial distribution map of the study area

4.2. Sodium Percentage (Na %)

The percentage of sodium is a communal factor in the evaluation of all natural waters, their appropriateness for irrigation purposes, and their influence on the physical and chemical properties of the soil. Sodium can have a great effect on the soil permeability infiltration process. When sodium is highly concentrated, the soil becomes solid, and compact when dry. This affects the structure of the soil and leads to reduce the rates of air and water leakage to the soil (USSL Staff, 1954; Tijani, 1994). In the studied water samples Na^+% values ranged between (13.9) and (50.9); the spatial distribution map of the sodium content was prepared and shown in Figure 3.

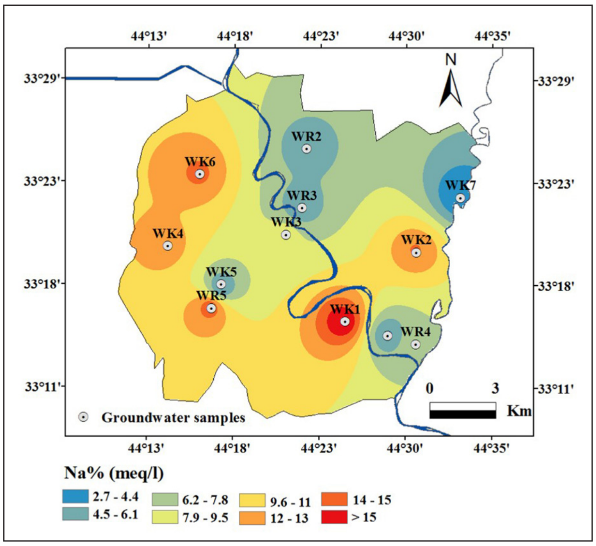

Figure 3. Na% Spatial distribution map of the study area

4.3. Alkalinity Hazard

Alkaline hazard is expressed as the ratio of sodium adsorption (SAR) which is the most common water quality factor that influences the normal rate of infiltration of water. It is calculated according to (Ayers and Westcot, 1994) as shown in equation 1. The values of SAR in the studied samples range from 1.2 meq/L to 5.01 meq/L. These values have been inputted to the GIS environment to create a spatial distribution of SAR map as displayed in Figure 4. If the value of the SAR is more than eighteen, the groundwater is considered unsuitable for irrigation purposes according to (Varol and Davraz, 2015). Based on SAR values in the studied groundwater, all the samples were found suitable for irrigation purposes.

4.4. Toxicity and Miscellaneous Effects

Chloride concentrations are presented as the parameter defining the specific ion toxicity. Although chloride ion is an influential factor in some regional water classifications, it is usually not included in modern water classifications because it does not affect the physical properties of the soil. The chemical analysis of the water samples showed that the minimum value of chloride is 2.5 meq/l (i.e 88.75 mg/l), and the maximum value is 30.1 meq/l (i.e 1068.55 mg/l) as presented in Table 1. The spatial distribution of chloride concentrations is shown in Figure 5. It has been observed that chloride concentrations were relatively high in all the water samples. Chloride is essential for plants in very low amounts, yet it can cause toxicity to sensitive crops at high concentrations. In comparison with the criteria presented in Table 7, plants were very sensitive to the amount of chloride in 33.3 % of the water samples (well no. 5, 7, 8,10), and were moderately tolerant to it in 41.7 % of the samples (well no. 11,12, 3, 9, 6). Moreover, 20 % of the water samples (well no.1, 2, 4, 10) can cause severe problems to plants as a result of the amount of chloride.

Table 7. Chloride classification of irrigation water (Bauder et al. 2003)

Chloride (mg\l)	Effect on Crops
Below 70	Generally safe for all plants
70-140	Sensitive plants show injury
141-350	Moderately tolerant plants show injury
Above 350	Can cause severe problems

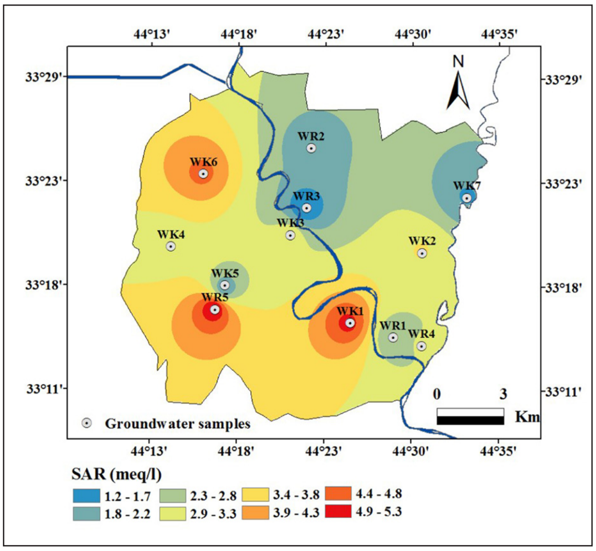

Figure 4. (SAR) Spatial distribution map of the study area

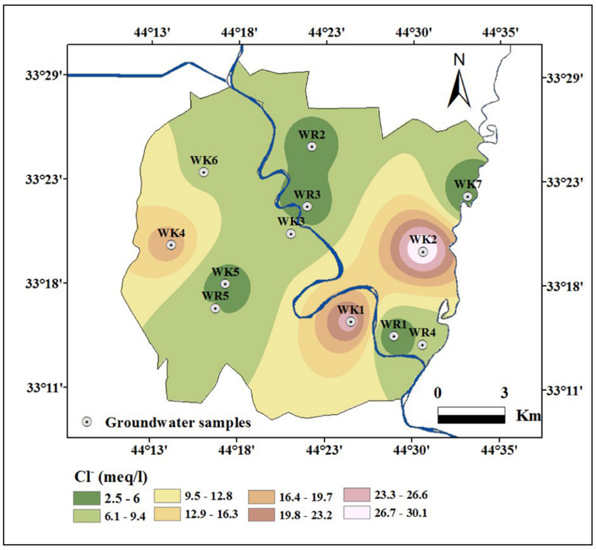

Figure 5. (Cl-) Spatial distribution map of the study area

Bicarbonate and pH parameters were found to be within the range of the miscellaneous effects on sensitive crops. The pH values range from 6.8 to 7.8 in the studied water samples as shown in Figure 6. It is found that all studied water samples were within the range reported by (Rizwan and Gurdeep, 2010) which is ranging from 6.5 to 8.4 in the irrigation groundwater. The reason for the high pH values to more than 8.5 in the groundwater are bicarbonate ions and thus can be considered the main component of alkalinity in groundwater (Charmaine and Anitha, 2010). The ability of the plant to take nutrients from the soil varies depending on the pH values. If the value of the pH is high or low it limits its ability to absorb nutrients. When the pH is low, the solubility of the ammonium and manganese salts increases and their concentration may be harmful to the plant.

Bicarbonate ion (HCO_3^-) concentration in the water samples ranged from (9.84 meq/l) to (2.3 meq/l) as shown in Figure 7. According to (Ayers and Westcot, 1994), the bicarbonate concentration values below 90 mg/l (i.e. 1.5 meq/l) are considered to be ideal for irrigation. Accordingly, all the studied samples containing more than 90 mg / L are not suitable for irrigation.

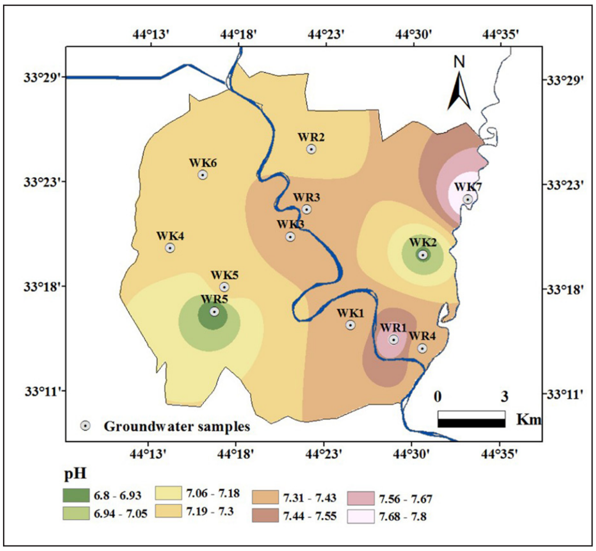

Figure 6. pH spatial distribution map of the study area

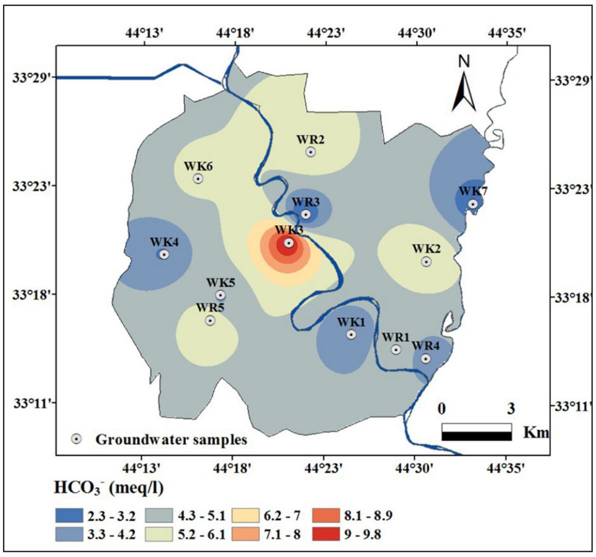

Figure 7. (HCO3-) Spatial distribution map of the study area

The spatial distribution maps of all the parameters which have been discussed above have been generated using inverse interpolation technique (IDW) to create the database of groundwater quality for irrigation water based on the data of twelve wells representing the Baghdad region. Maps of the spatial distribution of contaminant concentrations in groundwater in the study area provide a suitable presentation of the distribution of groundwater quality. Hence, these maps could be used to evaluate the groundwater quality, and estimate the suitable sites of new wells having lowest harmful pollutants.

4.5. Irrigation Water Quality Index (IWQI) Map

The EC, SAR, Na^+, Cl^- and HCO_3^- parameters have been used to calculate IWQI in the study area. Spatial distribution maps were prepared for each parameter and were integrated using ArcGIS /spatial analyst extension according to Equation (3). This integration gives the IWQI index map as a result of geostatistical analysis as shown in Figure 8.

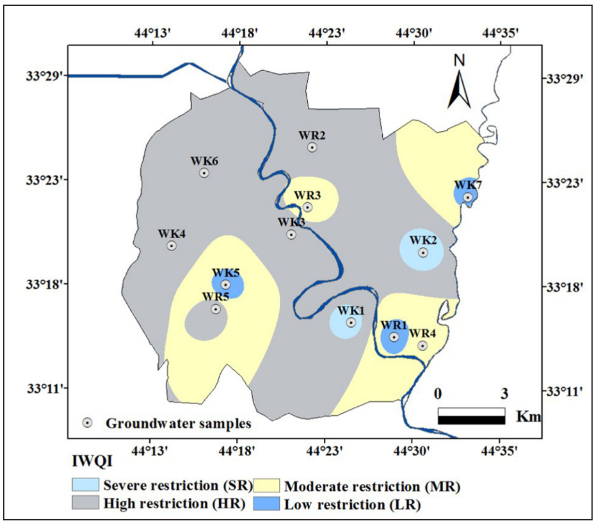

Figure 8. IWQI spatial distribution map of the study area

The analysis of IWQI map shows that the suitability of groundwater for irrigation in the studied area is divided into four classifications of water use restrictions. Only 25 % of groundwater fall in the low-restricted categories and could be used for irrigation directly without any processing. 49 % of the studied samples fall in the moderate to highly restricted for use classification, which means they can be used in soils with high permeability without compact layers, requiring moderate leaching of salts to ensure no harm to plants. The remaining (26 %) of the studied samples fall in the severe restriction (SR) categories, which means that this water should be avoided, and not used for irrigation under normal conditions. However, this water can sometimes be used if the soil permeability is high, and the excess of water is applied to avoid the accumulation of salt.

5. Conclusions

The integration of the spatial distribution map of EC, SAR, Na^+, Cl^- and HCO_3^- parameters have been conducted using the GIS technique to give the IWQI index map as a result of geostatistical analysis. Since the map shows the spatial distribution of the quality of irrigation water in the plain as index values, it provides a comprehensive view, and gives the results concerning the state of the groundwater. This facilitates the task of decision makers to assess the quality of groundwater used for irrigation in the study area. An analysis of the results of the IWQI maps confirms that 25 % of the groundwater in the study area is found to be suitable for irrigation purposes.

References

AL-Musawi, W.H. (2014). Assessment of Groundwater Quality in UMM ER Radhuma Aquifer (Iraqi Western Desert) by Integration between Irrigation Water Quality Index and GIS, Report submitted by Civil Engineering, University of Karbala, Iraq.

Ayers, R.S., and Westcot, D.W. (1994). Water quality for agriculture: FAO Irrigation and Drainage Paper 29, Revision 1, 1-130.

Bernardo, S. (1995). Manual de Irrigacao, 4th edition, Vicosa: UFV, 488 p.

Bauder, T.A., Waskom, R.M., Sutherland, P.L., Davis, J.G. (2003). Irrigation water quality criteria – 0.506, Colorado State University.

Charmaine, K.S.J., and Anitha, P. (2010). Evaluation of water quality index and its impact on the quality of life in an industrial area in Bangalore, American Journal of Scientific and Industrial Research, 1(3): 595-603.

Jackson, M.L. (1976). Soil Chemical Analysis. Prentice Hall Inc. Englewood Cliffs, NJ, USA, 227-267.

Jassim, S.Z., and Goff, J.C. (2006). Geology of Iraq, Dolin Prague and Moravian Museum, Brno, 341p.

Jerome, C., and Pius, A. (2010). Evaluation of water quality index and its impact on the quality of life in an industrial area in Bangalore, South India, American, Journal of Scientific and Industrial Research, 1 (3): 595-603.

Meireles, A., Andrade, E.M., Chaves, L., Frischkorn, H., Crisostomo, L.A. (2010). A new proposal of the classification of irrigation water, Revista Ciencia A gronomica, 41(3): 349-357.

Omran, I., and Marwa, F. (2015). Evaluation of Drainage Water Quality for Irrigation by Integration between Irrigation Water Quality Index and GIS, International Journal of Technical Research and Applications, 3(4): 24 – 32.

Rao, N.S. (1986). Hydrogeology and hydrogeochemistry of Visakhapatanam. Ph.D Thesis unpublished.

Rasul, M.K., and Waqed, H.H. (2015). Evaluation of irrigation water quality index (IWQI) for al-dammam confined aquifer in the west and southwest of karbala city, iraq, International Journal of Civil Engineering (IJCE), 2(3): 21-34

Rizwan, R., and Gurdeep, S. (2010). Assessment of Ground Water Quality Status by Using Water Quality Index Method in Orissa, India, World Applied Sciences Journal, 9(2): 1392-1397.

Rokbani, M.K., Gueddari N., Bouhlila, R. (2011). Use of Geographical Information System and Water Quality Index to Assess Groundwater Quality in El Khairat Deep Aquifer (Enfidha, Tunisian Sahel), Iranica Journal of Energy and Environment, 2(2): 133-144.

Tijani, M.N. (1994). Hydrochemical assessment of groundwater in Moro Area, Kwara State, Nigeria. Environmental Geology, 24:194–202.

United State Salinity Laboratory Staff. (1954). Diagnosis and improvement of saline and alkali soils. USDA Agr Handbook No. 60, Washington DC.

Varol, S., and Davraz, A. (2015). Evaluation of the groundwater quality with WQI (Water Quality Index) and multivariate analysis: a case study of the Tefenni plain (Burdur/Turkey), Environmental Earth Science, 73: 1725–1744.

Wilcox, L.V. (1955). Classification and use of irrigation water, U.S.A Dept. Ag. Circ. 696, Washington DC. 19p.

JJEES

Jordan Journal of Earth and Environmental Sciences

JJEES (2019) 10 (1): 21-27
ISSN 1995-6681

Total Petroleum Hydrocarbon and Heavy Metal Reduction: A Case Study of Enhanced Degradation Potential of Animal Waste by Fungal Isolates

Akiri-Obaroakpo, Imarhiagbe Eseosa, Ekhaise Frederick

University of Benin, Faculty of Life Sciences, Department of Environmental Management and Toxicology, Nigeria

Received 21 September, 2018; Accepted 3 January, 2019

Abstract

This study is conducted to determine the role of poultry litter and cow dung in enhancing the degradation of diesel in contaminated soils by fungal isolates. The treatment sets were used for soils with three levels of diesel pollution (50 ml, 100 ml and 150 ml). The microbiological properties, total petroleum hydrocarbon content and heavy metals were analyzed for six months using standard analytical procedures. The highest and lowest levels of total petroleum hydrocarbon utilization percentages were observed for C_1 as (98.5 %), soil with 50 ml diesel, amended with poultry and cow dung, and also for Control 1 as (31.6 %). The results of heavy metal analysis revealed Pb having the highest value of 3.20 mg kg^{-1} recorded for C_3, soil with 150 ml diesel amended with poultry litter and cow dung in the month of July, 2016; Cr had its highest value of 2.8 $mgkg^{-1}$ recorded for B_3, soil with 150 ml diesel amended with cow dung in July, 2016, and Fe had its highest value of 182 mg $kg^{-1}$for C_3 also in the month of July, 2016. The results of the total heterotrophic and hydrocarbon-utilizing fungal counts ranged from 22.0±2.0 to 42.5±2.5 x10^4 cfu/g for C_1 and B_3 and 24.0±2.0 to 51.0± 2.0 x10^4 cfu/g for C_3 and B_1, soils with 50 ml diesel amended with cow dung respectively. Seventeen fungal species were isolated. *Aspergillus* spp. had the highest frequency of occurrence, 31.69 % and the least percentage of frequency of occurrence was recorded for *Candida albicans* (0.7 %) and *Botrydiplodia* sp. (0.7 %). This study stresses the enhanced potential of fungal population in the reclamation of diesel-contaminated soils.

Keywords: Diesel oil pollution, animal waste, hydrocarbon-utilizing fungi, Total Petroleum Hydrocarbon, Heavy metals.

1. Introduction

Diesel oil is one of the major products of crude oil and it constitutes a major source of pollution to the environment (Nwaogu et al., 2008). Diesel pollution is on the rise in Nigeria as well as in other developing countries in the world (Stephen et al., 2010). Contaminations occurs through leakage from diesel-powered vehicles, generators, through wrecks of oil tankers carrying diesel oil, cleaning of diesel tanks by merchants, war ships carrying diesel oil and motor mechanics (Hill and Moxey, 1980). Poultry litter is a mixture of feces, wasted feeds, bedding materials, and feathers (Wilkinson et al., 2011, Kim et al., 2012). It contains significant amounts of nitrogen because of the presence of high levels of protein and amino acids. Owing to its high nutrient content, poultry litters has been considered one of the most valuable animal waste to be used as organic fertilizer (Wilkinson, 1979). Cow dung, on the other hand, is the waste product of bovine animal species. It contains a vast reservoir of the following nutrients (Akinde and Obire, 2008): 3 % nitrogen, 2 % phosphorus, and 1 % potassium (3-2-1 NPK) essential for microbial growth and metabolism, and hence has a wide array of microorganisms with a potential hydrocarbon-degrading capacity.

Bioremediation is a waste management technique that involves the use of organisms to remove or neutralize pollutants from a contaminated site (Omotayo et al., 2012). It can also be defined as the treatment that uses naturally occurring organisms to break-down hazardous substances into less toxic or non-toxic substances. This process is an efficient remediation method of petroleum by-products, pesticides, and other harmful chemical (Castro-Gutierrez et al., 2012). It is an environmentally friendly technique, cost effective and efficient process (Gadd, 2000).

Fungi have been shown to play a major role in the bioremediation of polluted environments. Amongst their features which enable them to play a great role in bioremediation are: the secretion of extracellular enzymes, the ability to grow under stressed environmental conditions (low nutrient, pH, and water activity), extension in biomass location through hyphal growth, easy and rapid growth on agricultural or forest waste, and other enzyme systems (Obire and Putheti, 2008; George-Okafor et al., 2009). Fungi are known to secrete extracellular enzymes during biodegradation. These inherent capabilities make fungi initiate primary attack of more complex and recalcitrant pollutants thereby facilitating secondary attacks by bacteria. Fungal genera (*Amorphoteca, Neosartorya, Talomyces*, and *Graphium*), yeast such as *Candida*, *Yarrowia,* and *Pichia* and terrestrial fungi; *Aspergillus, Cephalosporium*, and *Penicillium* have been

---

* Corresponding author e-mail: mercy.akiri-obaroakpo@uniben.edu

implicated in hydrocarbon degradation (Chaillan et al., 2004; Singh, 2006; Das and Chandran, 2011).

The presence of heavy metals in the soil has been attributed to pedogenetic processes of weathering of parent materials and anthropogenic sources (Kabata-Pendias and Pendias, 2001). The presence of heavy metals in the soil has been attributed to petroleum prospecting and mining as well as oil spills, (Osuji and Onojake, 2004). The most significant natural sources are weathering of minerals, erosion and volcanic activity, while the anthropogenic sources depend upon human activities such as mining, smelting, electroplating, use of pesticides and phosphate fertilizer discharge, as well biosolids (e.g., livestock manures, composts, and municipal sewage sludge), atmospheric deposition, *etc.* (Summer, 2000). Bioremediation is based on their catalyzed redox conversion to insoluble forms. These reduction or oxidation reactions take place due to enzymatic activity and the biomass concentration of microbes (Khan et al., 2005). More work is being done on the use of organic waste to remediate oil-polluted sites. The remediation of crude oil-polluted soil using cow dung manure in relations to the growth of maize (*Zea mays l.*) has also been demonstrated (Oyedele and Amoo, 2014). Obasi et al., (2013) conducted a comparative study using horse manure, cow dung and poultry litter to remediate polluted soil, and discovered that poultry litter remediated most contaminated soils compared with the other organic manures. The aim of this study is to determine the role of poultry litter and cow dung in enhancing degradation of diesel- contaminated soils by fungal isolates.

2. Materials and Methods

2.1. Soil and Animal Waste Collection

The soil samples were collected from the Animal and Environmental Biology (AEB) Experimental Garden, Faculty of Life Sciences, University of Benin, Benin City at a depth of 15 cm. The animal waste samples including cow dung and poultry litter were collected from the University of Benin Agricultural Farm and the Cattle Ranch at Benin Technical College Road, Benin City respectively. The samples of petroleum products (diesel) were collected from a Commercial Petroleum Products Station in Benin, Benin storage facility, Edo State.

2.2. Soil and Animal Waste Collection

A total of eleven treatments were set up in triplicate for the assessment of enhanced biodegradation. The experiments were monitored for a period of six months between July, 2016 and December, 2016. The experimental designs are as follows:

Table 1. TREATMENT SET-UP

	Treatments	Soil (g)	Diesel (ml)	PL (g)	CD (g)	PL+ CD (g)	Total
	Control 1	2000	–	–	–	–	2000
	Control 2	2000	50	–	–	–	2050
1	A_1	2000	50	100	–	–	2150
	A_2	2000	100	100	–	–	2200
	A_3	2000	150	100	–	–	2250
2	B_1	2000	50	–	100	–	2150
	B_2	2000	100	–	100	–	2200
	B_3	2000	150	–	100	–	2250
3	C_1	2000	50	–	–	100	2150
	C_2	2000	100	–	–	100	2200
	C_3	2000	150	–	–	100	2250

KEYS: *CD = Cow Dung; PL = Poultry Litter*

Control 1: soil only, control 2: soil + 50 ml diesel, A_1*: soil + 100 g poultry litter + 50 ml diesel,* A_2*: soil + 100 g poultry litter + 100 ml diesel,* A_3*: soil + 100 g poultry litter + 150 ml diesel,* B_1*: soil + 100 g cow dung + 50 ml diesel,* B_2*: soil + 100 g cow dung + 100 ml diesel,* B_3*: soil + 100 g cow dung + 150 ml diesel,* C_1*: soil + 50 g cow dung + 50 g poultry litter + 50 ml diesel,* C_2*: soil + 50 g cow dung + 50 g poultry litter + 100 ml diesel,* C_3*: soil + 50 g cow dung + 50 g poultry litter + 150 ml diesel*

The experiments were conducted over a period of six months (three months of rain and three months of dry weather). The perforated buckets containing the soil samples were kept in the open, but they were protected from the direct effect of rain. During this period, the soil samples were stirred, and the temperature of the soils were taken at regular intervals. The soil samples were bi-monthly collected for analysis.

2.3. Enumeration of Total Heterotrophic Fungal Counts

Total fungal analysis was carried out on treatments by weighing 10 g of the soil samples into 90 ml of distilled water and was serially diluted to obtain a ten-fold diluent. Aliquot (1 ml) of 10^{-4} and 10^{-6} dilutions were dispensed unto Potato Dextrose Agar (PDA), amended with chloramphenicol (0.02-1 μg/ml) and used for the isolation of fungi. The plates were prepared and inoculated in duplicates, and were incubated at room temperature for five days. After incubation, the colonies of the isolates were counted and expressed in cfu/g; the isolated colonies were further purified by sub-culturing and were identified by comparing their growth with the standard manual and microscopy (Barnett and Hunter, 1998).

2.4. Screening for Hydrocarbon Utilizing Fungal Populations

The vapor phase transfer technique was employed for the screening of hydrocarbon- utilizing fungi. Sterile Whatman filter papers soaked in diesel were aseptically placed into the lids of each inoculated Bushnell-Haas Agar plates. Aliquots (1 ml) of 10^{-4} and 10^{-6} dilutions of the crude oil soil suspension were seeded onto Bushnell-Haas Agar and incubated at room temperature for six days (Chikere and Azubuike, 2014). Average colony counts were recorded and used for hydrocarbon utilizers within the fungal population. The isolated colonies were further purified by sub-culturing onto Potato Dextrose Agar (PDA) medium to obtain a pure culture. They were examined both macroscopically and microscopically for the identification of the fungi (Barnett and Hunter, 1998).

2.5. Heavy Metal Analysis

The soil samples were initially digested using concentrated nitric acid (HNO_3) before being analyzed for heavy metals (chromium, lead and iron). The digested samples were analyzed for heavy metals using Atomic Absorbance Spectrophotometer (AAS) (Onyeonwu, 2000).

2.6. Determination of Total Petroleum Hydrocarbon (TPH)

TPH was analyzed using organic solvent extraction procedures (Onyeonwu, 2000). Ten grams (10 g) of the soil were weighed and 5 g of anhydrous sodium sulfate ($NaSO_4$) were added and stirred with a stirring rod. Thereafter, 100 ml of HPLC n-Hexane were then added into the sample and stirred with a magnetic stirrer for thirty minutes. The extract was then cleaned up and fractionated using silica gel Solid Phase Extraction (SPE). The TPH was analyzed using Gas Chromatograph Agilent 6890 Series, with an Agilent FID detector under the following conditions. Column Temperature Program 60 °C to 280 °C 10°C/min to 280 °C at 10 °C/min for 8 mins, Injector Temperature 200°C, Detector Temperature 300 °C, Carrier gas Nitrogen gas, Pressure Program (Setpoint) 14.5 psi, injected volume 1 µl and Column Dimensions was Capillary 30.0 m x 320 µm x 0.00 µm. The total cycle of time run was forty-two minutes for each sample injected. External calibration was carried out using TPH's Standards. The retention times of the standards were used for the identification and quantization of the individual TPH. All solvents used were of high-purity analytical grade. The percentage of crude oil degraded after six months was determined using the equation:

% Crude oil degraded = x 100

Weight of crude oil degraded = Original weight of crude oil – Weight of residual crude oil.

2.7. Statistical Analysis

Results obtained were subjected to test using Two Way Analysis of Variance (ANOVA) without replication to test the level of significance between the groups of means for the different treatment samples. Microsoft excel package was used.

3. Results

3.1. Total Heterotrophic and Hydrocarbon Utilizing Fungal Counts

Figure 1 shows the total heterotrophic fungal counts, Control 1: 21.0±1.0 to 28.0±14.5 x10^4 cfu/g, Control 2: 24.5±0.5 to 39.0±6.0 x10^4 cfu/g, Treatments A_1, A_2 and A_3 counts range between 25.0±1.0 to 41.5±4.5 x10^4 cfu/g, 26.5±9.5 to 39.0±3.0 x10^4 cfu/g, 23.5±0.5 to 36.0±1.0 x10^4 cfu/g respectively. Treatments B_1, B_2, B_3 counts range between 24.0±2.0 to 32.5±3.5 x10^4 cfu/g, 23.5±0.5 to 24.5±6.5 x10^4 cfu/g, and 22.0±2.0 to 28.0±7.0 x10^4 cfu/g respectively and for treatments C_1, C_2 and C_3, they ranged between 22.5± 0.5 to 42.5± 5.5 x10^4 cfu/g, 27.5±5.0 to 37.5±8.5 x10^4 cfu/g, 27.0±3.0 to 38.5±6.5 x10^4 cfu/g respectively. Higher fungal counts were observed between July to September, 2016 and decreased slightly between October to December, 2016 for total heterotrophic fungal counts. Figure 2 shows the mean total hydrocarbon utilizing fungal counts, Control 1: 23.0±1.0 to 34.0±4.0 x10^4 cfu/g, Control 2: 28.5±0.5 to 39.5±2.5 x10^4 cfu/g, Treatments A_1, A_2 and A_3 counts range between 28.5±1.5 to 38.5±1.5 x10^4 cfu/g, 35.0±3.0 to 41.5±3.5 x10^4 cfu/g, 29.5±5.5 to 40.5±0.5 x10^4 cfu/g respectively. Treatments B_1, B_2, B_3 counts range between 24.0±2.0 to 38.0±0.0 x10^4 cfu/g, 30.5±0.5 to 38.5±0.5 x10^4 cfu/g, and 33.0±2.0 to 41.0±2.0 x10^4 cfu/g respectively and for treatments C_1, C_2 and C_3, they ranged between 38.0± 2.0 to 43.5± 4.5 x10^4 cfu/g, 36.0±1.0 to 47.5±1.0x10^4 cfu/g, 44.5±2.5 to 51.0±2.0 x10^4 cfu/g respectively. Also, for total hydrocarbon-utilizing fungal counts, higher fungal counts were observed between July to September, 2016 and decreased slightly between October to December, 2016.

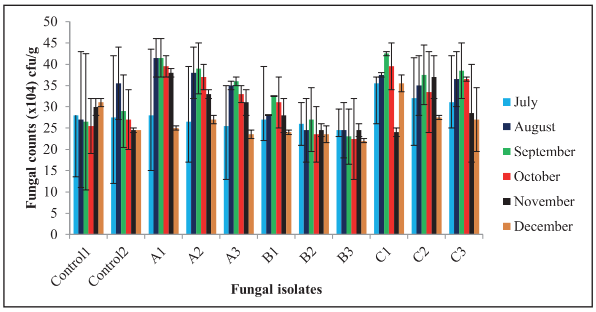

Figure 1. Total heterotrophic fungal counts (July- December 2016)
Keys: control 1: soil only, control 2: soil + 50ml diesel, A_1: soil + 100 g poultry litter + 50 ml diesel, A_2: soil + 100 g poultry litter + 100 ml diesel, A_3: soil + 100 g poultry litter + 150 ml diesel, B_1: soil + 100 g cow dung + 50 ml diesel, B_2: soil + 100 g cow dung + 100 ml diesel, B_3: soil + 100 g cow dung + 150 ml diesel, C_1: soil + 50 g cow dung + 50 g poultry litter + 50 ml diesel, C_2: soil + 50 g cow dung + 50 g poultry litter + 100 ml diesel, C_3: soil + 50 g cow dung + 50 g poultry litter + 150 ml diesel.

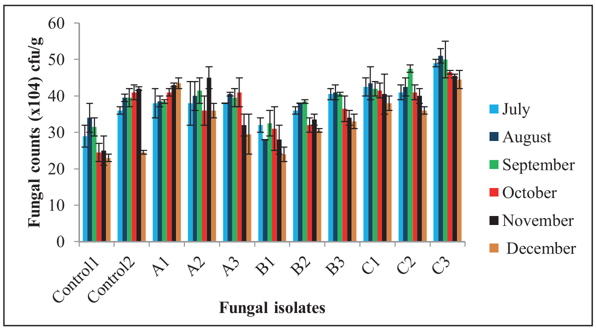

Figure 2. Total petroleum hydrocarbon utilizing fungal counts (July- December 2016)
Keys: control 1: soil only, control 2: soil + 50ml diesel, A1: soil + 100 g poultry litter + 50 ml diesel, A2: soil + 100 g poultry litter + 100 ml diesel, A3: soil + 100 g poultry litter + 150 ml diesel, B1: soil + 100 g cow dung + 50 ml diesel, B2: soil + 100 g cow dung + 100 ml diesel, B3: soil + 100 g cow dung + 150 ml diesel, C1: soil + 50 g cow dung + 50 g poultry litter + 50 ml diesel, C2: soil + 50 g cow dung + 50 g poultry litter + 100 ml diesel, C3: soil + 50 g cow dung + 50 g poultry litter + 150 ml diesel.

Seventeen heterotrophic and Five petroleum hydrocarbon utilizing fungal species were isolated. Among the fungal isolates, *Aspergillus* spp. (31.6 9%) had the highest percentage of frequency of occurrence and the least percentages were recorded for *Botryodiplodia* sp. (0.7 %) and *Candida* sp. (0.7 %).

Table 2. Percentage frequency of occurrence of the fungal isolates in the various treatments

Isolates	Control 1	Control 2	A (A_1,A_2,A_3)	B(B_1,B_2,B_3)	C(C_1,C_2,C_3)	Total
**Aspergillus* spp.	8	6	11	8	12	45(31.69 %)
**Penicillium* spp.	7	6	4	1	4	22 (15.49 %)
Helmintosporium sp.	1	1	3	2	2	9(6.34 %)
Rhizopus sp.	-	-	2	1	-	3(2.11 %)
**Mucor* sp.	1	1	3	2	3	10(7.04 %)
**Trichorderma* spp.	2	2	3	4	6	17(11.97 %)
Fusarium sp	-	-	1	-	3	4(2.82 %)
Candida albican	1	-	-	-	-	1(0.70 %)
**Cladosporium* sp	1	2	3	3	3	12(8.45 %)
Neurospora crassa	-	-	2	1	1	4(2.82 %)
Curvularia sp.	-	-	-	1	1	2(1.41 %)
Sclerotium sp	-	-	1	1	1	3(2.11 %)
Rhodoturula sp	-	-	1	-	1	2(1.41 %)
Saccharomyces sp.	1	1	-	1	-	3(2.11 %)
Geotrichium sp	-	1	1	1	-	3(2.11 %)
Botrydiplodia sp	-	-	-	-	1	1(0.70 %)
Botrytis sp	-	-	-	1	1	2(1.41 %)
Total	**22(15.38%)**	**20(13.99)**	**35(24.48%)**	**27(18.88%)**	**39(27.27%)**	**143(100 %)**

* *Total petroleum hydrocarbon degrading fungi species*

Keys: control 1: soil only, control 2: soil + 50ml diesel, A_1*: soil + 100 g poultry litter + 50 ml diesel,* A_2*: soil + 100 g poultry litter + 100 ml diesel,* A_3*: soil + 100 g poultry litter + 150 ml diesel,* B_1*: soil + 100 g cow dung + 50 ml diesel,* B_2*: soil + 100 g cow dung + 100 ml diesel,* B_3*: soil + 100 g cow dung + 150 ml diesel,* C_1*: soil + 50 g cow dung + 50 g poultry litter + 50 ml diesel,* C_2*: soil + 50 g cow dung + 50 g poultry litter + 100 ml diesel,* C_3*: soil + 50 g cow dung + 50 g poultry litter + 150 ml diesel.*

Results of heavy metals analyses conducted on chromium, lead and iron (fig. 3-8) revealed that Pb had its lowest value as 0.00 mg kg^{-1} in control 2 in the month of September, 2016 (fig. 5) and its highest value of 3.20 mg kg^{-1} in C_3 in the month of July, 2016 (fig. 3). Chromium (Cr) had its lowest value of 0.10 mg kg^{-1} in control 1 in the month of December, 2016 (fig.8) and its highest value of 2.80 mg kg^{-1} in B_2 in the month of July, 2016 (fig. 3). The lowest and highest values for Iron (Fe) were 71.0 and 182.0 mg kg^{-1} recorded for Control 1 and C_3 in the months of December and July, 2016 respectively. In all the three metals analyzed (lead (Pb), chromium (Cr) and iron (Fe)), there was a reduction in the concentration of heavy metals in both control and the amended soils throughout the months (July- December, 2016) of analysis. Also, there was an increase in the concentrations of heavy metals in the various treatments as the volume of diesel pollution increased. Table 3 shows the initial and the final TPH utilization with treated soil with $P < 0.05$, and also the percentages of degradation which were 31.6 %, 39.3 %, 94.8 %, 93.0 %, 89.8 %, 93.2 %, 92.2 %, 85.9 %, 98.5 %, 97.7 %, 96.2 % for control 1, control 2, A_1, A_2, A_3, B_1, B_2, B_3, C_1, C_2 and C_3 treatments respectively. Diesel-oil degradation was highest in C_1 (98.5 %) and lowest in control 1 (31.6 %).

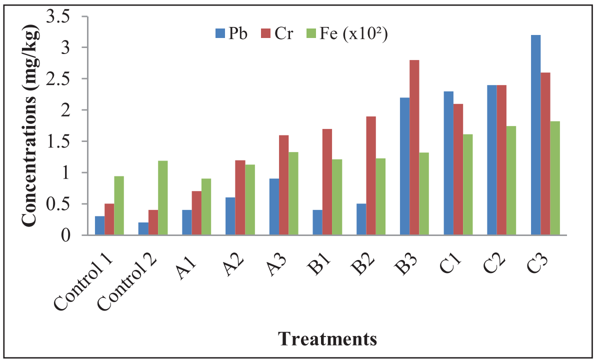

Figure 3. Heavy metal concentrations (July, 2016)

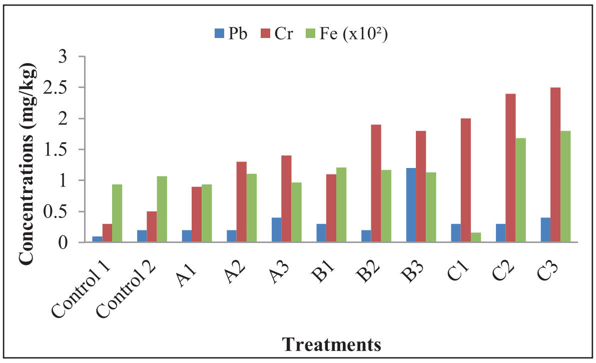

Figure 4. Heavy metal concentrations (August, 2016)

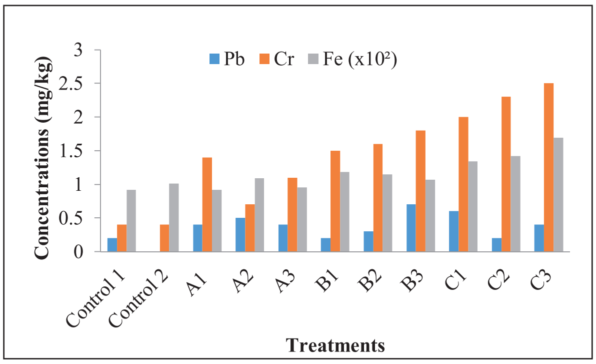

Figure 5. Heavy metal concentrations (September, 2016)

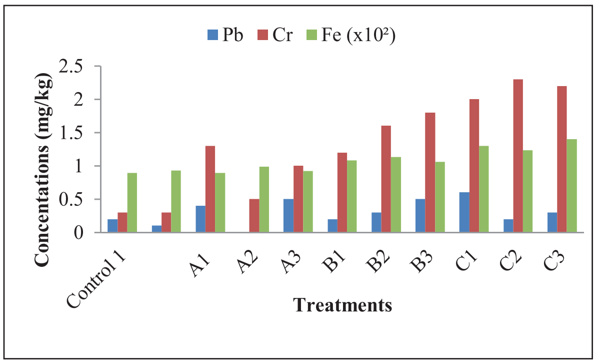

Figure 6. Heavy metal concentrations (October, 2016)

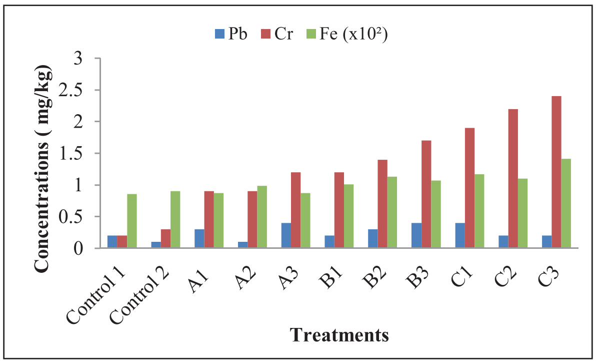

Figure 7. Heavy metal concentrations (November, 2016)

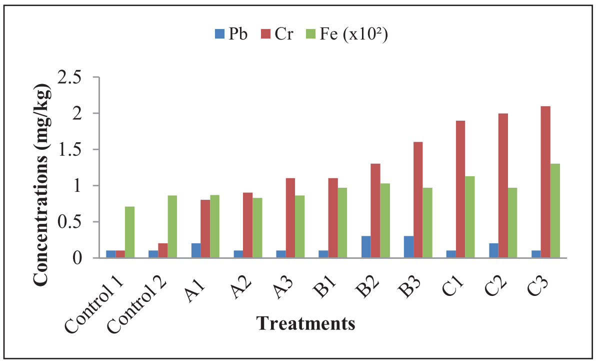

Figure 8. Heavy metal concentrations (December, 2016)

Keys: control 1: soil only, control 2: soil + 50ml diesel, A_1: soil + 100 g poultry litter + 50 ml diesel, A_2: soil + 100 g poultry litter + 100 ml diesel, A_3: soil + 100 g poultry litter + 150 ml diesel, B_1: soil + 100 g cow dung + 50 ml diesel, B_2: soil + 100 g cow dung + 100 ml diesel, B_3: soil + 100 g cow dung + 150 ml diesel, C_1: soil + 50 g cow dung + 50 g poultry litter + 50 ml diesel, C_2: soil + 50 g cow dung + 50 g poultry litter + 100 ml diesel, C_3: soil + 50 g cow dung + 50 g poultry litter + 150 ml diesel.

Table 5. Percentage (%) total petroleum hydrocarbon (TPH) utilization with treated soil (July 2016 – December 2016)

Treatments	Control 1	Control 2	A_1	A_2	A_3	B_1	B_2	B_3	C_1	C_2	C_3	P-value
Initial TPH (mg/kg)	3.8917	13292.4	11362.3	12140.5	13595.4	11656.7	12193.7	12576.5	11447.1	11558.2	11622.3	P<0.05
Final TPH (mg/kg)	2.6618	8056.41	592.25	848.766	1392.57	796.067	957.015	1774.65	169.69	270.164	446.83	P< 0.05
% Degradation	31.6	39.3	94.8	93.0	89.8	93.2	92.2	85.9	98.5	97.7	96.2	

Keys: control 1: soil only, control 2: soil + 50ml diesel, A_1: soil + 100 g poultry litter + 50 ml diesel, A_2: soil + 100 g poultry litter + 100 ml diesel, A_3: soil + 100 g poultry litter + 150 ml diesel, B_1: soil + 100 g cow dung + 50 ml diesel, B_2: soil + 100 g cow dung + 100 ml diesel, B_3: soil + 100 g cow dung + 150 ml diesel, C_1: soil + 50 g cow dung + 50 g poultry litter + 50 ml diesel, C_2: soil + 50 g cow dung + 50 g poultry litter + 100 ml diesel, C_3: soil + 50 g cow dung + 50 g poultry litter + 150 ml diesel..

4. Discussion

The total heterotrophic fungal counts were in this order; $C_1 > C_2 > C_3 > A_1 > A_2 > A_3 > B_1 > B_2 > B_3 >$ Control 1 > Control 2. The greater fungal counts observed in the combined amendment could be attributed to the synergism of the fungal population in the organic waste. It was observed that fungal counts were higher in poultry-amended soils than in soils amended with cow dung; this agrees with the report of Obasi *et al.* (2013), which showed a higher microbial count in soils amended with poultry litter than soils amended with cow dung, sawdust and horse manure. Control 1 had a more fungal population than Control 2, although both decreased with time. The reason for this difference could be attributed to the toxicity of the pollutant (diesel) that was applied. Within each treatment, with increasing levels of diesel pollution, there was slight reduction in fungal counts in this order: ($A_1 < A_2 < A_3$, $B_1 < B_2 < B_3$, $C_1 < C_2 < C_3$). For Total Petroleum Hydrocarbon Utilizing Fungal (TPHUB) counts, the reverse was the case as the fungi were able to utilize the hydrocarbon as sole source of carbon and energy, and thus increased in number as the volume of hydrocarbon increased. This finding corroborates with the results of Adebusoye et al. (2007), who reported an increase in TPHUC. Findings also revealed an observable decrease from July-December, 2016, this agrees with the work done by Stephen et al. (2015), who observed that the microbial count reduces with time. This could be attributed to the exhaustion of nutrients with time.

This observation is in consonance with the findings of Stephen et al, (2015), who observed higher microbial counts in oil-free soils than in oil-polluted soils. There was a significant difference ($P < 0.05$) in fungal counts isolated from individual amendment (poultry litters, cow dung) compared to that of the combined amended soil.

Further observations showed a significant difference ($P<0.05$) in the percentage of degradation between the amended and non-amended soils, and also between the initial and the final percentages of the total petroleum hydrocarbon values. The percentage of degradation in soils amended with poultry litter was greater than that in the soils amended with cow dung, but a greater percentage of degradation was observed in the soils amended with poultry litter and cow dung.

Findings from this experiment showed that there was a reduction in the concentration of lead (Pb) and chromium (Cr) with time (July- December, 2016). This observation supports the fact that fungi are able to accumulate these metals, and convert them to insoluble forms where some are reduced, volatilized or precipitated (Gadd, 1990). The lead (Pb) concentration as well as Cr and Fe in the amended soil were slightly higher than the control soil which confirms the results of Essien et al. (2015)*,* who reported that lead (Pb) content in soils amended with cow dung were higher than those in oil-free soils. Most striking was the fact that the concentrations of all the metals increased with increasing levels of diesel pollution indicating the presence of these heavy metals in the diesel oil applied. This is in agreement with earlier reports by Tanee and Kinako (2008) and Obasi et al. (2013) who reported a marked decrease in the total hydrocarbon content of amended soils polluted with crude oil relative to the control soils. Atuanya and Ibeh, (2004) and Chijioke-Osuji et al. (2014) reported that, the treatments amended with poultry litter showed enhanced utilization of petroleum product. Umar et al. (2012) also reported that bioremediated soils using cow dung and chicken droppings have a high removal rate of TPH compared to control soil. A higher loss of TPH was evident in the combined compost amendment followed by poultry litter-amended soil and then by cow dung-amended soil. It was observed that the percentage of degradation reduced slightly within each set of treatment with increasing the levels of pollution. The control soils percentage of degradation was slow when compared to the amended soils. This shows that organic waste is a good source of nutrients that stimulate the resident microorganisms to degrade the pollutants.

5. Conclusions

The results of the current study confirm that diesel oil impacts the soil ecology negatively, but with the application of organic waste as amendments (in the form of poultry litter and cow dung), the resident fungal population was stimulated bringing about an enhanced degradation. The combined compost amendment had a better percentage of degradation, and is recommended for bioremediation processes. However, this study has shown that poultry litter offered better degradation potentials than the cow dung, and is therefore preferred when recommending organic waste for bioremediative purposes.

References

Adams, G.O., Tawari-Fufeyin, P, Ehinomen, I. (2014). Bioremediation of spent oil contaminated soils using poultry litter. Research Journal in Engineering and Applied Sciences, 3(2):118-124.

Adebusoye, S.A., Ilori, M.O., Amund, O.O., Teniola, O.D. and Olatope, S.O. (2007). Microbial degradation of petroleum hydrocarbons in a polluted tropical stream. World Journal of Microbiology and Biotechnology, 23:1149-1159.

Akinde S., and Obire O. (2008). Aerobic heterotrophic bacteria and petroleum-utilizing bacteria from cow dung and poultry manure, World Journal of Microbiology and Biotechnology, 24(9):1999-2002.

Atuanya, E.I., and Ibeh, I.N. (2004). Bioremediation of crude oil contaminated loamy sand and clay6 soils. Nigerian Journal of Microbiology, 18(1-2):373-386.

Barnett, H.L., and Hunter, B.B. (1998). Illustrated Genera of Imperfecti Fungi. 4th Edition, APS Press, St. Paul. 218p.

Castro-Gutierrez, V.M, Rodriguez-Rodriguez. C.E., Vargas-Azofeifa, I. (2012). Hydrocarbon-degrading microflora in a tropical fuel contaminated aquifer: assessing the feasibility of PAH bioremediation. International Journal of Environmental Research, 6:345-352.

Chaillan, F., Le Fl`eche, A., Bury, E. (2004). Identification and biodegradation potential of tropical aerobic hydrocarbon degrading microorganisms. Journal of Microbiology Research, 155 (7): 587–595.

Chijioke-Osuji, C.C., Ibegbulam-Njoku, P.N., Belford, E.J.D. (2014). Biodegradation of Crude oil polluted soil by co-composting with agricultural wastes and inorganic fertilizer. Journal of Natural Science Research, 4(6):28-39.

Chikere, C.B., and Azubuike, C.C. (2014). Characterization of hydrocarbon utilizing fungi from hydrocarbon polluted sediments and water Nigerian Journal of Biotechnology, 27:49-54.

Das, N., and Chandran, P. (2011). Microbial degradation of petroleum hydrocarbon contaminants: An overview. International Journal of Biotechnology Research, 2001: 1-13.

Essien, E.B., Ifenacho, M.O., Nwanchukwu, G.A. (2015). The impact of cow dung augumentation for remediation of crude oil polluted soil by Eleusine indica Journal of Applied Science and Environmental Management, 19(1):103-107.

Gadd, G.M. (1990). Heavy metal accumulation by bacteria and other microorganisms. Cellular and Molecular Life Sciences, 48(8):834-840.

Gadd, G.M. (2000). Bioremedial potential of microbial mechanisms of metal mobilization and immobilization. Current Opinion in Biotechnology, 11:271-279.

George-Okafor, U., Tasie, F., Muotoe-Okafor, F. (2009). Hydrocarbon Degradation Potentials of Indigenous Fungal Isolates from Petroleum Contaminated Soils. Journal of Natural and Physical Sciences, 3(1): 1-6.

Hill, G.B., and Moxey J.G. (1980). Gasoline and Diesel Oil, pp.1-4. In: Gathee V.B(ed) Petroleum Product Handbook. 4th edition, McGraw Hill, New York.

Kabata-Pendias, A., and Pendias H. (2001). Trace Metals in Soils and Plants. 3rd edition. CRC Press, Boca Raton, Florida, USA. 413pp.

Khan, R., Isradi, S.H., Ahmad, H., Mohan, A. (2005). Heavy metal pollution Assessment in surface water bodies and its suitability for irrigation around the Neyevli Lignite mines and associated industrial complex, Tamil Nadu, India. Mine Water and the Environment, 24:151-161.

Kim, J., Diao, J., Shepherd, M.W., Jr., Singh, R., Heringa, S.D.,Gong, C., Jiang, X. (2012). Validating thermal inactivation of Salmonella spp. in fresh and aged chicken litter. Applied Environmental Microbiology, 78: 1302–1307.

Nwaogu, L.A., Onyeze, G.O.C., Nwabueze, R.N. (2008). Degradation of diesel oil in polluted soil using Bacillus subtilis. African Journal of Biotechnology, 7(12): 1939-1943.

Obasi, N.A., Eze, E., Anyanwu, D.I. Okorie, U.C. (2013).

Effects of organic manures on the physicochemical properties of crude oil polluted soils. African Journal of Biochemistry Research, 7(6):67-75.

Obire, O., and Putheti, R.R. (2008). Fungi in bioremediation of oil polluted sediments. Journal of. Applied Science and Environmental Management, 7:61-67.

Omotayo, A.E., Ojo, O.Y., Amund O.O. (2012). Crude oil degradation by microorganisms in soil compost. Research Journal of Microbiology, 7(4):209-218.

Onyeonwu, R.O. (2000). Manual for Waste/Wastewater; Soil Sediment, Plant and Fish Analysis. MacGll Environmental Research Laboratory Manual. Benin City. 81pp.

Osuji, L.C., and Onojake, C.M. (2004). Trace heavy metals associated with crude oil: A case study of Ebocha-8 oil spill polluted site in Niger Delta, Nigeria. Chemistry of Biodiversity, 1:1708–1715.

Oyedele, A.O., and Amoo, I.A. (2014). Remediation of crude oil polluted soil using cow dung manure in relations to the growth of maize (Zea Mays L.) Canadian Open Agricultural and Soil Science Journal, 1(1):1-16.

Singh, H. (2006). Mycoremediation: Fungal Bioremediation. Wiley-Interscience, New York, NY, USA. 614pp

Stephen, E., Onuche, H.A., Ijah, U.J.J. (2010). Physiochemical properties of wastes lubricating oil simulated soil in Lokoja, Koji state, Nigeria. International Journal of Applied Biological Research, 28(1):21-32.

Stephen, E., Okwute, L.O., Okai, A.I. (2015). Bioremediation of mechanic workshop polluted soil amended with poultry litter. Bioscience Research in Today's World, 1(1):77-83.

Sumner, M.E. (2000). Beneficial use of effluents, wastes, and biosolids. Journal of Commununity Soil Science and Plant Analysis, 31:1701–1715.

Tanee, F.B.G., and Kinako, P.D.S. (2008). Comparative Studies of Biostimulation and phytoremediation in the mitigation of crude oil toxicity in tropical soil. Journal of Applied. Science and Environmental Management, 12(2):143-147.

Umar, A. F., Tahir, F., Larkin, M., Oyawoye, O. M., Musa, B. L., Yerima, M. B., Agbo, E. B. (2012). In-Situ biostimulatory effect of selected organic wastes on bacterial atrazine biodegradation. Advances in Microbiology, 2:587-592.

Wilkinson, K.G.; Tee, E.; Tomkins, R.B.; Hepworth, G.; Premier, R. (2011). Effect of heating and aging of poultry litter on the persistence of enteric bacteria. Poultry Science, 90:10–18.

Wilkinson, S.R. (1979). Plant nutrient and economic value of animal manures. Journal of Animal Science, 48:121–133.

JJEES

Jordan Journal of Earth and Environmental Sciences

JJEES (2019) 10 (1): 28-34
ISSN 1995-6681

The Potential of the Application of Olive Cake and Stone Cutting Waste for Soil Amendment

Jalal Al-Tabbal[1] and Kamel Al-Zboon[2]

[1]Al-Balqa Applied University, Al-Huson University College, Department of Nutrition and Food Processing, Irbid, Jordan
[2]Al-Balqa Applied University, Al-Huson University College,Department of Environmental Engineering, Irbid, Jordan

Received 15 September, 2018; Accepted 2 February, 2019

Abstract

The recycling of waste is considered an attractive solution for the high amounts of waste generated worldwide. Some waste including olive waste and stone cutting waste present considerable environmental challenges for environmental planners and local communities. Due to their impacts on the environment and human health, this paper investigates the recycling of olive cake (OC) and stone cutting sludge (SCS) and their use for soil amendment. It evaluates their effect on soil pH, soil permeability, and maize growth. Thirteen different treatments containing clay soil (CS), OC, and SCS with different proportions to be used as maize seed growing media. The media were placed in pots and each treatment had three replicates with a randomized complete block design and was irrigated with fresh water. OC had high permeability, low pH, while SCS had low permeability and alkaline ph. The growing media which contained CS and SCS at 70:30 (w/w) ratio (T8) exhibited an increase in the number of leaves (8.7 %), plant height (5.5 %), stem diameter (34.3 %), shoot fresh weight (18.2 %), shoot dry weight (23.5 %), fresh root weight (4.29 %), dry root weight (38.10 %), leaf length (31.9 %), and leaf width (4.86%), while OC application resulted in significant reductions in all the above-mentioned parameters. In the treatments containing the three mixtures (CS, OC, and SCS), stone cutting sludge countered the negative effects of OC and enhanced the performance of the mixed soil, resulting in significant improvements of the growth indicators.

The obtained results highlighted the potential of using waste as a soil amendment technique instead of the disposal of waste. This could decrease the destructive impact of waste on the environment and reduce the costs of transportation and disposal.

Keywords: Olive Cake, Stone Cutting Waste, Soil Amendments, Maize, Recycling.

1. Introduction

A high increase in the global population has led to a corresponding high demand for food. An intensive use of land for continuous cropping has been adopted to meet the increasing demand for food. Intensive land use activities, in addition to soil erosion, nutrient leaching, and low rainfall have considerably reduced soil fertility (Moges and Holden, 2008). To compensate for soil exhaustion, fertilizers are often applied intensively, which has numerous negative impacts on the environment, such as contributing to acid rain and global warming, ground water contamination, air pollution, soil acidity, and eutrophication in surface water (Al-Tabbal and Al-Zboon, 2012). Soil amendment is an attractive route for improving soil fertility through the improvement of soil characteristics, in turn providing a suitable environment for root growth (McGeehan, 2012). The recycling of waste to be used in soil amendment can reduce the environmental loads of such waste and contribute to soil fertility and food production (Petersen et al., 2003). Several organic (compost, manure, sawdust, wood chips) (Lima et al., 2009; Breton et al., 2016.) and inorganic materials (gravel, tire waste) (Braun and Flückiger, 1998; William and Shenker, 2016) have been used to amend soils. Soil amendment may enhance soil physical properties (water retention, aeration, water infiltration, permeability, porosity, and texture), adjust soil acidity, and increase soil organic contents (Tester, 1990).

Chan et al. (2008) investigated the impact of biochar produced from poultry litter as soil amendment on the yield of radish and soil characteristics. They reported that yield increased by 42 % and 96 % with the biochar application rates of 10 and 50 t ha^{-1}, respectively. Soil Carbon (C), Nitrogen (N), pH, and Phosphorus (P) increased significantly following the amendment. The application of different organic wastes (municipal biosolids, food waste compost, composted hog manure solids, mined peat moss) in soil amendment resulted in considerable increases in soil water retention and a marginal increase in organic matter, while soil bulk density decreased significantly (Zebarth et al., 1999).

Olive Cake (OC) is a byproduct of olive fruit milling with an average production rate of 0.4 kg of cake per kg of olive fruit. More than 50,000 tons of OC is produced annually in Jordan (Al-Zboon, 2017). Today, this material is stored in open ditches for long periods and is left to dry, which results in an unpleasant odor, risks to groundwater and the attraction and spread of flies. After drying, OC is often used for energy production, particularly in rural areas. OC has a high organic matter content with volatile solid contents >82 % (Al-Zboon, 2017). Therefore, OC can be used for soil amendment, particularly in soils poor in organic matter such as the soils of arid and semi-arid regions. Compost OC is used as soil amendment with the application rates of 2 %,

---

* Corresponding author e-mail: jaltabbal@bau.edu.jo

4 %, and 8 %,; the soil organic matter content increased by 1.25 %–4.54 % depending on soil type. Moreover, it resulted in an increase in water penetration, water-holding capacity, and accumulated water intake (Al-Widyan et al., 2005).

In Jordan, stone cutting waste is considered a major environmental problem and is only associated with the construction sector. High quantities of slurry water containing solid particles are generated from stone cutting. This water is often collected and stored in open basins for long periods to condensate the solids (sludge), while the supernatant water is recycled inside the plant. The generated sludge is disposed-off in uncontrolled sites or in landfills which have numerous environmental effects on surface water and groundwater, in addition to harming flora, polluting soils, altering the natural drainage, and negatively affecting and disrupting the aesthetic appearance of environments (Al-Zboon et al., 2010). Stone cutting sludge (SCS) consists mainly of Calcium Oxide (CaO), Magnesium Oxide (MgO), Aluminum Oxide (Al_2O_3), and Iron (III) Oxide (Fe_2O_3), which means that it can be a great potential source of nutrients for the soil (Al-Zboon and Al-Zou'by, 2014). Carrao and Castelli (2008) reported that the application of stone sludge mixtures, at suitable proportions (40–50 %) relative to soil weight, may result in greater water retention. The addition of 20–40 % sludge to porous acidic soils could enrich them with potassium, magnesium, phosphorus, and numerous other micro-elements, which are beneficial to vegetable production. Tozsin et al. (2014) reported that the application of marble cutting waste as soil amendment increased the soil pH from 4.71 to 5.88, and increased the hazelnut yield by approximately 43 %. Furthermore, Pérez-Sirvent et al. (2011) observed that the addition of marble cutting sludge to soils contaminated with heavy metals modified the soil pH and enhanced the adsorption and precipitation of the metals, subsequently minimizing their mobility and toxicity. From an environmental and economic perspective, the recycling of waste is an efficient process for the reducing of the negative effects of waste on the environment, and for reducing the cost of waste management, and costs of crop production, while at the same time increasing the value addition from byproducts.

Both materials (OC and SCS) present serious environmental challenges in Jordan. The control of waste represents a heavy economic and environmental burden on their owners, municipalities, and local communities. Recycling is considered the optimal strategy for reducing waste quantities, the cost of waste management, in addition to adding values and creating job opportunities. To achieve the aforementioned goals, the present study was conducted and is aimed at investigating the impact of using OC and SCS waste as a soil amendment on maize (Zea mays) growth.

2. Materials and Methodology

2.1. Materials

In the present study, two types of waste are used for the soil amendment including OC and SCS. The control soils were collected from a field experimental station at Al-Huson University Collage, Al-Balqa Applied University. The soil samples were taken from the upper 25 cm zone, and were air-dried, and sieved through a 5-mm sieve. Naturally, dried OC was collected from a local three-phase centrifuge-system olive mill. A dried SCS sample was obtained from a local plant in Irbid area. An X-Ray fluorescence (XRF) spectrometer (SHIMADZU-XRF-1800) was used to determine the chemical composition of both materials (OC and SCS). Water content was determined by drying the samples in a drying oven at 105°C, and the water content was calculated as follows:

$$\%\ \text{Soil water conten} = \frac{(Weight\ of\ Wet\ soil - Weight\ of\ dry\ soil)}{Weight\ of\ dry\ soil} x100 \ldots\ldots.1$$

The organic contents of the sample were determined by measuring the sample volatility after being burnt in a muffle furnace at 550°C for four hours. A Euro EA 3000 elemental analyzer (Euro Vector, Milano, Italy) was used to determine the mass fraction of C, hydrogen (H_2), N, and oxygen (O_2) in the OC sample.

2.2. Experimental Layout

The experiments were carried out in a controlled environment in a greenhouse. Plastic pots with a diameter of 30 cm and a depth of 45 cm were used to plant Zea mays seeds after being filled with various media. The pots were divided into thirteen treatments according to different soil mixtures as shown in Table 1.

Table 1. Soil mixtures for different treatments(Dry-weight basis)

Treatment	Clay soil (%)	Olive cake (%)	Stone cutting sludge (%)
T1	100	0	0
T2	90	10	0
T3	80	20	0
T4	70	30	0
T5	60	40	0
T6	90	0	10
T7	80	0	20
T8	70	0	30
T9	60	0	40
T10	90	5	5
T11	80	10	10
T12	70	15	15
T13	60	20	20

The treatments were arranged based on a randomized complete block design with three replicates. The plants were irrigated daily using tap water to maintain the water-holding capacity at 80 %. Material permeability was determined using a constant-head test according to the standard test method for permeability in granular soils (ASTM D2434-68). pH was measured using an Ino Lab pH meter model (Model 7110, WTW Ino Labs, Germany).

2.3. Morphological Data Collection

The morphological parameters were recorded sixty days after sowing the maize *(Zea mays)* plants. The fresh weights of roots and shoots were measured and recorded in addition to the following measurements: the number of leaves per plant was determined by the visual counting of the leaves in a plant per pot (Tanko and Hassan, 2016); plant height (cm) was measured sixty days after being planted from the ground surface to the tip of the plant (Sabiel et al., 2014); stem diameter (mm) was measured using a vernier caliper at 10 cm above the ground level (Sabiel et al., 2014); leaf length was measured to the nearest millimeter from the leaf tip to the point at which the lamina is attached to the petiole (Sezer et al., 209); and the leaf width was measured from edge to edge at the widest part of the leaf lamina (Sezer et al., 2009). Roots and shoots were then dried at 105°C for dry-weight measurements.

2.4. Statistical Analysis

Analysis of variance, using randomized complete block design, was estimated for all the characters evaluated on SAS (SAS, 2008). The results are the means of three replicates. Data were statistically examined by the analysis of variance, and the least significant difference test was used to determine the significance of the differences between treatments.

3. Results

3.1. Properties of the Amendment Materials

OC and SCS had particle sizes ranging from 0.035 (N.400) to 16 mm (5/8) and from 0.50 to 177 µm (N.80) with an average size of 5.66 mm and 9.0 µm, respectively. The water contents of the OC and SCS samples were 11.6 % and 4.3 %, with soil content of 88.4 % and 95.7 % respectively. The average volatile organic matter content in the OC samples was 82.1 %.

The XRF analyses revealed that SCS contained a high level of CaO (54.7%), which indicates a carbonate origin of the stones (Table 2). OC had higher LOI lost on ignition (LOI) (80.4 %) than SCS (42.3 %) due to the high volatility of the organic matter in the OC samples, while SCS mostly had inorganic constituents. In addition, a higher Silicone dioxide (SiO_2) concentration was detected in the OC samples than in the SCS samples. High volatile organic compounds in OC (82.4 %) demonstrated its potential benefits as a source of organic matter, and that it could be used to improve the soil fertility and plant growth. The average element fractions in the OC samples were: C (50.1 %), O_2 (41.2 %), H_2 (6.3 %), N_2 (2.3and sulfur (0.1 %).

Table 2. Results of XRF analyses of the olive cake and stone cutting waste samples

Parameter	Olive cake	stone cutting sludge
	Average %	
CaO	7.65	54.7
SiO_2	6.45	0.85
Al_2O_3	1.37	0.20
K_2O	0.97	ND^+
Fe_2O_3	0.90	0.10
MgO	0.60	0.90
Na_2O	0.19	ND^+
SO_3	0.16	0.10
LOI*	80.4	42.3

**: loss on ignition, + not detected*

pH values of the different soils in the present study are presented in table (3). OC was acidic, while SCS and the control soil were alkaline. The acidity of OC could be useful in neutralizing alkaline soils, which is the case for most soils in Jordan.

Table 3. pH values for different soil samples

Treatment	pH
T1	7.7
T2	7.29
T3	6.91
T4	6.52
T5	6.5
T6	8.12
T7	8.15
T8	8.22
T9	8.26
T10	7.73
T11	7.37
T12	7.18
T13	7.19

The results of the permeability experiment revealed that the OC samples had high filtration rates, which were three and eight times higher than those in CS and SCS, respectively (Table 4). Based on the permeability results, CS, OC, and SCS, are be classified as slow, rapid, and very slow permeability (FAO, 2017). Al-Widyan et al. (2005) observed that the addition of OC to the soil increased its infiltration rate by 20, 24, and 27 % with the OC application loads of 2, 4, and 8 %, respectively after sixty-two minutes. Adequate permeability in the soil enhances soil aeration, biological activity, water infiltration, root development, and subsequently, plant growth. In contrast, low permeability causes disconnected soil channels, alters water filtration, and holds water within the top layer making it unavailable in the root zone, in addition to resulting in poor aeration. Very high permeability increases water filtration, decreases water availability for plants, and results in wastage of water resources. OC utilization considerably improved the permeability of CS and SCS, which makes it a potential material to increase soil infiltration, when applied at suitable rates.

Table 4. Permeability and filtration rate of various selected soil mixture.

Treatment	Permeability cm/min.
Olive cake	0.068
Stone cutting	0.0084
T1 (100:0:0)	0.0196
T5 (60:40:0)	0.0476
T9 (60:0: 40)	0.00939

3.2. Morphological characteristics of maize

The morphological parameters (number of leaves, plant height, stem diameter, fresh and dry weight of shoots, fresh and dry weight of roots, leaf length, leaf width, and shoot to root ratio) for all treatments are illustrated in Figures 1 to 10. Significant differences ($p \leq 0.05$) were observed among all treatments and for all morphological parameters, as illustrated in Table 5.

Table 5. Analyses of variance for growth parameters of maize (Zea Mays L.) plants grown in different mixtures of media (clay soil, olive cake and stone cutting).

Source of variation	Number of leaves	Plant height (cm)	Stem diameter (cm)	Fresh weight of shoot (g)	Dry weight of shoot (g)	Fresh weight of root (g)	Dry weight of root (g)	Leaf length (cm)	Leaf width (cm)	Shoot to root ratio
Treatment	17.87 **	863.8 **	0.25 **	609.6 **	38.92 **	20.93 **	0.89 **	1223 **	4.005 **	5.87 **
Error	0.58	13.47	0.03	25.57	1.7	0.84	0.04	4.34	0.035	0.78

*** indicates significant difference at 5 % probability.*

3.2.1. Number of Leaves

The number of leaves was significantly influenced by the growing medium, as illustrated in Figure 1. The effect was positive for some treatments and negative for others. The positive effects were found for plants grown in pots containing a combination of clay soil (CS) and SCS compared to control treatment (CS) with the highest number of leaves obtained from the treatment containing a combination of CS and SCS at the proportion of 70 % : 30 % (Figure 1). The number of leaves decreased progressively for all treatments that contained OC compared to the control treatment and the reduction was more obvious as he OC proportion increased to 40 % in the growing media. The reduction percentage for this treatment was 68.35 % compared with the control.

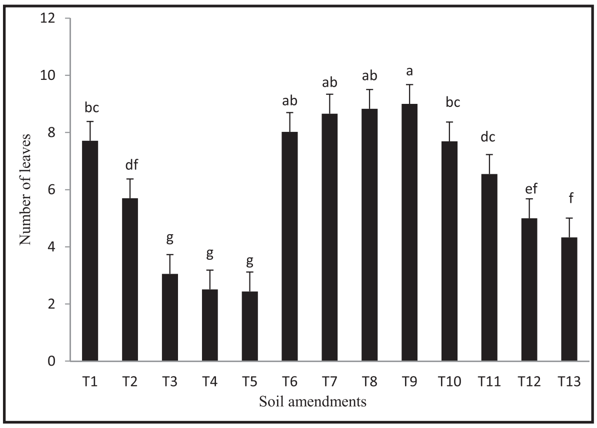

Figure 1. Effect of olive cake and stone cutting waste as soil amendment on the number of leaves of maize. Columns denoted by a different letter indicate significantly different values at P ≤ % 0.05 in one-way ANOVA.

3.2.2. Plant Height

OC exerted adverse effects on all other growth attributes. Plant height decreased progressively as OC concentration increased in the growth media (Figure 2). The most adverse effect was observed from the treatment that contained 40 % of OC resulting in a reduction in the plant height by 85.54 %. However, mixing SCS with OC mitigated the negative effects of OC. When comparing the treatment which contained OC only with the treatment that has the same percentage of OC mixed with SCS, it becomes clear that the treatment with SCS showed clear positive effects in improving the plant height.

3.2.3. Stem Diameter

The growing media exhibited significant differences for stem diameter. T8 that contained CS and SCS (70 % : 30) produced the highest stem diameter compared to other treatments (Figure 3). Plants grown in media that contained OC exhibited considerable decline in stem diameter. Maximum reduction was noted in T5, which resulted in 79 % reduction in stem diameter compared with T1 (control).

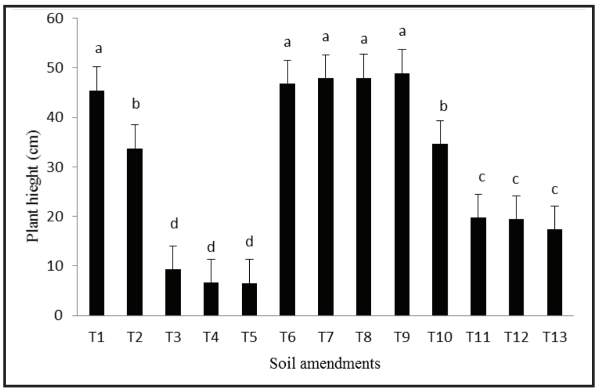

Figure 2. Effect of olive cake and stone cutting waste as soil amendment on plant height of maize. Columns denoted by a different letter indicate significantly different values at P ≤ % 0.05 in one-way ANOVA.

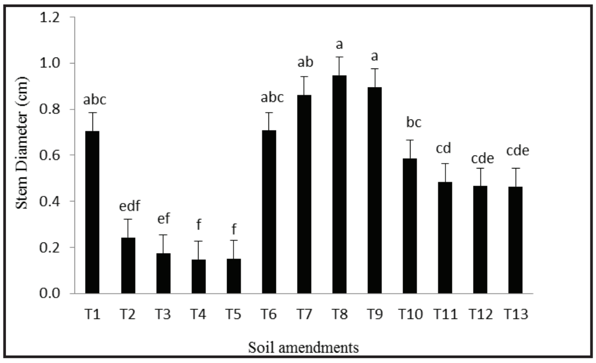

Figure 3. Effect of olive cake and stone cutting waste as soil amendment on stem diameter of maize. Columns denoted by a different letter indicate significantly different values at P ≤ % 0.05 in one-way ANOVA.

3.2.4. Leaf Length and Width

OC caused a significant reduction up to 79.4 % and 60.19 % in leaf length and leaf width, respectively, as compared to control plants (Figure 4 Figure 5). However, this inhibition was alleviated in the presence of SCS, the length and width of leaf in the combination treatment of CS, OC, and SCS decreased to 65 % and 56 %, respectively.

3.2.5. Fresh and Dry Weight of Shoot

The effects of OC and SCS on plant growth expressed as the fresh and dry weights of shoots are shown in Figures 6 and 7. The fresh and dry weights of shoots after treatments containing OC with CS alone remarkably decreased. The decrease was the highest in T5 while the fresh and dry weights of shoot after the treatment that contained SCS in addition to CS increased. The highest SCS–mediated OC stress alleviation was recorded in T13 (60 % CS: 20 % SCS: 20 % OC), in which the application of SCS improved the shoot fresh and dry weight by 557 % and 605 %, respectively compared with that in T3 (80 % CS: 20 % OC).

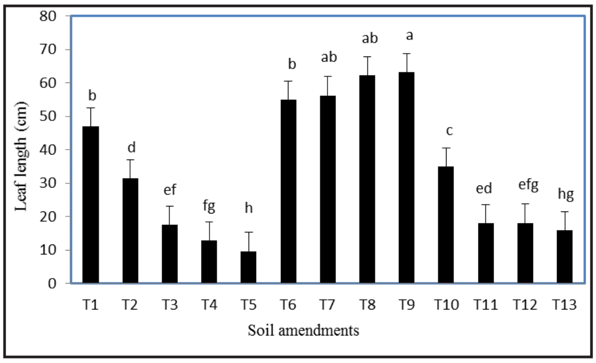

Figure 4. Effect of olive cake and stone cutting waste as soil amendment on leaf length of maize. Columns denoted by a different letter indicate significantly different values at P ≤ % 0.05 in one-way ANOVA.

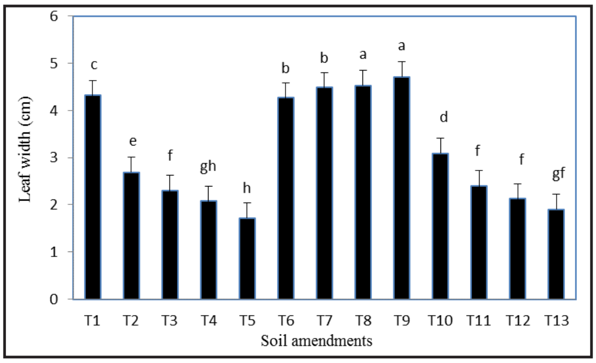

Figure 5. Effect of olive cake and stone cutting waste as soil amendment on leaf width of maize. Columns denoted by a different letter indicate significantly different values at P ≤ % 0.05 in one-way ANOVA.

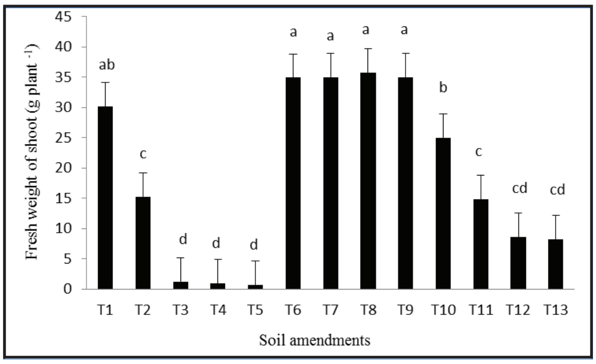

Figure 6. Effect of olive cake and stone cutting waste as soil amendment on shoot fresh weight of maize. Columns denoted by a different letter indicate significantly different values at P ≤ % 0.05 in one-way ANOVA.

3.2.6. Fresh and Dry Weight of Roots

The addition of OC to the growing media reduced the fresh and dry weights of roots, up to 70 % and 97 %, respectively, compared with the controls as shown in figures 8 and 9. Mixing SCS with both CS and OC mitigates the negative effects of OC in terms of the fresh and dry weights of roots. On the other hand, CS with SCS alone (CS and SCS, 70:30) increased the fresh and dry weights of roots by 8.42 % and 25 %, respectively compared to control.

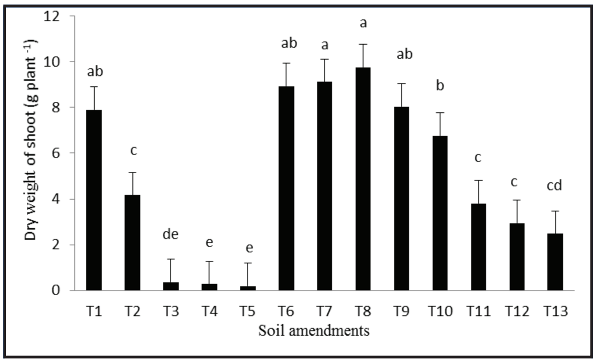

Figure 7. Effect of olive cake and stone cutting waste as soil amendment on dry weight of maize .Columns denoted by a different letter indicates significantly different values at P ≤ % 0.05 in one-way ANOVA.

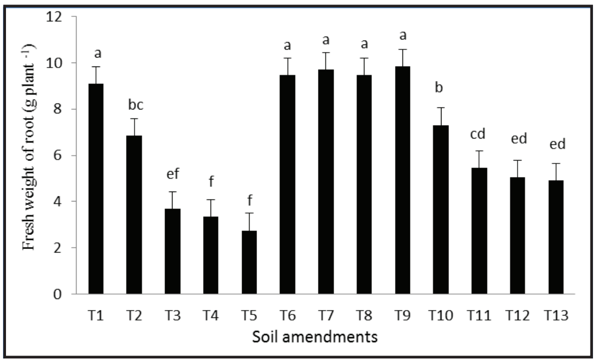

Figure 8. Effect of olive cake and stone cutting waste as soil amendment on root fresh weight of maize. Columns denoted by a different letter indicate significantly different values at P ≤ % 0.05 in one-way ANOVA.

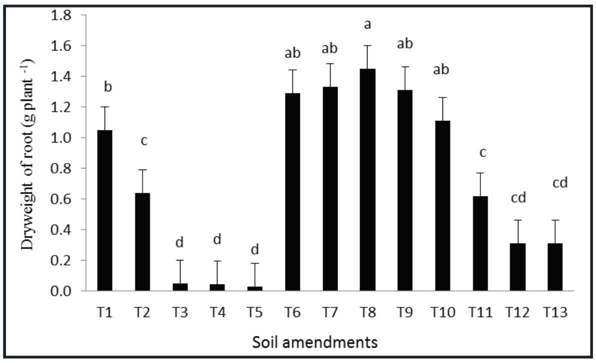

Figure 9. Effect of olive cake and stone cutting waste as soil amendment on root dry weight of maize. Columns denoted by a different letter indicate significantly different values at P ≤ % 0.05 in one-way ANOVA.

3.2.7. Shoot to Root Ratio

Shoot to root ratio decreased up to 92 % as a result of growing on CS containing OC alone (Figure 10). This reduction was decreased to 50 % when SCS mixed with previous media. The maximum alleviatory effect of SCS application on the growing media which contain OC was achieved when the concentration of SCS in the media increased to 20 %. However, an increase in shoot to root ratio was obtained in the growing media containing CS mixed with SCS only, reaching up to 15 % more than the control (CS).

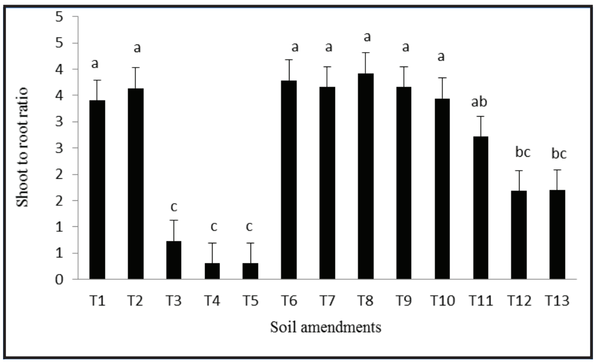

Figure 10. Effect of olive cake and stone cutting waste as soil amendment on shoot to root ratio of maize. Columns denoted by a different letter indicate significantly different values at P ≤ % 0.05in one-way ANOVA.

4. Discussion

The results of element analyses of the OC samples highlighted its importance as a bio-energy source in addition to its potential value as a source of organic matter. In the present study, OC significantly inhibited the growth of Zea mays. All application ratios of OC (10 %, 20 %, and 30 %) resulted significantly in lower growth parameters compared to the control soil, but greater reductions were achieved with higher percentages of OC in the mixtures. Olive mill waste has high phenolic, fatty acid, and ethanol compound contents, which have high lipophilicity and could alter the accessibility of nutrients within biological membranes which could explain the poor plant growth (El Hadrami et al., 2004; Tayeh et al., 2014; Pasten et al., 2017).

Moreover, the high infiltration rate of OC increases water loss, and could reduce the amount of water available to the plants (Abu-Rumman, 2016). Seferoglu (2011) reported that using olive fruit solid waste negatively influenced the germination of radish (Raphanus raphanistrum) and plant height in onions (Allium cepa) and radish (Raphanus raphanistrum), whereas it showed minor effects on onion germination and the plant height of faba beans (Vicia faba).

With regard to plant nutrient uptake, olive mill waste negatively influenced nutrient uptake rates in radish (Raphanus raphanistrum), while it positively influenced nutrient uptake rates in faba beans (Vicia faba) and onions (Allium cepa) at low application rates (20 t/ha). Higher application rates (40 t/ha) had adverse effects on all plants. Similarly, El Hadrami et al. (2004) reported that the addition of undiluted olive mill waste led considerably to the reduction of shoot and root weight and leaf extension, and significantly reduced yield in maize (Zea mays), chick peas (Cicer arietinum), tomatos (Solanum lycopersicum), and wheat (Triticum aestivum).

It has been reported that pH influences the solubility and availability of plant nutrients, and organic matter decomposition (McCauley et al., 2017). On the whole, soil pH near seven is the optimal pH for nutrient availability, crop tolerance, and soil microorganism activity (McCauley et al., 2017). Mixing OC with SCS resulted in a neutralized soil, which could decrease the negative effects of extreme pH on soil and plants.

Mixing CS and SCS at various proportions (T6-T9) and particularly at a ratio of 70:30 (T8) resulted in significant improvement of growth parameters compared to other treatments. Similarly, Tozsin et al. (2014) found that mixing marble waste with soil increased pH from 4.71 to 5.88, which resulted in the increase of hazelnut yield by 43 %. The increase in growth parameters for T9 (CS and SCS, 70:30), compared to the control soil, were 8.7 %, 5.5 %, 34.3 %, 18.2 % 23.5 %, 4.29 %, 38.10 %, 31.9 %, and 4.86 % for the number of leaves, plant height, stem diameter, fresh weight of shoot, dry weight of shoot, fresh weight of root, dry weight of root, leaf length, and leaf width, respectively. The increase in all morphological parameters in T6-T9 could be attributed to the presence of soluble nutrients in the treated soil (Ch'ng et al., 2014). The nutrients are essential for plant growth and development, and play key roles in various metabolic and physiological processes in plants, such as chlorophyll development, photosynthesis, starch synthesis, and phosphorylation (Dalcorso et al., 2014).

In the T10-T13 treatments, stone cutting waste countered and minimized the negative effects of OC, resulting in better growth of plants. Growing maize in pots containing a mixture of the three substances (CS, OC, and SCS) enhanced growth parameters compared with pots containing only a mixture of CS and OC. For example, in T13 (60:20:20) there were 4.3 leaves compared to 2.4 leaves in T5 (60:0:40), representing a 77.5 % increase. Plant height, stem diameter, fresh and dry weight of shoot, fresh and dry weight of root, leaf length, and width and shoot of root also increased. The improvement in plants' morphological parameters could be attributed to four reasons. T5 had a pH of 6.5, while stone cutting waste, which has good buffering capacity, increased pH in T13 to 7.19, which is more appropriate for plant growth. In addition to that, stone cutting waste decreased soil permeability, and subsequently increased the amount of water available to plants. Moreover, stone cutting waste added substantial amounts of nutrients to the soil as mentioned previously. Moreover, at higher pH rates (in the case of T13), the soil's capacity to adsorb phenol is low (Das et al., 2015), which could minimize the negative effects of phenol on plant growth.

5. Conclusions

OC and SCS have been assessed as potential materials for soil amendment for the production of Zea mays. Mixing OC and CS only at various proportions results in a decrease in key morphological parameters in Zea mays. Mixtures of OC and SCS, in addition to CS, at various proportions, facilitate suitable vegetative growth and plant productivity compared to OC alone or OC with CS. On the whole, stone cutting waste facilitates the recycling of OC for agricultural purposes.

The findings of the present study support the recycling of organic and industrial waste for soil amendment and food production.

Acknowledgments

The researchers express their appreciation and thanks to Al-Balqa Applied University for their assistance and support.

References

Abu-Rumman, G. (2016). Effect of Olive Mill Solid Waste on Soil Physical Properties. International Journal of Soil Science, 11(3): 94-101.

Al-Tabbal, J.A., and Al-Zboon, K.K. (2012). Suitability assessment of groundwater for irrigation and drinking purpose in the northern region of Jordan, Journal of Environmental Science and Technology, 5(5): 274-290.

Al-Widyan, M., Al-Abed, N., Al-Jalil, H. (2005). Effect of Composted Olive Cake on Soil Physical Properties, Communications in Soil Science and Plant Analysis, 36(9-10): 1199-1212.

Al-Zboon, K., and Al-Zou'by, J. (2014). Recycling of stone cutting slurry in concrete mixes, Journal of Material Cycles and Waste Management, 17(2): 324–335.

Al-Zboon, K., Tahat, M., Abu-Hamatteh, Z., Al-Harahsheh, M. (2010). Recycling of stone cutting sludge in formulations of bricks and terrazzo tiles, Waste management and Research, 28(6): 568-574.

Al-Zboon, K.K. (2017). Indoor air pollution due to household use of olive cake as a source of energy, International Journal of Environment and Waste Management, 19(3):248 - 267.

Braun, S., and Flückiger, W. (1998). Soil amendments for plantings of urban trees. Soil and Tillage Research, 49(3):201-209.

Breton, V., Crosaz, Y., Rey, F. (2016). Effects of wood chip amendments on the revegetation performance of plant species on eroded marly terrains in a Mediterranean mountainous climate (Southern Alps, Alpes), Solid Earth Discussion, 7(2): 1-21.

Carrao, G., and Castelli, G.S. (2008). Guidelines for the correct management and possible reuse of cutting process sludge, exploitation of sludge from stone working synthesis of the research, http://www.aigt.ch/download/rapporto_interreg-en.pdf.

Ch'ng, H.Y., Ahmed, O.H., Majid, N.M. (2014). Improving phosphorus availability in an acid soil using organic amendments produced from agroindustrial wastes, The Scientific World Journal,2014:1-6. doi.org/10.1155/2014/506356.

Chan, K.Y., Van Zwieten, L., Meszaros, I., Downie, A., Joseph, S. (2008). Using poultry litter biochars as soil amendments, Australian Journal of Soil Research, 46(5): 437-444.

Dalcorso, G., Manara, A., Piasentin, S., Furini, A. (2014). Nutrient metal elements in plants, Metallomics, 6(10):1770-88.

Das, P., Goswami, S., Banerjee, P., Datta, S. (2015). Phenol Adsorption onto Various Soil Composite Membranes: Insight into Process Kinetics, Modelling and Optimisation Using Response Surface Methodology, Hydrol Current Res, 6: 203. Doi: 10.4172/2157-7587.1000203.

El Hadrami, A., Belaqziz, M., El Hassni, M., Hanifi, S., Abbad, A., Capasso, R., Gianfreda,L., El Hadrami, I. (2004). Physico-chemical characterization and effects of olive oil mill wastewaters fertirrigation on the growth of some Mediterranean crops, J. Agron, 3 (4): 247–254.

FAO. (2017). Soil permeability, http://www.fao.org/fishery/static/FAO_Training/FAO_Training/General/x6706e/x6706e09.htm.

Lima, D.L.D., Santos, S.M., Scherer, H.W., Schneider, R.J., Duarte, A.C., Santos, E.B.H., Esteves, V.I. (2009). Effects of organic and inorganic amendments on soil organic matte properties. Geoderma 150(1-2): 38-45.

McGeehan, S., 2012. Impact of waste materials and organic amendments on soil properties and vegetative performance. Applied and Environmental Soil Science, 2012, doi: 10.1155/2012/907831.

McCauley, A., Jones, C., Olson-Rutz, K. (2017). Nutrient management module no.8, Soil pH and Organic Matter, Montana state university, http://landresources.montana.edu/nm/documents/NM8.pdf.

Moges, A., and Holden, N. M. (2008). Soil fertility in relation to slope position and agricultural land use: a case study of umbulo catchment in Southern Ethiopia, Environmental Management. 42(5): 753–763.

Pasten, A., Urib, E., Stucken, K., Rodrguez, A., Vega-Galvez, A. (2017). Influence of Drying on the Recoverable High-Value Products from Olive (cv. Arbequina) Waste Cake. Waste and Biomass Valorization, 2017, https://doi.org/10.1007/s12649-017-0187-4.

Pérez-Sirvent, C., García-Lorenzo, M.L., Martínez-Sánchez, M.J., Molina-Ruiz, J., Marimon, J. y., Navarro, M.C. (2011). Use of marble cutting sludges for remediating soils and sediments contaminated by heavy metals, Environmental Progress. & Sustainable Energy, 30(4): 533–539.

Petersen, S.O., Henriksen, K., Mortensen, G.K., Krogh, P.H., Brandt, K.K., Sorensen, J., Madsen, T., Petersen, J., Gron, C. (2003). Recycling of sewage sludge and household compost toarable land: fate and effects of organic contaminants, and impact on soil fertility, Soil Tillage Res, 72(2): 139–152.

Sabiel, S.A.I., Abdumula, A.A., Bashir, E.M.A., Khan, S., Yinying, S., Yank, Y., Baloch, S.U., Bashir, W. (2014). Genetic variation of plant height and stem diameter traits in maize (Zea mays L.) under drought stress at different growth stages. Journal of Natural Sciences Research, 4 (23): 116 – 122.

SAS Institute. (2008). SAS/STAT User's Guide Version 9.2. SAS Institute Cary NC.

Seferoglu, S. (2011). Effects of olive oil solid waste on growth and nutrient uptake of faba bean, onion, and radish plants. African Journal of Biotechnology, 10(34): 6510-6515.

Sezer, I., Oner, F., Mut, Z. (2009). Non-destructive leaf area measurement in maize (Zea mays L.). Journal of Environmental Biology, 30 (5): 785-790.

Tanko M.U., and Hassan, U.T. (2016). Leaf Area Determination for Maize (Zea mays L), Okra (Abelmoschus esculentus L) and Cowpea (Vigna unguiculata L) Crops Using Linear Measurements, Journal of Biology, Agriculture and Healthcare. 6(4): 103-111.

Tayeh, H. A., Najami, N., Dosoretz, C., Tafesh, A., Azaizeh, H. (2014). Potential of bioethanol production from olive mill solid wastes. Bioresource Technology, 152(2): 24–30.

Tester, C.F. (1990). Organic amendment effects on physical and chemical properties of a sandy soil, Soil Sci. Soc. Am. J., 54(3):827–831.

Tozsin, G., Oztas, T., Arol, A.I., Kalkan, E. and Duyare, O. (2014). The effects of marble wastes on soil properties and hazelnut yield, Journal of Cleaner Production, 81(15): 146-149.

William, M., and Shenker, M. (2016). Pulverized Tires as Soil Amendment for Plant Growth. International Journal of Scientific & Engineering Research, 7(6): 161-167.

Zebarth, B.J., Neilsen, G.H., Hogue, E., Neilsen, D. (1999). Influence of organic waste amendments on selected soil physical and chemical properties, Canadian Journal of Soil Science, 79(3): 501-504.

JJEES
Jordan Journal of Earth and Environmental Sciences

JJEES (2019) 10 (1): 35-45
ISSN 1995-6681

Adsorption Modeling of Cr^{+3} on Volcanic Tuff-Based Geopolymer

Kamel Al-Zboon[1], Bashar Al-Smadi[2],
Mohammad Al-Harahsheh[3], Sajedh Al-Khawaldh[2]

[1]Al-Balqa Applied University, Al-Huson University College,Department of Environmental Engineering, Irbid, Jordan
[2]University of Jordan, Department of Civil Engineering, Faculty of Engineering and Technology, Amman, Jordan
[3]Jordan University of Science and Technology, Faculty of Engineering, Department of Chemical Engineering, Irbid, Jordan

Received 30 June, 2018; Accepted 3 February, 2019

Abstract

In the current work, geopolymer was synthesized from volcanic tuff and was then used as a sorbent for Cr^{+3} from aqueous solutions. An adsorption batch experiment was conducted to study the factors affecting the adsorption process. The obtained results showed a high removal efficiency of geopolymer (96 %) against 70 % for the volcanic tuff with an uptake capacity of 21.24 and 14.76 mg/g for both materials, respectively. The removal efficiency increased with increasing the pH up to 5, geopolymer dosage, contact time up to thirty minutes, temperature, and the decrease of Cr^{+3} initial concentration in the studied ranges. The validity of the isotherm models to the experimental data can be ranked in the order of Langmuir > Temkin > Frundilch > Dubinin–Radushkevich. The kinetic study showed that the second order model provided the best fit with R^2 of 0.97 against 0.44 and 0.62 for the first order and the intra-particle model. The sorption process can be described as endothermic, monolayer, physical, and of a high ion affinity to the surface of the geopolymer. The results obtained buttressed the applicability of using a volcanic tuff-based geopolymer for the Cr^{+3} removal as a low-cost natural material at low concentrations.

Keywords: Geopolymer, Volcanic tuff, Adsorption, Chromium, isotherm, kinetic modeling.

1. Introduction

Chromium is generated as waste stream from numerous industries including textile, leather, pigments and paints, metal finishing, chromium alloy, the ceramic and glass industry, production of catalysts, photography, fungicides, refractories, drilling mud, and corrosion control (Krishna and Sree, 2013; Jacobs and Testa, 2004). Poor housekeeping of Cr^{+3} waste leads to the spill and leakage into the environment which causes serious contamination to the soil and groundwater (Jacobs and Testa, 2004). The ingestion of 1–5 g of chromate results in severe effects including gastrointestinal disorders, haemorrhagic diathesis, and convulsions (WHO, 2003). Mutagenicity effects include increase in incidences of genotoxic effects such as sister chromatid exchanges and chromosomal aberrations (Janus and Krajnc, 1990; WHO, 2003). Due to its impact on human health, the California Office of Environmental Health Hazard Assessment (OEHHA) recommended a public health goal (PHG) of 2.5 mg/l for total chromium and 0.02 mg/l for Cr(VI) (Jacobs and Testa, 2004). Stricter standards were set by EPA with a drinking water level of 0.10 mg/l for total chromium (EPA, 2010).

Traditional removal methods of chromium include, but are not limited to: ion exchange, revers osmoses, adsorption, membrane filtration, soil flushing, and electrokinetics (Hawley et al., 2004). Chromium transformation options include: chemical (oxidation-reduction, sorption, and precipitation), biological and physical transformation. Although precipitation is the most commonly used method, the main drawback of this method is the formation of high quantity of sludge (Pansini et al., 1991). Recent researches focus on the use of low cost treatment as an attractive option for Cr removal such as coconut fibers waste (Mohan et al., 2006), powdered marble waste (Ghazy et al., 2010), waste newspaper (Dehghani et al., 2015), eggshell (Ghazy et al., 2008), rice husk (Bansal et al., 2008), fruit skins (Rane et al., 2008), saw dust (Bansal et al., 2008), activated neem leaves, activated tamarind seeds, activated fly ash, sawdust, (Gupta and Babu, 2008) and geopolymers (Chen et al., 2016).

Geopolymer showed superior physical, chemical, and mechanical properties such as compressive strength, thermal insulation, low permeability, acid and fire resistance, quick setting, freeze-thaw cycle resistance, and low heavy metal mobility contained within the geopolymeric structure (Al-Zboon et al., 2011). Such properties nominated it successfully to be used for many engineering applications including: cements and high tensile and compression strength concrete, heat resistance concretes, resin, paint, binder, grout, and in ceramic industries. In the environmental field, geopolymer was used for the removal of Cu (Al-Harahsheh et al., 2015; Cheng et al., 2012), Pb (López et al., 2014; Al-Zboon et al., 2011), Zn (Al-Zboon et al., 2016), Cs^+ (López et al., 2014), Cd (Cheng et al., 2012), cobalt (Mužeka et al., 2016), ammonium (Luukkonen et al., 2016), dyes (Li et al., 2006), and for the stabilization of radioactive materials (Hanzlicek et al., 2006).

Several researchers have investigated the possibility of producing geopolymer from different materials such as metakaoline (López et al., 2014; Hamaideh et al., 2014), fly ash (Mužeka et al., 2016, Al-Zboon et al., 2011), volcanic tuff (Al-Zboon et al., 2016), Aluminium hydroxide waste

---

* Corresponding author e-mail: kazboon@yahoo.com

(Onutai et al., 2015), waste glass (Christiansen, 2013), rice husk (He et al., 2013), waste foundry sand (Devi and Kumar, 2015), waste serpentine cutting (Cheng, 2003), fly ash from the incinerators of municipal solid waste (Lancellotti et al., 2011), slag (Astutiningsih and Liu, 2005) and red mud (He et al., 2013).

The heavy metal removal efficiency of geopolymer is influenced by many parameters including: pH, geopolymer dosage, contact time, contaminant initial concentration, temperature and the composition of geopolymer.

Since its discovery in Jordan in 1968, volcanic tuff opened the door for research depending on its inventive characteristics. Because of the availability, good porosity, low cost, volcanic tuff is used in numerous engineering applications such as in light-weight concrete production (Al-Zboon and Al-Zou'by, 2016), water and wastewater treatment (El-Eswed et al., 2012; Al-Zou'by et al., 2013; Ibrahim, 2001), air-pollution control (Al-Harahsheh et al., 2014), soil improvement (Al-Tabbal et al., 2016), cooling and heating systems (Sqoor et al., 2015) and heavy metal removal (Ibrahim et al., 2016).

For this study, volcanic tuff samples were collected from Jabal Aritien site located north east of Jordan. The collected samples were used for the production of geopolymer and for Cr^{+3} removal. To the authors' best knowledge, this is the first time volcanic tuff- based geopolymer is used for Cr removal. The results of this study may open the door for future researches regarding the production of geopolymer from natural materials to be used for many environmental applications such as gases and heavy metal removal. The possible parameters affecting the adsorption process were considered. Adsorption isotherm, kinetic, and the thermodynamic behavior of the adsorbate were also investigated.

2. Materials and Methodology

2.1. Materials

A volcanic tuff sample of two cubic meter volume was obtained from Jabal Aritin (30 km east of Al Mafraq city), one of the identified volcanic tuff sites in Jordan. The collected sample was reduced to the required volume by cone and quartering dividing method. The obtained sample was sieved, and the sieve fraction of <45 µm was used for geopolymer production (Al-Zboon et al., 2011). Reagent grade chemicals (Nitric acid and sodium hydroxide) and chromium nitrate stock solution with a concentration of 1000 ppm was obtained from Merck- Germany.

2.2. Instrumentation

X-ray diffraction (XRD) analysis for feed material (tuff) and the product (geopolymer) samples were performed using (SHIMADZU-XRD-6000). The chemical composition was obtained using X-ray fluorescence (XRF) spectrometer (SHIMADZU-XRF-1800). Chromium concentration in the aqueous solution was measured using Inductively Coupled Plasma Optical Emission Spectrometer (ICP-OES) (SHIMADZU-ICPS-7510). The pH measurements were performed using pH meter model inoLab® pH 7110 from WTW. A water bath shaker equipped with a digital thermostat was used to regulate the temperature to perform the sorption tests at different temperatures.

2.3. Synthesis of Geopolymer

The geopolymer samples were produced according to the procedure followed by (Al-Zboon, et al., 2011), as demonstrated in Figure 1. A certain mass of volcanic tuff with the size of <45 µm was mixed with NaOH (14 M) with the ratio of 1:1.25, where NaOH is considered the best activator (Abdul Rahim et al., 2014). The vibration process will de-foam the geopolymer matrix. To enhance the dissolution of material in the NaOH solution, ultrasonication was used (Álvarez et al., 2008).

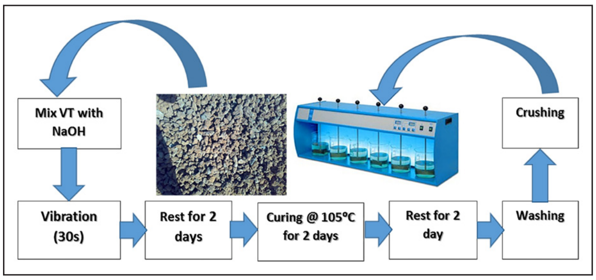

Figure 1. Procedure for the synthesis of geopolymer

High-temperature curing (105 ºC) will accelerate the formation of geopolymer and increase its strength. It was reported that the temperature range of 60-100 ºC yielded the highest strength under compression (Al Bakri et al., 2012); however, the higher temperature did not affect the compressive strength (Rangan, 2008). After geopolymerization, the geopolymer was washed with water to remove the excess of NaOH. The process of washing continued until reaching constant pH of the washing water, which was achieved after three washing times. The produced geopolymer was ground to 100 % < 200µm to be used for further adsorption, isotherm, and kinetic studies.

2.4. Adsorption Tests

A Jar test (model B-KER) with six jars made by Philipps & Bird was used to perform the adsorption tests. Specific geopolymer dosage (0.25 g) was added to the batch containing different concentrations of chromium (10-160 ppm), at different pH (1 - 6), and variable contact times (5 – 180 min). The temperature effect on adsorption behavior was studied at 25, 35, and 45 °C. After mixing; a liquid sample was separated from the solution through decantation followed by filtration.

2.5. Adsorption Performance

Three indicators were used to evaluate the performance of adsorption; these are: uptake capacity (q), efficiency (E), and Partition Coefficient (k). These indicators were calculated according to equations 1-3 below (Al-Zboon et al., 2016).

$$E = \frac{C_0 - C_e}{C_0} \times 100\% \tag{1}$$

$$q = \frac{(C_0 - C_e) \times V}{m} \tag{2}$$

$$K_d = \frac{(C_0 - C_e) \times V}{C_e \times m} \ (\text{ml/g}) \tag{3}$$

Where C_o is Cr^{+3} initial concentration of (ppm), C_e is the equilibrium Cr^{+3} concentration (ppm), q is Cr^{+3} uptake (mg

Cr/g of geopolymer), V is the solution volume (liters) and m is the mass of the geopolymer (dosage) (g).

2.6. Modeling of Adsorption Isotherms

Four models were tested to describe the adsorption of Cr^{+3} on the geopolymer mass. These are Langmuir's, Freundlich's, Dubinin–Radushkevich, and Temkin model. These models explained the adsorption process based on the models' assumption. Langmuir assumed a homogenous and monolayer adsorption process, whereas, Freundlich's model assumes a heterogeneous and multilayer adsorption (Foo and Hameed, 2010). Dubinin–Radushkevich's model is used to express the adsorption mechanism with a Gaussian energy distribution onto a heterogeneous surface (Dada et al., 2012). Temkin's model is based on the fact that the heat of adsorption of all molecules in the layer would decrease linearly as a function of temperature (Dada et al., 2012). The fitness of the applied models was tested by comparing the experimental data with the model predicted results.

2.7. Error Analysis

Mean Square Error (MSE) and Chi-square test (χ^2) were used as error evaluation parameters to evaluate the degree of models' fitness to the experimental data. The following equations were used for this purpose (Sampranpiboon et al., 2014):

$$MSE = \frac{1}{n}\sum(q_{exp} - q_{cal})^2 \quad (4)$$

$$\chi^2 = \frac{\sum(q_{exp.} - q_{cal.})^2}{q_{cal}} \quad (5)$$

where q_{exp} and q_{cal} are the experimental and calculated uptake capacities in mg/g.

2.8. Adsorption Kinetics

The kinetics of chromium adsorption on the synthesized geopolymer was modeled using pseudo-first-order (Equation 6) Lagergren's pseudo second order (Equation 7) and the intraparticle diffusion (Equation 8) models (Amenaghawon et al., 2013.):

$$Ln(q_e - q_t) = Lnq_e - k_1 t \quad (6)$$

$$\frac{t}{q_t} = \frac{1}{k_2(q_e)^2} + \frac{t}{q_e} \quad (7)$$

$$q_t = k_3(t)^{0.5} + I \quad (8)$$

where q_e and q_t stand for adsorption capacities at equilibrium and at contact time t (mg/g), k_1, K_2, K_3 are the rate constants for pseudo-first-order, Lagergren's pseudo second order and the intraparticle diffusion models , respectively (1/min) retrieved by plotting a graph of $\ln(q_e - q_t)$ versus t, t/q versus t, and q_t versus $t^{0.5}$, respectively.

2.8. Thermodynamic Calculations

To be able to calculate the thermodynamic parameters of chromium adsorption on the geopolymer, the adsorption tests were carried out at three temperatures (25, 35, and 45 ºC) and at three pH values (3, 4, and 5). The enthalpy (ΔH^o, kJ/mol), and entropy (ΔS^o, kJ/mol.K) were calculated using the following equation (Misra et al., 2003):

$$\ln K_d = (\Delta S^o/R) - (\Delta H^o/RT) \quad (9)$$

where T is the temperature (Kelvin), R is gas constant. A plot of ln K_d versus 1/T yields a slope of $\Delta H^o/R$ and an intercept of $\Delta S^o/R$,

The delta Gibbs free energy (ΔG^o, kJ/mol) was obtained according to Equation 10 below:

$$\Delta G^o = \Delta H^o - T\Delta S^o \quad (10)$$

3. Results and Discussion

3.1. Characteristics of the Natural and Synthesized Materials

The chemical and mineralogical composition of the raw volcanic tuff and the geopolymer were reported previously (Al-Zboon et al, 2016). The volcanic tuff is zeolite rich containing mainly phillipsite and chabazite minerals as main zeolite phases. These phases disappeared after geopolymerization, whereas, sodalite appeared as a new phase in the geopolymer structure. The main elements present in the volcanic tuff were Ca, Si, Mg, Al, and Fe; after geopolymerization, the sodium content increased by factor of 7 as where it incorporated in the geopolymer structure (Al-Zboon et al., 2016).

3.2. Performance of Volcanic Tuff and Geopolymer

In order to determine the benefit of using geopolymer instead of the volcanic tuff used for Cr removal, both materials were used for Cr adsorption with an initial concentration of 100 ppm, adsorbent dosage = 0.25 g, pH=5 at a temperature of 25 °C. It was found that the percentage uptake for volcanic tuff was 70.38 % against 93.65 % for geopolymer which indicated an improvement of 33 % in removal efficiency under the specified experimental conditions. Similarly, the uptake capacity increased from 14.76 to 19.3 mg Cr /g of volcanic tuff and geopolymer, respectively. Al-Zboon et al. (2016) found that the geopolymrization succeeded in producing additional pores in comparison with the raw tuff, which explains the higher adsorption capability of geopolymer. Balan et al. (2009), used Sphagnum moss peat for Cr^{+3} removal, and they obtained an uptake capacity of 18.6 mg Cr^{+3} /g of peat. Tangjuank, et al. (2009) prepared activated carbon from cashew nut shells and obtained 13.93 mg/g of Cr^{+3} uptake capacity. A lower uptake capacity was obtained by using two sources of coal (Lakhra and Thar coalfields) with the maximum Cr^{+3} uptake ranging from 2.61- 2.55 mg/g (Anwar, et al., 2009). Dam silt provided a very low adsorption capacity of 0.97 mg/g Cr^{+3} (Ouadjenia-Marouf et al., 2013). A synthesized Amberlite (IR 120 Resin) showed higher adsorption capacity toward Cr^{+3} which provided 142.86 mg Cr^{+3} /g of the resin (Meshram et al., 2012). Also, polystyrene and styrene/acrylonitrile copolymer provided a high uptake capacity up to 37.8 and 37.2 mg/g, respectively (Kanwal et al., 2012). Al Dwairi (2017) achieved a higher removal efficiency for Cr^{+6} using natural zeolitic tuff (56.3mg/g), and the smaller the particles' size, the higher the removal efficiency.

This comparison indicates that the produced geopolymer provides a high removal efficiency in comparison with a natural material which buttressed the benefit of using it for heavy metal removal.

3.3. Effect of pH:

The impact of pH on the adsorption behavior of Cr on the geopolymer was studied in the pH range of 1-7. Figure 2 below shows that the removal efficiency and the uptake capacity increased sharply as pH increased up to 5; afterwards, it decreased slightly in the studied range. The max removal efficiency was 96 % with a max uptake of 19.2 mg/g. As pH increases, the surface of the geopolymer becomes negatively charged which enhances the positive ions of Cr to contact the geopolymer surface decreasing the repulsion forces in the system and subsequently enhancing the adsorption process (Meroufel et al., 2013). The decrease in the Cr^{+3} adsorption at the low pH can be attributed to the competition between H^+ ions and Cr^{+3} ions for the adsorption sites (Nikagolla et al., 2013).

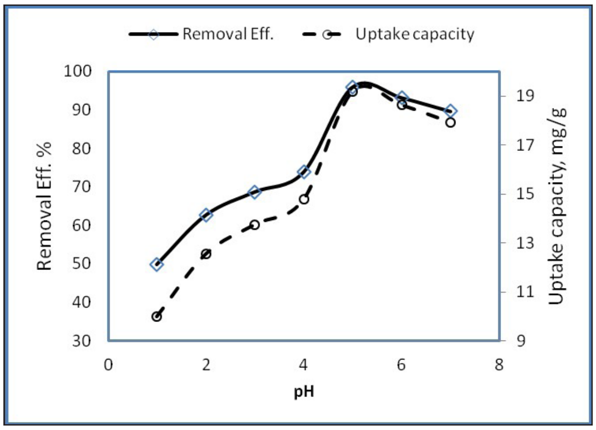

Figure 2. Impact of pH on Cr^{+3} adsorption (C_0=100 ppm, dosage=0.25g, T=25ºC, time=120 min.)

At a higher pH (>5) chromium hydroxide starts to precipitate, making true adsorption studies impossible (Kanwal et al., 2012). It was reported that the mechanism of removal appears to be ion exchange of Cr $(OH)^{2+}$ at pH≤ 6.0 and adsorption on zeolite surface of fine $Cr(OH)_3$ precipitate at pH> 6.0 (Al-Haj-Ali and Marashdeh, 2014). Bellú et al. (2008) found that the adsorption of Cr^{+3} on Grain–less Stalk of Corn increased with the increasing of pH, and there is no adsorption of Cr^{+3} at pH < 3. Balan et al. (2009) found that at a pH < 2.0, the Cr^{+3} adsorption was insignificant but increased rapidly with the increase of pH value reaching a maximum adsorption in the range of 4.0–5.5.

Tofan et al. (2015) found that the maximum removal of Cr^{+3} by alizarin pretreated hemp occurred at pH 5.8. Meshram et al. (2012) found that the extraction of Cr^{+3} from Amberlite Resin was found to be invariant in the pH range from 1.0 to 4.5; however, it decreases with a further increase in pH. Kanwal et al. (2012) reported that pH substantially affects the adsorption of Cr^{+3} on Synthetic Polymers, Copolymers and the maximum adsorption takes place at pH = 7. Tangjuank et al. (2009) used a lower pH (3.5) as the optimum for Cr^{+3} uptake on activated carbon prepared from cashew nut shells.

The best pH for the adsorption process depends on many interactive parameters such as the type, physiochemical properties, structure, and the mineral compositions of the adsorbent.

3.4. Effect of Geopolymer Dosage:

The effect of geopolymer dosage on the removal efficiency was investigated in the range of 0.03 – 1.00 g, at pH (5), temperature (25 °C), Cr concentration (100 ppm) and contact time (120 min.). Figure 3 shows that the removal efficiency increased from 67.33 to 98.93 % when the geopolymer dosage increased from 0.03 to 1.00 g. As the geopolymer dosage increased, the available pores and surface area for bending increased which also increased the opportunity for Cr ions to connect with the geopolymer surface. Many researchers reported that the removal efficiency increased with the increase of geopolymer dosage (Tangjuank et al., 2009; Balan et al., 2009; Al-Zboon et al., 2011; Al-Harahsheh et al., 2015; Odeh et al., 2015; Al-Zboon et al., 2016,).

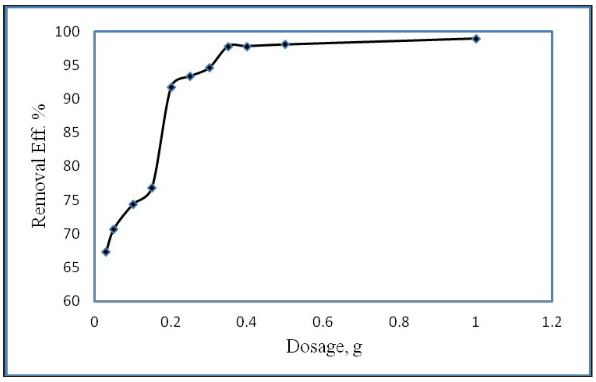

Figure 3. Impact of geopolymer dosage on Cr^{+3} adsorption (C_0= 100 ppm, pH=5, T=25 ºC, time =120 min.)

Krishna and Sree (2013) reported that the removal percentage of chromium increased from 58.25 % to 90.07 % with the increase of the adsorbent dosage (Custard Apple Peel Powder) from 0.10 to 0.60 g.

3.5. Effect of Initial Concentration

The effect of Cr^{+3} initial concentration on its removal efficiency was studied with the initial concentration ranging between 10- 160 ppm, pH=5, dosage of 0.25 g and a temperature of 25 °C. It was found that the removal efficiency decreased from 99.2 % at C_o of 10 ppm to 67.4 % at C_o of 160 ppm, while the uptake capacity increased from 1.98 to 21.58 mg/g for the same concentrations respectively as shown in Figure 4.

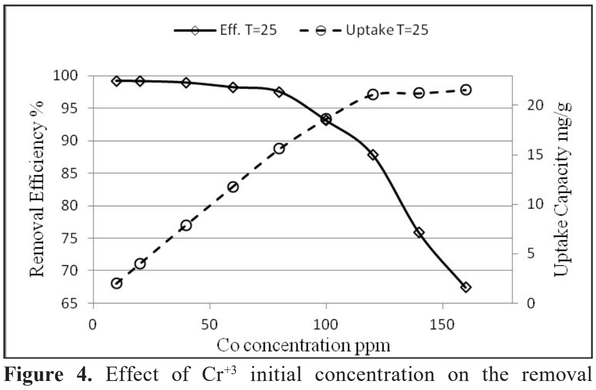

Figure 4. Effect of Cr^{+3} initial concentration on the removal efficiency (uptake capacity) by the geopolymer (pH = 5, dosage = 0.25g, T= 25 °C, time = 120 min.).

At a low concentration of Cr^{+3}, the available pores are enough to host most of the ions, whereas, at a higher concentration, some of the metal ions will not find the required pores due to the high competition on the available bending sites.

Similar results were obtained by Kanwal et al. (2012), who found that all the tested adsorbents (polystyrene, polyacrylonitrile, polymmethylmethacrylate, and polyacrylicacid) showed a reduction in chromium removal in the concentration range of 200 - 400 ppm due to the fact that the active sites are limited and occupied with Cr^{+3} as the concentration of Cr^{+3} is increased. Yousef et al. (2015) also reported that with the gradual increase of Cr^{+3} concentration, there is a decrease in its removal by cation-exchange resin.

The increase of the Cr^{+3} concentration from 10 mg/l to 104 mg/l at pH 4 decreased the removal percentage of Cr^{+3} by Sphagnum moss peat from about 86.5 to 28.5 % (Balan, et al., 2009). Tofan et al. (2015) found that the increase in the Cr^{+3} concentration from 13 to 26 mg/l increased the breakthrough adsorption capacity of Hemp fibers from 4.2 to 6.2 mg/g and decreased the percentage of removal from 73.6 to 62.6 %. Different results were found by Tangjuank et al. (2009) who mentioned that increasing the initial Cr^{+3} concentration caused an increase in Cr^{+3} adsorbed on activated carbons due to the sufficiency of pores.

3.6. Effect of Contact Time

Figure 5 shows the removal efficiency and uptake capacity with time. It was observed that about 96 % of Cr^{+3} was adsorbed within thirty minutes, whereas, a slight improvement (0.4 %) was noticed until 180 minutes. Similarly, the uptake capacity increased with the increase of time and reached 19.18 mg/g after thirty minutes and 19.2 mg/g after 180 minutes. A longer contact time will enhance the opportunity of metal ions to bind with the adsorbent which increases the removal efficiency; whereas, when most of the metal ions bind to the geopolymer surface, any additional contact time becomes not useful. Based on this result, it can be concluded that a time of thirty minutes is feasible for the Cr^{+3} removal on geopolymer-based volcanic tuff.

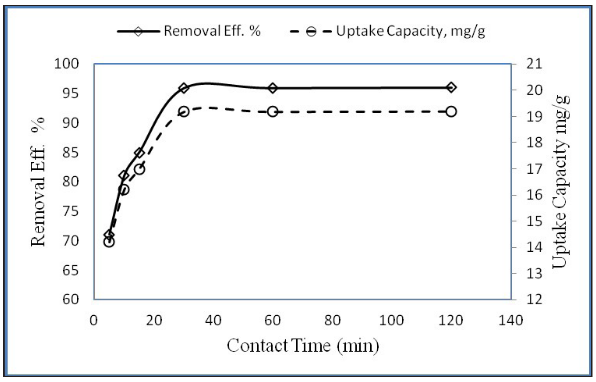

Figure 5. Impact of contact time on Cr^{+3} adsorption (pH = 5, dosage = 0.25g, T = 25 °C, C_0= 100 ppm)

Meshram et al. (2012) found that the major amount of Cr^{+3} was removed after five minutes and 99 % Cr^{+3} was removed in fifteen minutes from a 500 ppm Cr^{+3} solution. Nikagolla et al. (2013) observed that the adsorption increased rapidly and 95 % of Cr^{+3} was absorbed on natural red earth within the first ten minutes, and reached 95 % after ninety minutes.

Danielsson and Söderberg (2013) reported that the time for optimal chromium adsorption with Bauxite was determined to be forty minutes. The equilibrium contact time of sixty minutes for the adsorption of Cr^{+3} on activated carbon prepared from cashew nut shells was determined by Tangjuank et al. (2009). However, Bellú et al. (2008) found that the removal of chromium on Grain–less Stalk of Corn increased with time up to 120 minutes. and thereafter became almost constant.

3.7. Effect of Temperature

The removal efficiency increased from 89.3 to 98.6 % when the temperature increased from 25 to 45 °C at constant pH=5, dosage =0.20 g, C_0=100 ppm (Figure 6). The uptake capacity also increased from 21.24 to 24.53 mg/g for the same temperature range. The higher removal efficiency at higher temperatures is attributed to the improved diffusion through the pores of adsorbate which is known to be temperature-dependent. No significant impact of temperature on the removal efficiency at a lower concentration (<100 ppm) was observed; however, the impact of temperature was more significant at a higher concentration (Figure 7). Al-Zboon et al. (2016) found the same result confirming that at high temperature a better removal efficiency of Zn was obtained using a volcanic tuff-based Geopolymer.

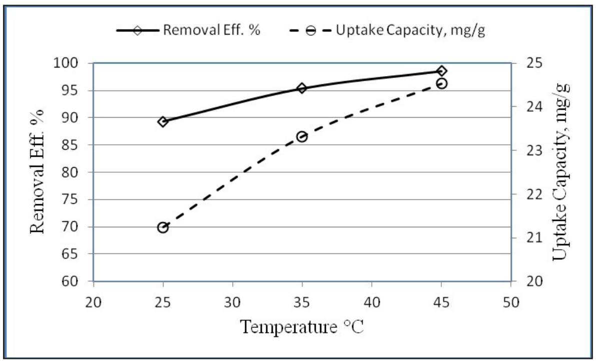

Figure 6. Impact of temperature on Cr^{+3} adsorption (pH=5, dosage = 0.25g, C_0= 100 ppm, time = 120 min.)

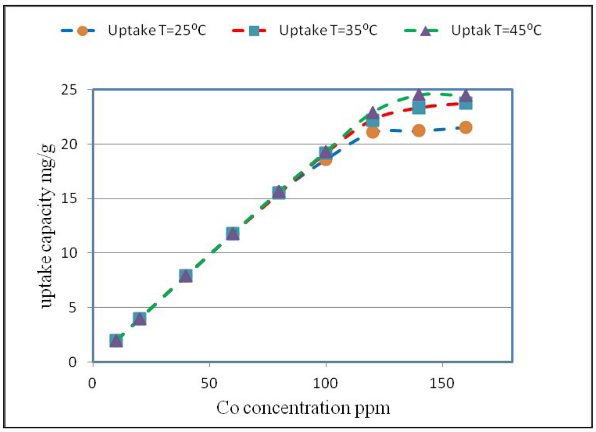

Figure 7. Impact of temperature and initial concentration on Cr^{+3} adsorption (pH=5, dosage=0.25g, T= (25, 35 and 45 ºC) t= 120 min).

3.8. Adsorption Isotherm

3.8.1. Langmuir Model

The most common form of Langmuir model is given by the following linearized form (Al-Harahsheh et al., 2015):

$$\frac{1}{q_e}=\frac{1}{q_m K_L}\frac{1}{C_e}+\frac{1}{q_m} \qquad \text{...} (11)$$

where K_L is the Langmuir equilibrium constant related to the heat of adsorption and q_m is the maximum monolayer adsorption capacity.

The validity of Langmuir model was determined by plotting the experimental data, C_e versus C_e/q for the three pH values (3, 4, and 5). The equilibrium uptake capacity (q_m), the reaction rate (k_a), and the correlation coefficient (R^2) were determined from the graph (see Table 1). It was found that q_m increased as pH and temperature increased in the studied range suggesting an endothermic adsorption behavior. The experimental data at pH = 5 and different temperatures were plotted with the calculated ones, and correlation coefficients close to 1 were obtained at temperatures of 25, 35, and 45 °C, respectively (Figure 8). The fitness of Langmuir model suggests a monolayer homogenous adsorption process (Al-Zboon et al., 2016). At 25 °C and pH 5, the equilibrium uptake capacity calculated by Langmuir model was 21.88 mg/g. The higher K_a values (>0.68) at pH 5 indicate a high affinity of Cr^{+3} on the geopolymer surface at this pH (Sampranpiboon et al., 2014) against a lower affinity at pH 3 and 4 where low K_a values were found.

Table 1. Calculated parameters of Langmuir isotherm model at different temperatures and pH values

Model	pH=3			pH=4			pH=5		
	R^2	q_m	Ka	R^2	q_m	Ka	R^2	q_m	Ka
T= 25	0.996	10.53	0.045	0.996	16.92	0.072	0.999	21.88	1.18
T= 35	0.997	13.19	0.054	0.998	20.24	0.089	0.999	24.24	1.03
T= 45	0.997	15.84	0.072	0.998	25.12	0.095	0.999	25.06	1.30

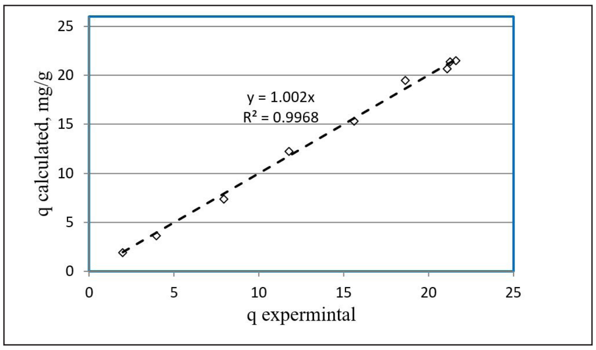

Figure 8. Correlation of calculated and experimental uptake capacity (pH=5, T=25 °C) for Langmuir model

Balan et al. (2009) found that the isotherms data of Cr^{+3} ions adsorption on sphagnum moss peat were better described by the Langmuir model, while Meshram et al. (2012) found the adsorption of Cr^{+3} on Amberlite (IR 120 resin) following Freundlich isotherm and Langmuir models, with a maximum adsorption capacity of 142.86 mg Cr^{+3} /g resin. Nikagolla et al. (2013) reported that the experimental results of Cr^{+3} adsorption on natural red earth fit well with the Langmuir isotherm only at pH = 2, while adsorption shows a nonconformity from the Langmuir isotherm at pH >2.

The values of the dimensionless separation factor (R_L) was determined from Langmuir model at pH 5 and a temperature of 25 °C according to the following equation (Al-Zboon et al., 2011):

$$R_L = \frac{1}{1 + K_a C_0} \quad (12)$$

where K_a is the Langmuir coefficient, C_o is the equilibrium concentration. The values of R_L were 0.021, 0.024, and 0.019 at temperatures of 25, 35 and 45 °C, respectively. The values of R_L was close to zero suggesting that the adsorption is a highly advantageous and irreversible (Dada et al., 2012) and the adsorbate will not dissolve back into the solution.

3.8.2. Freundlich Model

The logarithmic form of Freundlich isotherm is expressed by the following equation (Al-Harahsheh et al., 2015):

$$\ln q_e = \ln K_F + \frac{1}{n} \ln C_e \quad (13)$$

where q_e is the quantity of the solute adsorbed per unit weight of adsorbent at equilibrium, C_e is the equilibrium concentration of the adsorbing compound, and K_F ($mg^{1-1/n} \cdot g^{-1} \cdot l^{1/n}$) represents the adsorption capacity when metal ion equilibrium concentration equals 1, and n represents the degree of the dependence of adsorption on equilibrium concentration

The Log q_e was plotted against Log C_e at three pH values (4, 5, 6) and temperatures (25, 35, 45 °C) to determine the Freundlich model parameters yielding an intercept ($\log K_F$)), and a slop (1/n). The values of K_f ranged from 1.05 at pH=3 and T=25 °C to 9.66 at pH=5 and T=45 °C, with a significant increase as the pH and temperature increased which suggests more adsorption at higher temperatures (Donat et al., 2005). The impact of pH on K_f values was higher than the impact of temperature, where K_f values increased more than 5 times with the pH increase from 3 to 5. Its value increased only by 22-58 % as the temperature increased from 25 to 45 °C. The n values ranged from 1.66 at pH=3 and T=35 °C to 2.96 at pH=5 and T=25 °C; a insignificant increasing trend with temperature. It was reported that if value 1/n <1, it indicates a normal adsorption (Dada et al., 2012). All n values >1 and <10 indicating a favorable adsorption process (Donat et al., 2005). The correlation coefficient (R^2) values ranged from 0.84 to 0.96 with a better correlation at a lower pH (Table 2). Freundlich model has less fitness with the adsorption data than the Langmuir models, which suggests that the homogenous adsorption is better at describing the process compared with heterogeneous adsorption. A higher fitness of Freundlich model at lower pH values (3, 4) may indicate that the adsorption process at this pH range has affinity to the heterogeneity and becomes homogenous at a higher pH (5). This behavior is attributed to the different adsorption sites of geopolymer with different adsorption energies at this range of pH (Nikagolla et al., 2013).

Table 2. Calculated parameters of Freundlich isotherm model at different temperatures and pH values

Temperature	pH= 3			pH =4			pH =5		
	R^2	K_f	n	R^2	K_f	n	R^2	K_f	n
25	0.96	1.05	1.99	0.96	1.85	1.99	0.84	8.13	2.966
35	0.96	1.29	1.66	0.95	2.23	1.86	0.87	8.76	1.86
45	0.95	1.66	1.94	0.95	2.61	1.7	0.86	9.66	2.61

3.8.3. Dubinin–Radushkevich Isotherm Model

The Dubinin–Radushkevich isotherm model is applied to express the adsorption process which happened onto both the homogeneous and heterogeneous surfaces (Chen, 2015). The general term of this model is shown in Equation 14 below:

$$q_e = q_m * \exp\left(-K * \varepsilon^2\right) \qquad (14)$$

Which can be linearized as:

$$\mathrm{Ln}(q_e) = \ln(q_m) - K\,\varepsilon^2 \qquad (15)$$

Where K is the Dubinin–Radushkevich isotherm constant. The value of ε can be determined from Equation 16 below (Dada et al., 2012):

$$\varepsilon = RT\ \ln(1+1/C_e) \qquad (16)$$

To calculate the model coefficient (K) and the equilibrium uptake (q_m), $\ln q_e$ was plotted with e^2 (Equation 15) resulting in a slope (K) and the intercept ($\ln(q_m)$).

The results of Dubinin–Radushkevich isotherm model showed high fitting at pH 5 (R^2 = 0.94-0.95) and less fitting at a lower pH (R^2 = 0.77 -0.84). This result indicated that the adsorption process is homogenous, so the Dubinin–Radushkevich isotherm model provided poorer fitting compared to the Langmuir model, but was better than Freundlich model. The obtained q_m values are less than the experimental ones (C_o=160 ppm) with ratios of -18 %, - 22 %, -17 % at the temperatures of 25, 35, and 45 ºC, respectively (see Table 3).

Table 3. Calculated parameters of Dubinin–Radushkevich isotherm model at different temperatures and pH values

Temperature	pH= 3		pH =4		pH =5	
	R^2	q_m	R^2	q_m	R^2	q_m
25	0.80	6.83	0.77	10.48	0.94	17.67
35	0.88	8.76	0.79	12.34	0.95	19.02
45	0.84	10.41	0.78	17.76	0.95	19.70

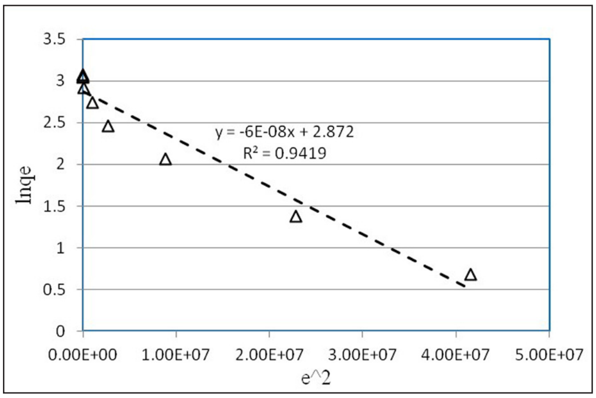

Figure 9. Validity of D-R model

3.8.4. Temkin Isotherm Model

This model takes in consideration the possible interaction between the geopolymer with chromium, where the heat of adsorption decreases linearly rather than logarithmically (Dada et al., 2012).

The linear form of Temkin isotherm model can be written as (Dada, 2012):

$$q_e = B\ \ln A_T + B\ \ln C_e \qquad (17)$$

where B= RT/b_t, A_T is Temkin isotherm equilibrium binding constant (l/g); b_t: Temkin isotherm constant; B: Constant related to the heat of adsorption (J/mol);

The obtained data indicated a high correlation (>0.96) at all temperatures and pH values with better fitting at lower pH values (Table 4).

Table 4. Calculated parameters of Temkin isotherm model at different temperatures and pH values

Temperature	**pH= 3**			**pH =4**			**pH =5**		
	R^2	B	A_T	R^2	B	A_T	R^2	B	A_T
25	0.99	2.17	0.54	0.98	3.28	1.01	0.96	3.24	29.68
35	0.99	2.69	0.66	0.98	4.02	1.17	0.97	3.75	24.01
45	0.98	3.22	0.88	0.98	4.99	1.27	0.96	3.98	26.57

3.8.5. Calculation of Errors

The experimental q values were compared with the predicted model ones. MSE and χ^2 were calculated for each model as presented in table 5.

Based on the obtained results, the model's validity can be ranked according to MSE and χ^2 values as: Langmuir > Temkin > Frundilch > Dubinin–Radushkevich. It is worth mentioning that at pH=5, Dubinin–Radushkevich has better fitness than the Frundlich model.

Table 5. Calculated MSE and χ^2 for the isotherm models

	pH=3			**pH=4**			**pH=5**		
	R^2	**MSE**	**χ^2**	**R^2**	**MSE**	**χ^2**	**R^2**	**MSE**	**χ^2**
Langmuir	0.99	0.041	0.062	0.99	0.18	0.23	0.99	0.17	0.13
Frindluch	0.96	0.46	0.58	0.96	1.61	1.29	0.84	19.02	10.0
Dubinin–Radushkevich	0.8	1.97	3.02	0.77	7.65	7.30	0.94	6.61	3.94
Temkin	0.99	0.065	0.160	0.98	0.33	1.061	0.96	2.08	1.52

3.9. Kinetics of the Adsorption Process

The three time-dependent models mentioned above were used to determine the fitness of these models to the experimental data. The results suggest that the second order model provided the highest R^2 (0.97) against 0.44 and 0.62 for the first order and the intraparticle models, respectively (Figure 10). Although the 2nd order model has high fitness, it provided a lower estimate at a longer contact time; this could be attributed to the insignificant change in q_t after thirty minutes. contact time. Balan et al. (2009) indicated that the adsorption of Cr^{+3} on the Sphagnum moss peat followed the pseudo-second order kinetic model, with $R^2 > 0.99$, whereas, Meshram et al., (2012) found that the adsorption of Cr^{+3} by Amberlite IR 120 Resin has a good fitting ($R^2 \geq 0.97$) to the Lagergren first order model. Similar results were obtained by Al-Zboon et al. (2016); the second order obtained better fitness to the experimental data than the first order and intraparticle models.

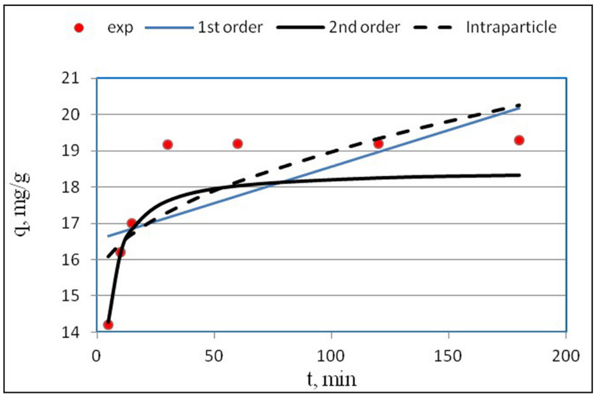

Figure 10. Validity of the kinetic models

3.10. Thermodynamic Study:

Table 6 shows that the distribution coefficient (K_d) values increased as pH and temperature increased. The higher value at higher temperatures and higher pH values indicate that a higher amount of metal is absorbed by the geopolymer (Al-Zboon et al., 2016).

The plot of $\ln K_d$ against 1/T yields a straight line with a slope of ΔH°, and an intersection of (ΔS^0). Gibbs free energy (ΔG^0) was determined by Equation 9 (see Table 6). The values of ΔH^0 and ΔS^0 ranged from 4.7 to 14.16 kJ/mol and 0.001 to 0.027 kJ/(mol.K) respectively. The positive sign of ΔH^0 and ΔS^0 and their decrease with the increase of pH buttress the favorability of the adsorption at higher pH. The positive value of ΔH^0 suggests that ΔS^0 of the system increases after the adsorption process.

The magnitude of ΔH^0 provides an idea about the nature of adsorption, where the heat of physical adsorption ranges from 2.1–20.9 kJ/ mol, whereas, the heat of chemisorption generally ranges from 80 to 200 kJ/mol (Saha and Chowdhury, 2011). Therefore, it is concluded that the physio adsorption is the predominant process during Cr adsorption on geopolymer.

Table 6. Thermodynamic parameters calculated for Cr^{+3} adsorption on geopolymer

T, Kelvin	pH =3				pH=4				pH=5			
	R^2	ΔH^0	ΔS^0	ΔG^0	R^2	ΔH^0	ΔS^0	ΔG^0	R^2	ΔH^0	ΔS^0	ΔG^0
	-	kJ/ mol	kJ/ mol.K	kJ/ mol	-	kJ/ mol	kJ/ mol.K	kJ/ mol	-	kJ/ mol	kJ/ mol.K	kJ/ mol
298	0.98	14.16	0.027	6.01	0.98	8.58	0.012	5.73	0.97	4.70	0.001	5.46
308				5.02				4.90				4.78
318				4.40				4.39				4.38

The adsorption process has low affinity for the heterogeneous system as suggested by the low values of entropy (ΔS^0) (Al-Zboon et al., 2016). A positive value of ΔS^0 mirrors the affinity of the adsorbent towards the adsorbate and increased randomness at the solid-solution interface with some structural changes in the adsorbate and the adsorbent (Saha and Chowdhury, 2011).

ΔG^0 values decreased from 6.01 at T= 298 K, pH =3 to 4.38 at T = 318 K, pH=5 suggesting an endothermic process and more favorable at higher temperature (Saha and Chowdhury, 2011). The impact of pH on ΔG^0 values decreased with the increase of temperature, where the difference becomes close to zero at temperature of 318 K indicating that temperature has a higher impact than pH (Figure 11).

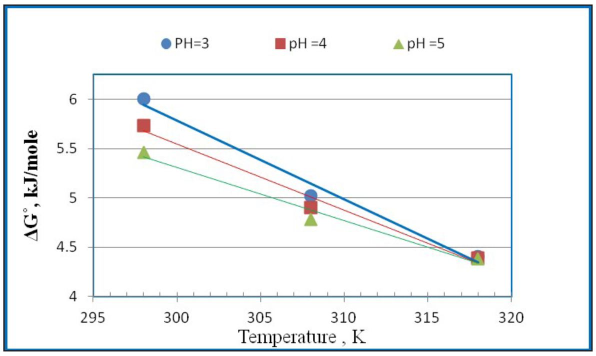

Figure 11. Relationship between temperature and ΔG^0 values at different temperatures and different pH values

3.11. Activation Energy and Sticking Probability

The activation energy is the energy required for the ion to overcome or interact with the adsorbent surface (Saha and Chowdhury, 2011). The removal efficiency, the activation energy (E_a) and the sticking probability (S*) are indicators of the adsorption effectiveness where the direct relationship between them is shown in Equation 16 below (Ayawei et al., 2015):

$$\ln(1-\theta) = \ln S^* + E_a/RT\ldots \qquad (18)$$

The plot of ln(1-θ) against 1/RT resulted in the slope of E_a, and intercept of S*. The positive value of E_a (28.54 kJ/mol at pH=5) suggesting that Cr adsorption by the geopolymer surface is a simple physical process, because the value of activation energy was in the range of 21 to 42 kJ/mol (Sismanoglu et al., 2004).

The calculated S* value was very low (<<<1) indicating a strong binding of the ions to the geopolymer surface (Saroj et al., 2013).

4. Conclusions

The current study focused on the adsorption of chromium (III) on volcanic tuff-based geopolymer from aqueous solutions. The impact of pH, contact time, dosage, and the adsorbent initial concentration on the performance of the adsorption process was investigated. An Isotherm study was conducted by applying four common models, while adsorption kinetic was investigated using three models. The results showed that the most applicable and feasible conditions for the adsorption of Cr^{+3} on the synthesized geopolymer were: pH=5, contact time= thirty minutes. geopolymer dosage =0.25 g. Natural volcanic tuff-based geopolymer is capable of achieving a removal efficiency of 93.65 % with an uptake capacity of 19.3 mg Cr/g of geopolymer. The adsorption process followed the Langmuir isotherm model with less fitness to the Freundlich model. The second order kinetic model provided good fitness to the kinetic data. The thermodynamic study revealed that the adsorption process is endothermic and encouraged at a higher temperature. It is irreversible and physical with the ions being highly stuck to the geopolymer surface. The present study concludes that volcanic tuff-based geopolymer can be used as a low-cost adsorbent for the removal of metal ions from aqueous solutions.

References

Abdul Rahim, R.H., Rahmiati, T., Azizli, K.A., Man, Z., Nuruddin, M.F., Ismail, L. (2014). Comparison of Using NaOH and KOH Activated Fly Ash-Based Geopolymer on the Mechanical Properties. Materials Science Forum, 803: 179-184.

Al Bakri, A.M.M., Kamarudin, H., Bnhussain, M., Khairul, Nizar I., Rafiza, A.R., Zarina Y. (2012). The processing, characterization, and properties of fly ash based geopolymer concrete. Reviews on advanced materials science, 30(2012): 90-97.

Al Dwairi, R. (2017). Modeling of chromium (VI) adsorption from aqueous solutions using Jordanian Zeolitic Tuff. Water Sci Technol., 75(9-10): 2064-2071.

Al-Haj-Ali, A.M., and Marashdeh, L.M. (2014). Removal of Aqueous Chromium (III) Ions Using Jordanian Natural Zeolite Tuff in Batch and Fixed Bed Modes. Jordan Journal of Earth and Environmental Sciences, 6(2): 45- 51.

Al-Harahsheh, M.S., Al-Zboon, K., Al-Makhadmeh, L., Hararah, M., Mahasneh, M. (2015). Fly ash based geopolymer for heavy metal removal: A case study on copper removal. Journal of Environmental Chemical Engineering, 3(3): 1669–1677.

Al-Harahsheh, M.S., Shawabkeh, R., Batiha, M., Al-Harahsheh, A., Al-Zboon, K. (2014). Sulfur Dioxide Removal using Natural Zeolitic Tuff. Fuel Processing Technology, 126: 249–258.

Al-Tabbal, J., Al-Zboon, K., Al-Zouby, J., Al-Smadi, B., Ammary, B.Y. (2016). Effect of zeolux use on sage (salvia officinalis) plant irrigated by fresh and Ro reject waters. Global NEST Journal, 18(2): 416 - 425.

Álvarez-Ayuso, E., Querol, X., Plana, F., Alastuey, A., Moreno, N., Izquierdo, M., Font, O., Moreno, T., Diez, S., Vazquez, E., Barra, M. (2008). Environmental, physical and structural characterization of geopolymer matrixes synthesized from coal (co- combustion fly ashes. Journal of Hazardous Materials, 154(1–3), 175–183.

Al-Zboon, K., Al-Harahsheh, M., Falah, B.H. (2011). fly ash based geopolymer for Pb removal. Journal of Hazardous Materials, 188(1–3): 414–421.

Al-Zboon, K.K., Al-Smadi, B.M., Al-Khawaldah, S. (2016). Natural Volcanic Tuff-Based Geopolymer for Zn Removal: Adsorption Isotherm, Kinetic, and Thermodynamic Study. Water Air Soil Pollution, 227(7): 227-248.

Al-Zboon, K.K., and Al-Zou'by, J. (2016). Effect of volcanic tuff on the characteristics of cement mortar. European Journal of Environmental and Civil Engineering, 20(5): 520-531.

Al-Zou'by, J.Y., Al-Zboon, K., Al-Tabbal, J.A. (2013). Low-cost treatment of grey water and reuse for irrigation of home garden plants. Environmental Engineering and Management Journal, 16(2): 351-359.

Amenaghawon, N.A., Aisien, F.A., Agho, O.E. (2013). Application of Recycled Rubber from Scrap Tyres in the Adsorption of Toluene from Aqueous Solution. Journal of Applied Sciences and Environmental Management, 17(3): 411-417.

Anwar, J., Shafique, U., Salman, M., Waheed, uz Z., Anwar, S., Anzano, J.M. (2009). Removal of chromium (III) by using coal as adsorbent. Journal of Hazardous Materials, 171(1–3): 797–801.

Astutiningsih, S., and Liu, Y. (2005). Geopolymerization of Australian Slag with Effective Dissolution by the alkali, in Geopolymer: green chemistry and sustainable solution, Proceeding of Geopolymer Congress 2005, edited by Joseph Davidovits, Institute of Geopolymer, Paris, 69-73.

Ayawei, N., Inengite, A.K., Wankasi, D., Dikio, E.D. (2015). Synthesis and Sorption Studies of Lead (II) on Zn/Fe Layered Double Hydroxide. American Journal of Applied Chemistry, 3(3): 124-133.

Balan, C., Bilba, D., Macoveanu, M. (2009). Studies on chromium (III) removal from aqueous solutions by sorption on Sphagnum moss peat. Journal of the Serbian Chemical Society, 74 (8–9): 953–964.

Bansal, M., Singh, D., Garg, V.K., Rose, P. (2008). Mechanisms of Cr(vi) removal from synthetic wastewater by low cost adsorbents. Journal of Environmental Research and Development, 3(1): 228-243.

Bellú, S., García, S., González, J.C., Atria, A.M., Sala, L.F., Signorella, S. (2008). Removal of Chromium(VI) and Chromium(III) from Aqueous Solution by Grain–less Stalk of Corn. Separation Science and Technology, 43(11): 3200-3220 .

Chen, J., Wang, Y., Wang, H., Zhou, S., Wu, H., Lei, X. (2016). Detoxification/immobilization of hexavalent chromium using metakaolin-based geopolymer coupled with ferrous chloride. Journal of Environmental Chemical Engineering, 4(2): 2084–2089.

Chen, X. (2015). Modeling of Experimental Adsorption Isotherm Data. Information, 6: 14-22.

Cheng, T.W. (2003). Fire-Resistant Geopolymer Produced By Waste Serpentine Cutting, Proceedings of the 7th International Symposium on East Asian Resources Recycling Technology November 10-14, 2003, Tainan, 431-434.

Cheng, T.W., Lee, M.L., Ko, M.S., Ueng, T.H., Yang, S.F. (2012). The heavy metal adsorption characteristics on metakaolin-based geopolymer. Applied Clay Science, 56: 90-96.

Christiansen, M.U. (2013). An Investigation of Waste Glass-Based Geopolymers Supplemented with Alumina. Dissertation, Michigan Technological University.

Dada, A.O., Olalekan, A.P., Olatunya, A.M., Dada, O. (2012). Langmuir, Freundlich, Temkin and Dubinin–Radushkevich Isotherms Studies of Equilibrium Sorption of Zn Un to Phosphoric Acid Modified Rice Husk. IOSR Journal of Applied Chemistry, 3(1): 38-45.

Danielsson, L., and Söderberg, L. (2013). Removal of chromium in wastewater with natural clays in southern Malawi. Projektarbete 15hp, available at https://www.diva-portal.org/smash/get/diva2:619424/FULLTEXT01.pdf.

Dehghani, M.H., Sanaei, D., Ali, I., Bhatnagar, A. (2015). Removal of chromium(VI) from aqueous solution using treated waste newspaper as a low-cost adsorbent: Kinetic modeling and isotherm studies. Journal of Molecular Liquids, 215: 671–679.

Devi, R., and Kumar, H. (2015). Utilization of Waste Foundry Sand in Geopolymer Concrete. International Research Journal of Engineering and Technology, 2(2): 904-908.

Donat, R., Akdogan, A., Erdem, E., Cetisli, H. (2005). Thermodynamics of Pb2+ and Ni2+ adsorption onto natural bentonite from aqueous solutions. Journal of Colloid and

Interface Science, 286(1): 43–52.

El-Eswed, B., Alshaaer, M., Rushdi, I.Y., Hamadneh, I, Khalili, F. (2012). Adsorption of Cu(II), Ni(II), Zn(II), Cd(II) and Pb(II) onto Kaolin/Zeolite Based-Geopolymers. Advances in Materials Physics and Chemistry, 2 (4B): 119-125.

EPA, (2010). chromium-drinking-water, available at: https://www.epa.gov/dwstandardsregulations/chromium-drinking-water.

Foo, K.Y., and Hameed, B.H. (2010). Insights into the modeling of adsorption isotherm systems. Chemical Engineering Journal, 156(1): 2–10.

Ghazy S.E. , El-Asmy A.A., El-Nokrashy A.M. (2008). Separation of Chromium(III) and Chromium(VI) from Environmental Water Samples Using Eggshell Sorbent. Indian Journal of Science and Technology, 1(6): 1-7.

Ghazy, S.E. , El-Asmy, A.A. , El-Nokrashy, A.M. (2010). Removal of chromium(III) from water samples by a low-cost sorbent: application to a mixture of chromium(III) and chromium(VI)'. International Journal of Environmental Technology and Management. 12(2-4): 240-256.

Gupta S., and Babu B.V. (2008). Economic feasibility analysis of low cost adsorbents for the removal of Cr(VI) from waste water. Proceedings of International Convention on Water Resources Development and Management (ICWRDM), BITS Pilani, October 23-26.

Hamaideh, A., Al-Qarallah, B., Hamdi, R.M., Abu Mallouh, S.A., Al-Kafawein, J.K., Alshaaer, M. (2014). Synthesis of Geopolymers Using Local Resources for Construction and Water Purification. Journal of Water Resource and Protection, 6(5): 507-513.

Hanzlicek, T., Steinerova, M., Straka P. (2006). Radioactive Metal Isotopes Stabilized in a Geopolymer Matrix: Determination of a Leaching Extract by a Radiotracer Method. Journal of the American Ceramic Society, 89 (11), 3541–3543.

Hawley, E.L., Deeb, R.A., Kavanaugh, M.C., Jacobs, J.R.G. (2004). Treatment Technologies for Chromium (VI). In Chromium (VI) Handbook, Edited by Guertin, J., Jacobs, J. A., Avakian C. P., CRC Press, Boca Raton.

He, J., Jie, Y., Zhang, J., Yu, Y., Zhang, G. (2013). Synthesis and characterization of red mud and rice husk ash-based geopolymer composites. Cement and Concrete Composites, 37, 108–118.

Ibrahim, K.M. (2001). Evaluation of Jordanian faujasite tuff by comparison with other natural and synthetic zeolites. Environmental Geology, 40(4–5): 440–44.

Ibrahim, K.M., Khoury, H.N., Tuffaha, R. (2016). Mo and Ni Removal from Drinking Water Using Zeolitic Tuff from Jordan. Minerals, 6(116):6-13.

Jacobs, J., and Testa, S.M. (2004). Overview of Chromium (VI) in the Environment: Background and History. Chromium (VI) Handbook, available at: http://www.engr.uconn.edu/~baholmen/docs/ENVE290W/National%20Chromium%20Files%20From%20Luke/Cr(VI)%20Handbook/L1608_C01.pdf.

Janus, J.A., and Krajnc, E.I. (1990). Integrated criteria document chromium: effects. Appendix. Bilthoven, Netherlands. National Institute of Public Health and Environmental Protection, Springfield, VA : NTIS.

Kanwal, F., Imran, M., Mitu, L., Rashid, Z., Razzaq, H., Qurat-Ul-Ain. (2012). Removal of Chromium (III) Using Synthetic Polymers, Copolymers and their Sulfonated Derivatives as Adsorbents. E-Journal of Chemistry, 9(2): 621-630.

Khoury, H.N. (2014). Importance of Clay Minerals in Jordan Case Study: Volkonskoite as a Sink for Hazardous Elements of a High pH Plume. Jordan Journal of Earth and Environmental Sciences, 6(3): 1-9.

Krishna, D., and Sree, R.P. (2013). Removal of Chromium from Aqueous Solution by Custard Apple (Annona Squamosa) Peel Powder as Adsorbent. International Journal of Applied Science and Engineering, 11(2): 171-194.

Lancellotti, I., Kamseu, E., Barbieri, L., Corradi, A., Leonelli, C. (2011). Municipal solid waste incinerator fly ash to obtain geopolymers. Second International Volarization Symposium, 18-20 April 2011, Leuven Belgium.

Li, L., Wang, S., Zhu, Z. (2006). Geopolymeric adsorbents from fly ash for dye removal from aqueous solution. Journal of Colloid and Interface Science, 300(1): 52–59.

López, F.J., Sugita, S., Tagaya, M., Kobayashi, T. (2014). Metakaolin-Based Geopolymers for Targeted Adsorbents to Heavy Metal Ion Separation. Journal of Materials Science and Chemical Engineering, 02(07):16-27.

Luukkonen, T., Sarkkinen, M., Kemppainen, K., Rämö, J., Lassi, U. (2016). Metakaolin geopolymer characterization and application for ammonium removal from model solutions and landfill leachate. Applied Clay Science, 119(2): 266–276.

Meroufel, B., Benali, O., Benyahia, M., Zenasni, M.A., Merlin, A., George, B. (2013). Removal of Zn (II) from Aqueous Solution onto Kaolin by Batch Design. Journal of Water Resource and Protection, 5: 669-680.

Meshram, P., Sahu, S.K., Pandey, B.D., Kumar, V., Mankhand, T.R. (2012). Removal of Chromium(III) from the Waste Solution of an Indian Tannery by Amberlite IR 120 Resin. International Journal of Nonferrous Metallurgy, 1(3): 32-41.

Misra, A., Gupta, R., Gupta, R.C. (2003). Utilization of marble slurry in construction materials, Workshop on Gainful Utilization of Marble Slurry and Other Stone Waste. in: Indian School of Mines, available from: http://www.cdosindia.com.

Mohan, D., Singh, K.P., Singh, V.K. (2006). Trivalent chromium removal from wastewater using low cost activated carbon derived from agricultural waste material and activated carbon fabric cloth. Journal of Hazardous Materials, 135(1-3): 280–295.

Mužek, M.N., Svilović, S., Ugrina, M., Zelić, J. (2016). Removal of copper and cobalt ions by fly ash-based geopolymer from solutions-equilibrium study. Desalination and Water Treatment, 57(23): 10689-10699.

Nikagolla, C., Chandrajith, R., Weerasooriya, R., Dissanayake, C.B. (2013). Adsorption kinetics of chromium(III) removal from aqueous solutions using natural red earth. Environmental Earth Sciences, 68(3): 641–645.

Odeh, L., Odeh, I., Khamis, M., Khatib, M., Qurie, M., Shakhsher, Z., Qutob, M. (2015). Hexavalent Chromium Removal and Reduction to Cr (III) by Polystyrene Tris(2-aminoethyl)amine. American Journal of Analytical Chemistry, 6(1): 26-37.

Onutai, S., Jiemsirilers, S., Thavorniti, P., Kobayashi, T. (2015). Aluminum hydroxide waste based geopolymer composed of fly ash for sustainable cement materials. Construction and Building Materials, 101(1): 298–308.

Ouadjenia-Marouf, F., Marouf, R., Schott, J., Yahiaoui, A. (2013). Removal of Cu(II), Cd(II) and Cr(III) ions from aqueous solution by dam silt. Arabian Journal of Chemistry, 6(4): 401–406.

Pansini, M., Colella, C., De Gennaro, M. (1991). Chromium removal from water by ion exchange using zeolite. Desalination, 83(1–3): 145-157.

Rane, N.M., Sapkal, R.S., Sapkal, V.S., Patil, M.B., Shewale, S.P. (2008). Use of naturally available low cost adsorbents for removal of Cr (VI) from waste water. International Journal of Chemical Sciences and Applications, 1(2): 65-69.

Rangan, B.V. (2008). Low-Calcium Fly Ash-Based Geopolymer Concrete. Chapter 26, Concrete Construction Engineering

Handbook, Second Edition, Editor-in-Chief: E.G. Nawy, CRC Press, New York, 2008, pp. 26.1-26.20.

Saha, P., and Chowdhury, Sh. (2011). Insight Into Adsorption Thermodynamics. Book: Thermodynamics, Edited by Mizutani T., INTECH, available at: http://cdn.intechweb.org/pdfs/13254.pdf.

Sampranpiboon, P., Charnkeitkong, P., Feng, X. (2014). Equilibrium Isotherm Models for Adsorption of Zinc (II) ion from Aqueous Solution on Pulp Waste. Wseas Transactions on Environment and Development, 10: 35-47.

Sismanoglu, T., Ercag, A., Pura, S., Ercag, E. (2004). Kinetics and isotherms of dazomet adsorption on natural adsorbents. Journal of Brazilian Chemical Society, 15(15): 669-675.

Sqoor, S., Sarireh, M., Alahmer, A., Tarawneh, W. (2015). Feasibility of using volcanic tuff stone in ground heat exchange for cooling and heating Systems in buildings. International Journal of Thermal & Environmental Engineering, 9(1): 33-39.

Tangjuank, S., Insuk, N., Udeye, V., Tontrakoon, J. (2009). Chromium (III) sorption from aqueous solutions using activated carbon prepared from cashew nut shells. International Journal of Physical Sciences, 4(8): 412-417.

Tofan, L., Paduraru, C., Teodosiu, C., Toma, O. (2015). Fixed Bed Column Study on the Removal of Chromium (Iii) Ions from Aqueous Solutions by Using Hemp Fibers with Improved Sorption Performance. Cellulose Chemical. Technology, 49(2): 219-229.

WHO (2003). Chromium in Drinking-water, available at: https://www.who.int/water_sanitation_health/dwq/chemicals/chromium.pdf.

Yousef, N.S., Hazzaa, R., Farouq, R. (2015). Adsorptive Removal of Chromium (III) from Aqueous Solution Using Cation-Exchange Resin: Development of an Empirical Model. International Proceedings of Chemical, Biological and Environmental Engineering, 88(5): 21-28.

JJEES

JJEES (2019) 10 (1): 46-51
ISSN 1995-6681

Jordan Journal of Earth and Environmental Sciences

The Economic and Environmental Effects of Water Harvesting in Arbaat Region Red Sea State

Mohammed Alzubair[1], Atiyat Nuri[2], Al Imam Ali[3]

[1]*University of Khartoum, Sudan.*
[2]*Red Sea University, Sudan.*
[3]*Africa International University, Kenya.*

Received 13 April, 2018; Accepted 6 February, 2019

Abstract

This research aims at assessing water harvesting and its economic and environmental impacts in the Arbaat Red Sea State area. The hydrological aspects of water resources namely rainfall groundwater and springs in this region were studied within the basin area of (23.040) Km^2. In addition, all the projects aimed at increasing water yield and its impact on agricultural production, pastoral life and forests were identified and studied. Geographic Information Systems (GIS) and Remote Sensing (RS) were used to map the water harvesting area in Arbaat. The data obtained were processed using statistical analytical methods. The results show that there is a correlation between water harvesting, agricultural and livestock production. This was clear in Khor Arbaat Reparation Program (KARP) from (1992-2004). Reports by engineering consultant for groundwater recharge between (1987-2011) expected the increasing of water harvesting from 0.1 m^3/ day in 2002 to 5205 m^3/day in 2011; the total production of 18000 Km^3/ day increased to 23205 Km^3/ day in 2011. Water potential can help achieve a comprehensive and sustainable development in the region concerning agriculture and livestock if it is well supported and financed. The agricultural land is about 4,600 acres, but 1500-2000 acres are cultivated covering 30 % of the Port Sudan market's needs.

Keywords: Khor Arbaat, Water harvesting, Khor Arbaat Reparation Program, Red Sea State.

1. Introduction

The Red Sea State is located between latitudes 17- 23.2° N and longitude 35- 38.5° E (Figure 1). Arbaat region is located in the north - east of the state, twenty kilometers from Port Sudan, with an area of 54.850 acres. Arbaat region consists of three areas, the first one is Arbaat Al Muwyh that lies between the upper and lower gates at the narrow entrance of khor Arbaat. This area is considered hilly with steep slopes of 1/120 meters degree with a limited agricultural potential (Bun, 1980). The second area is Arbaat Alziraa starting at the lower gate confined between the lower gate and the Red Sea coast with a steep slope of 1/200 meters degree. It is fan-shaped and the component delta covers an area of 25 km with stabilization in housing and agriculture, stretching up to the coast region, which represents the third area in the Arbaat region (Bailey, 1987).

As mentioned earlier, the average per capita daily water consumption in Port Sudan is less than ten liters per day. Water problems in the Red Sea State led to the flow of many investors and the migration of most of the productive sector to other locations inside or outside the country which left quite negative impacts on the economic activities of the rigion and led to the closure of about 70 % of the factories there.

2. Research Problem

Despite the efforts which had been made to tackle the issue of water harvesting in Khor Arbaat, the positive economic and the environmental impacts are still limited. This research shows that there are still natural hydrological, and biological problems, especially in farming, herding and in the forests, in addition to the lack of scientific and strategic plans which prevents projects from reaching the standards of sustainable development in the region.

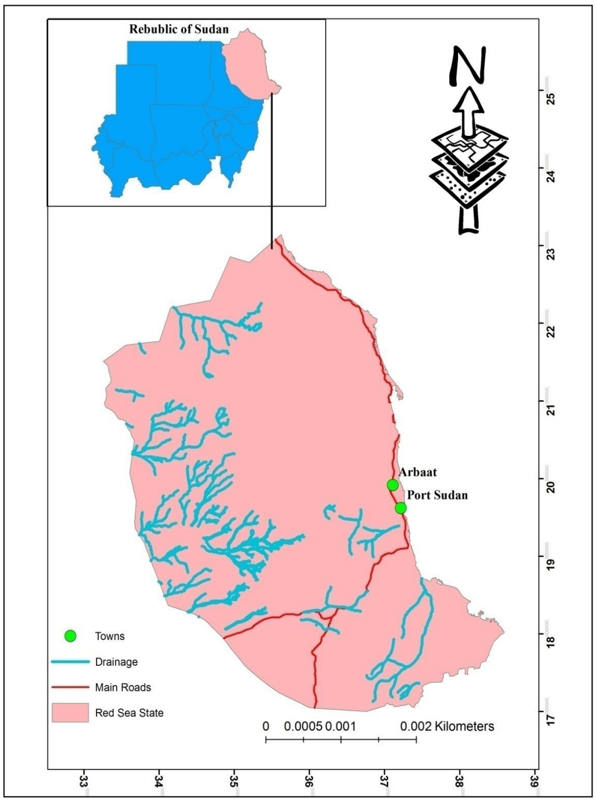

Figure 1. Red Sea State

---

* Corresponding author e-mail: Abozaker68@gmail.com

3. Research Objectives

The main objectives of this research include: (1) Assessing the strategic significance of Khor Arbaat as a main source of fresh water in the region, (2) Determining the water budget and how to manage it for various purposes, (3) Highlighting the obstacles and problems which reduce the optimum exploitation of Khor water, and (4) Submitting proposals and solutions for the sake of increasing the water yield in the region.

3.1. The Study Area

Arbaat region is classified as coastal arid and semi - arid regions, with the average annual rainfall in the northern part being 50 mm and increasing to the south to more than 200 mm in winter (Bashir, 1991). The wind is northwest. The climate of the region is affected by the Red Sea hills and the coast beside the orbital separator (Dabalob, 1999). The geology of the region is characterized by basement rocks, tertiary volcanic and surface sedimentary rocks, with barrier reefs at the coast (Musa,1989). The region has mixed soils, which consist of silt and sand, and a rough texture with limestone. Mangrove, that is naturally grown, dominates the area of the coastal plain, while Acacia sp dominates the area off the sea coast (Satter, 1989).

3.2. Drainage System

Khor Arbaat comes from the catchment area (Odroos) in the mountainous region, flowing from the west to the east towards the Red Sea. The storage capacity of Khor Odroos is about 2.7 million cubic meters (MCM) of water. The upper Khor reaches a distance of 90 km towards the north and 40 km towards the northeast and the width of the Khor is between 1500- 2000 meters forming a fan - shape delta following the upper gate. It has been divided into eleven branches (Dhrab, Aichenk, Ahgeor, Kspaa, Kmueb, Houphouet, Blonay, Balmiat, Kmoa, Waco). Figure 2 shows the drainage system of the Arbaat Basin.

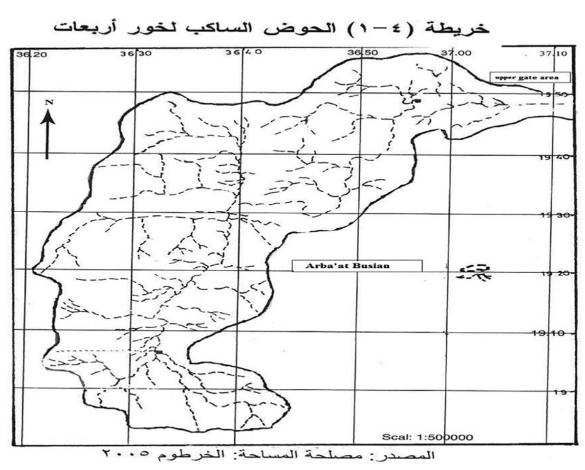

Figure 2. Drainage system of Arbaat Basin (Source: Remote Sensing Authority, 2007)

3.3. Khor Arbaat

Khor Arbaat is about 165 km long forming a fertile alluvial soil in the Arbaat Delta. The average annual discharge of Khor Arbaat is about 18.450.000 meter^3 (Baashr and ALmahey, 1998; Kabashy, 2002). It consists of a series of streams, which come from Odroos in the mountains. The total area is estimated to be about 50 thousand acres including forests, the housing area, and agricultural land. The estimated arable soil is approximately 33.000 acres, while the exploited area is between 2.000 -5.000 acres. Irrigation depends on spate irrigation and rain for the cultivation of maize, millet and some vegetables. (Kabbashi, 2002). Figure 3 shows Khor and the Arbaat's Delta location from Land sat 8 (2016).

3.4. Important Tributaries of Khor Arbaat

Following are the main important tributaries of Khor Arbaat:

- ***Khor Aychenk:*** This is the largest tributary of Khor Arbaat. It runs from west to east ending in the Arbaat Delta; its soil is characterized by sandy gravel. The flora of this Khor consists of Cappories deciduas and Prosopis chiliensis.
- ***Khor Oujor:*** This tributary covers a large area up to the position of the Delta; the soil is sandy gravel, the vegetation includes Prosopis chiliensis.
- ***Khor Hamshdow:*** is one of the important tributaries of Khor Arbaat.
- ***Khor Dhrab:*** This is the main branch of Khor Arbaat, running from the mountains towards the Delta, with a sandy soil, and arid-zone plants including Hyphaena thebaica, Salvadora persica, Capparis decidus (Dablob, 1998).

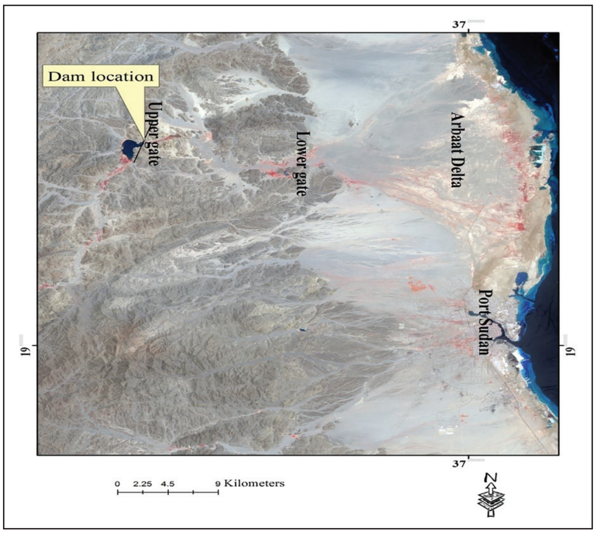

Figure 3. Khor and Arbaat Delta location from Landsat 8 (2016).

4. Materials and Methods

There are several difficulties encountered in the process of collecting information and conducting a field survey, including the lack of resources and studies on the region.. Moreover, the inhabitant local tribes are often found to be not cooperative enough to respond to researchers and their questions. The current research is based on personal interviews and research reviews to investigate the economic and environmental effects of water harvesting in that region. It also depends on a (KARP) project from 1992 – 2004. It studies the hydrological aspects of water sources from precipitation, groundwater and springs, based also on reports and some studies done by the Ministry of Irrigation and Water Resources and Metrology Department in the Red Sea

State. Geographic Information System (GIS) and Remote Sensing (RS) were used to map and locate the Arbaat basin and delta. The data obtained were processed using statistical analysis methods to analyze the available hydrological and metrological data for the detection of the impact of water harvesting on the environment and the economic activities in the Arbaat region.

5. Results and Discussion

5.1. Rainfall

Figure 4 shows the annual rainfall in the Arbaat basement from 1944 to 1990. The years 1950 and 1957 represent the highest rainfall records, while the period from 1958 to 1990 shows a lower rainfall representing the drought period in the state. Based on the temporal distribution, it is clear that the rainfall is scarce and irregular.

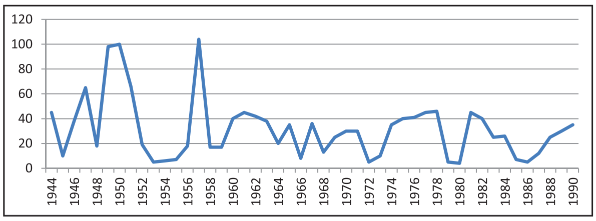

Figure 4. Annual rainfall/mm in Arbaat basement from (1944-1990).

Based on the seasonal distribution of rainfall, table 1 shows that most of the rainfall occurs in November, and thus most water recharge is derived from the winter season. According to the statistical analysis of annual rainfall moving average of 10 years, Table 2 shows that the arithmetic mean does not provide a clear explanation for the amount of precipitation due to the existence of huge variability in the annual precipitation.

Table 1. The seasonal distribution of rainfall

Rainy month (November)		Summer rain (July & September)		Winter rain (October & November)	
Rainfall (mm)	Annual rain%	Rainfall (mm)	Annual rain%	Rainfall (mm)	Annual rain%
20	47	9	21	26	60

Ministry of Irrigation and Water Resources (1999).

Table 2. Statistical Analysis of Rainfall / mm in 10 years

Years recorded	Arithmetic mean	standard deviation	Dry years 8 of 10	Average for the past (5 of 10)	Rainy years (2 of 10)
27	43mm	39mm	6mm	33mm	80mm

Source: Ministry of Irrigation and Water Resources (1999)

The maximum runoff, size of the flow and the duration of output have been analyzed and calculated using available hydrological data, metrological information and field work, which can be summarized as follows:

There is a lot of water entering the basin area and is dispersed in a large area used for agriculture and pastures which improved the Arbaat region environment. Table 3, shows the maximum surface runoff per cubic meter per second.

Table 3. The maximum runoff /m^3/sec.

Basement area (km2)	years	Maximum flow recorder	Flow (Return time)			
			2	10	50	100
4850	18	400 m^3	200 m^3/sec	450 m^3/sec	700 m^3/sec	800 m^3/sec

Source: Ministry of Irrigation and Water Resources (1999)

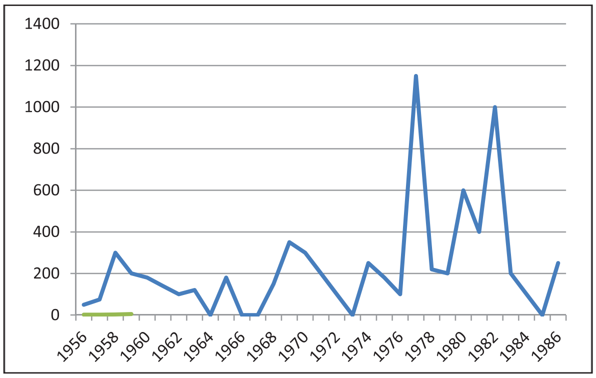

Figure 5. Annual floods rates/m^3 between 1956 – 1987.

From Tables 3 and 4, and Figure 5, it can be noted that there is a connection between the basin area and annual runoff. The duration of runoff increases the basin area. There is a relationship between the distribution of rainfall and the duration of runoff.

Table 4. Annual Runoff and Flood in the Basin.

Basin area	Years Surveillance	Maximum levels recorded	Dry years 8 of 10	Average for the years 5 of 10	Rainy years 2 of 10
Total annual runoff / MCM	18	67.8	4.5	11	26
Annual floods m^3 / year	17	990	250	430	820

Source: Ministry of Irrigation and Water Resources (1999)

5.2. Spring Water

The spring and seaport water is concentrated in the upper gate area which produces about 7,000 to 11,000 m^3 of water per day throughout the year. Winter rainfalls are the main source of the continuity of the spring water which reached 6.440 m^3. Figure 6 shows rates of monthly spring water.

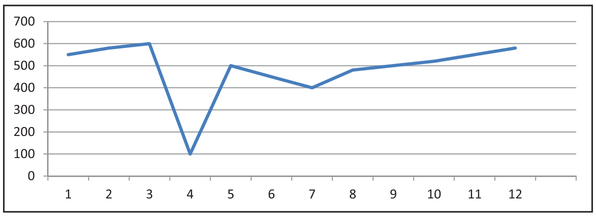

Figure 6. Rate of Monthly Spring Water Discharges/m^3.

5.3. Groundwater:

There are numerous studies of the groundwater wells in the region (e.g. Hussein, 1975; Musa, 1989) which explore the movements of the groundwater and identify the nature of the water rock features. From these studies, it is clear that the water stone rock for the well region extends to about 22 km, 12 km from the upper gate and 10 km from the lower gate. The variable depths of wells ranged between 3-15 meters or more depending on water strength and density This is associated with a high level of surface runoff and the extent of coverage of the rock layer; and the average of rock density and porosity coefficient is 0.2. The water storage capacity of the rocks of khor Arbaat is 48 MCM. The increasing of water and recharge in cubic meters per month was identified by studying the current annual runoff, and by analyzing the increasing level of water rock and natural water loss by evaporation, transpiration and drought, as shown in Table 5.

Table 5. Water increase per month in cubic meters

Month	Recharge /m^3
July	302 500
August	303 000
September	306 000
October	305000
November	405000
December	501 000

Source: Field work based on the Office of Engineering Consultants (2002)

According to the work done by researchers based on the information collected from Office of Engineering Consultants (2002), it is clear that groundwater rises in November and December on the basis of the flood compared with the rainfall. From Table 6, and according to the engineering consultant's studies in (2002), there was reserve water in the wells as a result of storage that can be exploited for various uses.

According to Hussein (1975), it is clear that in spite of the incomplete data, the application of various equations, there is no surplus water in the Khor due to the large quantities of water that flooded towards the sea and those are estimated at 359,000 m^3 / day. This water can be harvested and used in the development of that region.

5.4. Assessment of Traditional and Modern Water Harvesting:

1 / Diversion Dams:

These are earth dams built for agricultural purposes to divert water and irrigate farm land. Farmers built a number of dams, which take the form (U).They were traditionally weak and were destroyed by floods; therefore, they are considered less effective and have a negative impact on the soil texture due to flooding, siltation, escarpment in addition to the need for annual maintenance.

2 / Storage dams:

Three reservoirs exist in Arbaat area (the fourth tank, the entrance gate and upper gate tank). There has been a number of studies conducted to for the sake of constructing a storage dam in Arbaat (the upper gate dam). A study in 1987 recommended the constructing of a storage dam 20 km from the upper gate with a storage capacity of 5 million m^3 / hour. Another study in 1991 recommended that the dam must be constructed about 3.2 km from the upper gate with a storage capacity of 100 million m^3. According to a study conducted in 2002, a storage dame was constructed focusing on increasing the groundwater level. A report issued by some engineering consultants in 2002 stated that there will be an increasing in the groundwater recharge after the dam construction. Table 7, explains the increase in the groundwater recharge in different years.

Table 6. Assessment of wells recharge and the flow from 1972 to 2000

Year	Water Increase	Changes in storage (10^{6}m^3 / sec)	The amount of water with drawn (10^6 m^3)	Recharge (10^{6}m^3 / year)	The value of the budget (10^{6}m^3 / year)
1972	3.6	8.64	5.480	14:48	9
1973	2.3	5.2	6.278	11.80	5.52
1988	7.0	16.80	6.57	23:37	16.8
1991	4.0	9.60	6.94	16:54	9.6
1993	8.5	20.4	7.3	27.3	20
2001	2.5	6.0	6.21	12:11	5.59
Average	**4.65**	**11:16**	**6.52**	**17.68**	

Source: Ministry of Irrigation and Water Resources (1999)

The area of the dam lake is about 5 km$^{2.}$ It depends on the increase or decrease of seasonal water runoff and rainfall. It is one of the largest dams and is considered new because production began in 2004. Figure 7 shows the Arbaat basin and Delta location.

Table 7. Ground water recharge from (2002-2011) in m^3/day

years	No. Well	Expected production (m^3 / day)	Expected increase (m ^{3} / day)	Total production (km / day)
2002	10	18000	1.0	18000
2003	27	18000	7945	25,945
2004	27	18000	7123	25123
2005	27	18000	6849	24,849
2006	27	18000	6301	24301
2007	27	18000	6301	24301
2008	27	18000	6027	24027
2009	27	18000	5753	23,753
2010	27	18000	5479	23479
2011	27	18000	5205	23205

Source: Ministry of Irrigation and Water Resources (1999)

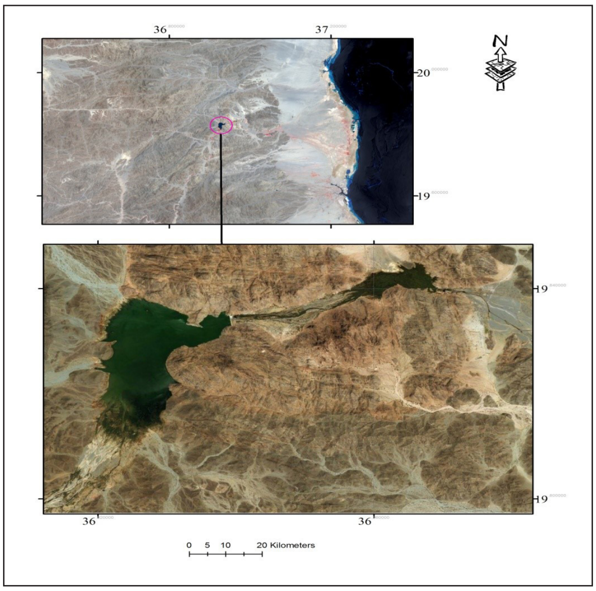

Figure 7. Khor and Arbaat Delta location from Land sat 8 (2016).

6. Arbaat Reservoir

6.1. Groundwater Levels

The fluctuation in the underground water level from one well to another has been different in a single season.

6.2. Feeding of the Reservoir

In the year 1971, the reservoir provided the city with about 12 million cubic meters, about with 9 million cubic meters in 1973.

Water-bearing Geological Formations

The presence of water in the composition of rocks occurs through the cracks, but it is relatively not much compared with the water found in sedimentary rocks.

The water-bearing rocks are mainly composed of homogeneous rock foundations such as stones and gravel deposited in Khor as result of weathering (Ahmedon, 2008).

6.3. Reservoirs Extension

The underground reservoir extends from the supreme gate to the lower gate over an area of approximately 10.177 $km^{2.}$ The average prone is between 1.310 km ^{2} and 13.3 km^{2} (Ahmedon, 2008).

6.4. Storage Capacity

The storage capacity of the reservoir ranges from 36 to 48 million cubic meters, with the highest amount of storage reaching about 54 million cubic meters during the flood season (winter. The lowest discharge is 3 million cubic meters in the summer season; however, the average storage capacity in summer is 10 million cubic meters. (Adam, 2006).

Water Harvesting and its Economic Dimensions in Arbaat Area

According to a report recorded by SOS (1995, 1996, 1997, 2001) the first economic agricultural project in Arbaat region was in 1918. It was a project about cotton and tobacco cultivation using flood irrigation. A report from Soil Conservation Management in (1944) recommended reforestation in the Arbaat Delta to produce fuelwood for Port Sudan city. Between 1950-1955, cotton production was increased and also exported. The project was developed with funding from the US for the years 1960- 1961 by constructing earth dams in the lower areas of delta toward the east direction in Khor Hmshdo and Khor Dhrab (SCE, 2004). Since the beginning of the eighties, agricultural production has deteriorated due to the lack of water, the poor conditions of the existing dams, and the unstable repairing and maintenance operations until the initiation of Khor Arbaat Reparation Program (KARP) in 1993 (SOS, 1997).

According to the (KARP) studies, it is clear that there is a positive connection between water harvesting and the agricultural production process, which can be clarified as follows:

The area of agricultural land is 4,600 acres, from which 1500-2000 acres were cultivated. This area covers about 30 % of the Port Sudan market's needs. According to a field study, there is a relationship between the increase in agricultural productions and the amounts of available water. Figure 8, shows the relationship between agricultural production and water harvesting in tons. The storage capacity of the reservoir ranges from 36 to 48 million cubic meters, with the highest amount of storage reaching about 54 million cubic meters during the flood season (winter. The lowest discharge is 3 million cubic meters in the summer season; however, the average storage capacity in summer is 10 million cubic meters. (Adam, 2006).

Water Harvesting and its Economic Dimensions in Arbaat Area

According to a report recorded by SOS (1995, 1996, 1997, 2001) the first economic agricultural project in Arbaat region was in 1918. It was a project about cotton and tobacco cultivation using flood irrigation. A report from Soil Conservation Management in (1944) recommended reforestation in the Arbaat Delta to produce fuelwood for Port Sudan city. Between 1950-1955, cotton production was increased and also exported. The project was developed with funding from the US for the years 1960- 1961 by constructing earth dams in the lower areas of delta toward the east direction in Khor Hmshdo and Khor Dhrab (SCE, 2004). Since the beginning of the eighties, agricultural production has deteriorated due to the lack of water, the poor conditions of the existing dams, and the unstable repairing and maintenance operations until the initiation of Khor Arbaat Reparation Program (KARP) in 1993 (SOS, 1997).

According to the (KARP) studies, it is clear that there is a positive connection between water harvesting and the agricultural production process, which can be clarified as follows:

The area of agricultural land is 4,600 acres, from which 1500-2000 acres were cultivated. This area covers about 30 % of the Port Sudan market's needs. According to a field study, there is a relationship between the increase in agricultural productions and the amounts of available water. Figure 8, shows the relationship between agricultural production and water harvesting in tons.

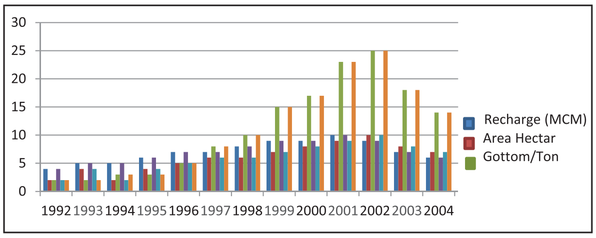

Source: Prepared according to a fieldwork research results (SOS, 2001)

Figure 8. The relationship between agricultural productions and water harvesting in tons

From figure 8, it is clear that the over the duration period of Khor Arbaat Reparation Program (KARP) (1996-2002) there was an increase in productivity per tons. During this time water has been harvested in eleven branches of khor Arbaat which feed the Delta.

When funding ended in 2002, the project began to decline gradually even at the present time as a result of lack of routine maintenance which led finally to the collapse of most of the dams.

6.5. Water Harvesting and Livestock

Khor Arbaat is a rich area where different varieties of livestock were found. Records from SOS (2001) show that 72 % of the population own goats and 13 % have sheep and 15 % own qualitative livestock. There are several problems faced by livestock owners and these can be summarized as follow:

- Mobility, where pastoralists move long distances seasonally with their families in the winter season to the coast; this is referred to as (gunap trip), and in summer they move to the mountains; this is called the (Alooulib trip) due to precipitation and its effects on the growth of the weeds in those seasons.These lead to a decline in specific plants including Panicum turgidum and Capparis deciduas and the increase of the invasive plants such as Prosopis chilensis.
- There is a clear shortage in water in this region. 66 % suffer from lack of water; 9 % rely on pipelines; 15 % rely on wells and 10 % on flood water (Cole, 1989). The technique of water harvesting can solve all these problems and may increase the cultivation of forests and rangelands in order to stabilize pastoralists and provide them with drinking water. This can increase animal livestock and production for the Port Sudan city market.
- The increasing of agricultural and livestock production in the region along with an improved chance of marketing in Port Sudan city can create jobs and intermediate trade. These local economic activities can raise the income of Arbaat communities, thus improving the living standards and health services in the region which suffers from poverty and lack of work opportunities. Water harvesting in the region is the perfect choice to achieve better and sustainable levels of development.

7. Conclusions

Through the evaluation of (KARP) projects for water harvesting in the Arbaat area over the period from 1992 to 2004, it becomes clear that the increasing of water output in the dams, led to a rise in the levels of well groundwater in the region This has enhanced the cultivated area and pastures. An open market for the livestock and agricultural products in Port Sudan city can create employment, intermediate trade, and transportation. This can in turn contribute to the per capita income of the Arbaat population and improve the living standards, health conditions, and health services in this region that has been suffering from poverty, very limited work opportunities and high unemployment rates for a long period of time. Water harvesting remains the best solution to achieve the best levels of sustainable development in the region.

In conclusion, this research paper offers the following set of recommendations that can hopefully help in the stability of this region in the future.

Recommendation

1- A sustainable maintenance and periodic monitoring of water harvesting projects.
2- Conducting geological and metrological studies continually on precipitation and runoff to reduce the risk of droughts.
3- A follow - up treatment of special problems of water reserve from sedimentation and silting and their impact on the soil types.
4- The cultivation of lands around valleys and dams is a source of benefit for the environment.
5- A follow-up evaluation of the agricultural expansion and the education of farmers to contribute to the production process.
6- Using modern irrigation techniques such as drip irrigation.
7- Protecting agricultural and livestock production to achieve attractive and stable prices.
8- Controlling the spread of Mesquite trees, especially in agricultural lands.
9- Developing the laws and legislation of water management.

References

Adam, E.T.B. (2006). Hydrology of Khor Arba'at - Faculty of Earth Sciences, Red Sea University (Port Sudan) (supplementary research for the degree of (BA).

Ahmedon, A.B.A. (2008). Chemical Characterization of Catchment Area and Water of Arbaat Region. Ph.D thesis in Environment and Resources. Red Sea University.

Bailey, K. (1987). Method of Social Research. ed. free press, New York .

Bashir, M.K.A. (1991). Rainfall in Red Sea Province.

Bun, (1980). Reconnaissance of groundwater and surface water Resources in coastal area of Sudan, Red Sea hills, Sudan, Report GRAS, Khartoum (1980).

Cole, R. (1989) Measuring Drought and Drought Impact in The Red Sea Province, Oxfam Publication, London.

Dablob, S.H. (1998). A working paper entitled: Program of priorities for combating drought and desertification in the Red Sea State, workshop.

Dabalob, S.H. (1999). Desertification in the Red Sea state.

Hussein, M.T. (1975). Hydrogelogical Investigation of Khor Arbaat Basin, Bull. No.28. Geological and Mineral Resources, Khartoum, Sudan.

Kabbashi, Mohamed El Amine, (2002). Red Sea State, Drinking Water Conference: Risks and Treatments - Khartoum - UNESCO Water Chair. Arab Organization for Agricultural Development.

Ministry of Irrigation and Water Resources (1999), Sudan.

Musa, M.M. (1989). Structural geological Study of the upper gate area (Arbaat ') for suggested dam site. GRAS. Port Sudan unpublished.

Satter, R.G. (1989). The Charcoal Producers of tambek: Integrated Study of Sea Hills, C and. Scient thesis, Oslo.

SOS, Sahel International Organization in Sudan. (1995). Soils and Use in Khor Arbaat Delta, Hunting Technical Services LTD.

SOS, Sahel International Organization in Sudan. (1996). Women of Khor Arbaat Delta.

SOS, Sahel International Organization in Sudan. (1997). Review of Khor Arbaat Rehabilitation Project.

SOS, Sahel International Organization in Sudan. (2001). Evaluation of Khor Arbaat. Rehabilitation Project.

JJEES

Jordan Journal of Earth and Environmental Sciences

JJEES (2019) 10 (1): 52-63
ISSN 1995-6681

Climate Monitoring and Damage Assessment Model: A Case Study from the Praetorium at Umm El-Jimal Archaeological Site, Jordan

Fadi Bala'awi[1] and Shatha Abu Aballi[2]

[1]*Queen Rania Faculty of Tourism and Heritage, Department of Conservation Science, The Hashemite University, Zarqa, Jordan.*
[2]*Queen Rania Faculty of Tourism and Heritage, Department of Sustainable Tourism, The Hashemite University, Zarqa, Jordan.*

Received 19th November 2018, Accepted 6th February 2019

Abstract

Umm el-Jimal is a Byzantine- Nabetean archeological site located on the edge of the southern Hawran plain. The site is notable among Jordan's premier archaeological sites for its wealth of Late Antique ruins. The architectural forms are illustrated in the ruins of the site by ground plans, the construction of the super structures of the buildings, their ornament, the girder arch, the corbel courses, and roofing slabs. There are principal details and constructive principles developed in the purely lithic architecture in basalt at Umm el-Jimal and these are not common in the architecture of Hawran.

The objective of this study is to carry out a detailed microclimate monitoring program in order to provide reliable information on the measurement and characteristics of the stone decay problem at Umm el-Jimal. Relative humidity, temperature, and the level of pollution (CO_2) will be measured for a limited period of time.

This study is focused on the Praetorium – one of the structures at Umm el-Jimal which enables us to determine elements that accelerate destruction. The Praetorium gives a glance at the damage to the stone in Umm el-Jimal, which is affected by microclimate. Climate changes such as the rise in the percentage of relative humidity during winter and humidity decline during summer, and vice versa with temperature all result in damages to the site. Both relative humidity and temperature appear in different types of mechanical, alteration, and solution decay forms at the site. In addition, it is notable that Umm el-Jimal suffers from high levels of CO_2, which contributes to the increasing growth of micro-organisms on stone surface, which accelerates many types of damage to the stone. Therefore, it is necessary to have a comprehensive conservation plan for the preservation of the site from loss and destruction in addition to the need for removing the damaged or deteriorated crust by using non-destructive methods as much as possible.

Keywords: Umm el-Jimal, microclimate, damage assessment, relative humidity, temperature, CO_2 and conservation plan

1. Introduction

1.1. General Introduction

Umm el-Jimal is a large settlement near the northern border of Jordan and is located in the semiarid region of north Jordan – on the edge of the basalt plain. It was created by prehistoric volcanic eruptions from the slopes of the Jebel Druze (De Vries, 1990). The ruins of Umm el-Jimal are situated at twenty kilometers from Mafraq, where the pipeline and road from Iraq cut the Hijaz railway on the way to Haifa city on the Mediterranean Sea (Horsfield, 1937).

Figure 1. Umm el-Jimal location (Google Earth, 2016).

Umm el-Jimal is situated in semi-arid steppe, 25km south of Busra and 40km southwest of Salkhad. This is the point where the southern Hawran plain meets al-harra, the formidable basalt plateau of north-eastern Transjordan. This remote lava city is interspersed with pockets of soil and vegetation. Today, the city hosts a few villages including Sabha and Umm al-Quttayn, which were built-up around the Late Antique ruins as local Bedouins settled, and as a result of the scattering of Druze families (Brown, 2009).

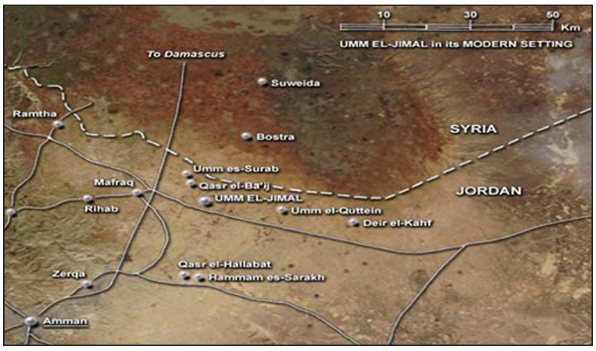

Figure 2. Umm el-Jimal location (Umm el-Jimal Project, 2016)

---

* Corresponding author e-mail: fadi.balaawi@gmail.com

Umm el-Jimal ranks second after Petra and Jerash in the state of preservation among Jordan's archaeological sites (De Vries, 1981). The city is considered as a substantial town compared with many of its neighboring towns (Kennedy, 2013).

In the Roman, Byzantine, and Umayyad periods, the desert population of Northern Jordan created a comfortable human habitat in the apparently hostile environment of the basaltic frontier. Umm el-Jimal formed more fertile parts of the basaltic regions where sparse agricultural resources were exploited and distributed along the Roman-Byzantine Arabic region. This also formed a secure buffer to prevent nomadic and military incursions into Syria and Palestine (De Vries, 1985).

Umm el-Jimal was occupied for 700 years from the 1st Century AD to the 8th Century AD. It was, then, completely abandoned and after that was occupied during the 20th century (De Vries, 1990). Umm el-Jimal has undergone several occupations in the Late Nabataean Roman, Byzantine and Umayyad periods (De Vries, 1995). It was finally reoccupied by the Druze who expanded their territories beyond their mountain to the North, and found Umm el-Jimal an attractive place to remodel (De Vries, 1990).

The landscape of the town resembles a rough parallelogram from south to north (Horsfield, 1937), with 800 meters in length and 500 meters in width. The site encompassed more than 150 buildings grouped into three irregular clusters (Whitcomb, 1996). However, some of the buildings had been destroyed for different reasons, while other structures still exist.

People who lived at Umm el-Jimal built a town of laboriously chiseled basalt ashlars and long beams (Brown, 2009). The town of Umm el-Jimal encompassed doorways and alleys that lead from room to room, and from building to building, reaching up to three or four stories high (Al-Kurdi, 2014). The town was surrounded by walls from four destinations and five gates. These held within them praetorians, churches, houses, several reservoirs, a channel system, civil buildings, stairways, barracks, and a number of other features. All of these features were scattered throughout the town, which contravened a late antiquity pattern (Obeidat, 2002).

Umm el-Jimal has many inscriptions found throughout the rubble of the buildings, churches and graves. The inscriptions are lingually diverse including Nabataean, Latin, Greek, Safaitic, and Arabic inscriptions written on basalt rocks. The inclusion of the various inscriptions facilitates the determination of the history of the site. Furthermore, the multilingual inscriptions allow the absolute dates of some of the structures at the site to be detected. Also, the inscriptions facilitate the understanding of the development of the Arabic language and provide information on who settled at this site (Obeidat, 2002).

1.2. Architecture of Umm el-Jimal

Since the Late Roman, Byzantine and Umayyad periods, Umm el-Jimal has had dozens of prosperous rural towns and villages scattered on the plains between Dera'a to the west and Deir el-Kahf to the east (De Vries, 1990).

The architecture of Umm el-Jimal has given it a unique stability through the one-hundred and eight of the town's structures which once stood three stories in height (Brown, 2009). Moreover, there were fifteen churches, a water system and barracks distributed at the site (Obeidat, 2002). These were grouped in compact masses, in the east, west and north, and a scattered group was found down the middle of the structure of the city (Horsfield, 1937). Further walls of structures run every direction without plan or order (Al-Kurdi, 2014).

Umm el-Jimal is built completely from basalt. Basalt exhibits a high structural resistance against erosion, climate and time (Al-Kurdi, 2014). People who occupied the site used special techniques to support the buildings and give more space to the structures, such as corbelling, the the cantilevered stairway rough wall finish, the building quality, doorway and window treatment, and lintel relieving illustrated by the circular window relief and double lintel relief (Obeidat, 2002).

Umm el-Jimal, has none of the formal lay-out or architecture which distinguished Syrian Graeco-Roman cities of the 2nd and 3rd centuries A.D. Although contiguous and contemporary with them (Horsfield, 1937), Umm el-Jimal is a non-grid town. The place is planned without frills or carving on any kind of its buildings. The churches present a far greater variety of ground plans and superstructure than can be found in any part of the surrounding area (Butler, 1913).

The houses of Umm el-Jimal consist of a single or more than one room, which overlooks a courtyard; some houses share walls (Obeidat, 2002). The houses are of two large arched stories at the front, but houses with four stories of narrow chambers are also common throughout the ruins (Al-Kurdi, 2014). Some of the houses were covered internally and externally with coatings of stucco, finished with a polished surface on walls. It should be noted that doors and window shutters were made of basalt (Horsfield, 1937), but unfortunately, people who reoccupied the site during the Umayyad period robbed and badly damaged some portions of the Byzantine buildings, such as the walls of the rooms (De Vries, 1995).

Churches of Umm el-Jimal appear in various types. Some of the churches can be identified by inscriptions upon the surface of the structure, like that of Numerianos. Others may be distinct through the observation of their architectural form, such as the cathedral church, of a basilica type built in 557 A.D. Furthermore, churches that include multiple arcades in their structure can also be found, such as the Chapel of the Barracks. The last type of churches to be found at Umm el-Jimal is known as the "hall type". This type is demonstrated by the churches of Julianos, built in 345 A.D., and of the Maeschos. The halls of these churches include roofs with black basaltic long beams and girder arches to carry the flat roofs. The largest church at Umm el-Jimal is known as the "cathedral church". The cathedral church is 23 meters in length and 25 meters in width. On the other hand, the smallest church is referred to as the "southeast church" which is 10 meters in length and 8 meters in width. In general, the churches of Umm el-Jimal are distinct in that they lack excessive decorations, while only a few are found at the base and capital of the columns which support the arches.in addition to some minor religious symbols carved on the walls (Horsfield, 1937).

Remarkably, the tribes who reoccupied the site during the 20th century changed the purpose of some ruins. They used the site as a campground, where domestic courtyards provided corrals and additional walled pens which could easily be created from the scatter of stones that littered the site (Brown, 2009).

2. Case Study

The Praetorium (371 A.D) is situated near the west wall, south of the Gate of Commodus, and beside the broad, open, space that extends through the middle of the city. Its major axis lies eastwards and westwards. It is a great courtyard, originally enclosed within a high wall. In the southwest angle of this yard, and extending for some distance along its western wall, is a row of residences of the same period, following the same general style, as the main building (Butler, 1913).

Figure 3. Front Façade of Praetorium, Umm el-Jimal (by researcher, 2016)

The plan of the Praetorium is a parallelogram divided longitudinally into two main sections; one to the south subdivided into three main apartments, and one to the north having five smaller divisions. The middle division of the three main apartments consists of a square atrium noricum. The south wall of the atrium contains the principal entrance to the building and two large windows above two rectangular niches. In the eastern wall of the atrium, to the right as one enters, is a single doorway between two pilasters which correspond to the columns (Obeidat, 2002).

The Praetorium is composed of two-storey superstructures. This is evident upon the observation of the ground-plan, with the aid of the parts of the building that are still in situ, and by the observation of the fallen parts (De Vries, 1993).

3. Literature Review

Butler, De Vries, and the Department of Antiquities of Jordan are principal investigators responsible for the start of the excavation project in 1905 continuing to present day. Butler started the excavation of the site in 1905. De Vries continued the excavation work at Umm el-Jimal during 1972. As such with any project, many archaeologists and specialists are involved in the actual excavations and subsequent studies and analysis required for publication.

Haddad (1991) presented an analytical study for nine of the Byzantine churches, in order to contrast the differences of the internal and external details of the structures. Moreover, Haddad made a comparison of the churches at Umm el-Jimal site, and those in the surrounding areas in Syria and Jordan. The ability to identify the differences and similarities among the churches allowed for the determination of approximate dates of the Churches. The study helped current researchers compare the structures for digital reconstruction and the theories on how the buildings were destroyed through time and were then introduced as a three-dimensional model.

In 2002, Dunn provided a new study of mortars and concretes from an Umm el-Jimal structure. Her study depended on the collection of many samples taken from random structures of Umm el-Jimal. She used many types of analysis such as Insoluble Residue Analysis, Grain Size Analysis, X-Ray Diffraction analysis, ICP Mass Spectroscopy, Petrographic and Microscopical Analysis. The formulation result gave the original mortar and concrete specific degrees of physical strength and durability, in addition to the effect of the geological origin of the raw materials. The evidence allowed Dunn to provide an explanation for the way through which the former inhabitants of Umm el-Jimal processed it, and how technology changed over time. Finally, Dunn used the results based on the analysis to create a comprehensive management plan of the site.

Smith et al., (2008) developed a way to evaluate damage done to stone using salt weathering simulated and salt-based durability tests which have largely relied on weight loss after each weathering cycle. One must take into consideration properties that are affected by environmentally-driven thermal and moisture cycles and association variation in relative humidity, and how stone reacts with atmospheric pollutants. In order to properly monitor the environmental agents, researchers have to use a specific environmental monitoring sensor. The apparatus is put into the stone and is left for a period of time. During this time, the change of physical properties of the stone will be observed and recorded.

Abo Ali (2012) created a development and marketing plan for Umm el-Jimal site. Abu Ali illustrated how individuals may utilize the site for cultural resources, by exploring the heritage or structure, like those of the Nabatean Temple, Barracks and many others. He submitted a comprehensive study of natural and human resources located around the site as clarification of how they can be explicated. These actions can be set into place to serve as promotion of Umm el-Jimal as a tourist destination.

4. Methodology

The current study relies on a theoretical as well as a practical approach as follows:

1. The theoretical approach: during this phase of the study, the researchers reviewed all the previous studies of Umm al-Jimal that are of a historical and archaeological significance in order to understand the detailed aspects of the site. After utilizing the practical approach, the researchers re-studied the results of the diagrams obtained from the devices. This allowed the researchers to evaluate the changes that occurred on site according to SWOT analysis and determine the strengths and weaknesses. Furthermore, this can contribute and aid in the drafting of opportunities to preserve Umm el-Jimal against decay by the determination of possible intervention techniques to

protect the site of Umm el-Jimal against threats which may deprive it of being a tourist destination. Lastly, together, the researchers would be able to set up a comprehensive conservation plan that may be applied at the site, based on the results from the practical approach.

2. The practical approach: This approach included several steps.

The first step entailed carrying out several fieldwork visits to the site for the assessment of stone decay. Also, the completion of a comprehensive environment-monitoring program in order to determine the risks threatening the site using two Gemini Tiny tag loggers. These loggers are installed at the site for several months to monitor three parameters of the microclimate. The readings of the loggers will then be discussed to link how these parameters have an effect on the damaging of the stone. Finally, fieldwork observation will be conducted to assess the decay of some features at site that are not visible to the naked eye. Such assessment will record the types and degree of damage; the degree of damage will be evaluated on a scale from one to five.

The reason behind choosing such types of loggers is mainly because they are designed for tough locations and they are ideal for external environmental monitoring due to their waterproofing qualities and their large detection range. The temperature ranges of these loggers are between -30 and 50º C, and the relative humidity ranges are from 0 to 100 %. Also, these loggers are capable of recording more than 15,000 readings, which means that they can run unattended for more than twenty months if set up to record one reading every hour (Gemini Data Loggers, 2015).

5. Microclimate Condition Assessment

The sustainability and preservation of the historical and cultural heritage preserved in stone required studies of the intrinsic and extrinsic deterioration factors causing the decay of such materials. The intrinsic factors include the composition and internal architecture. On the other hand, extrinsic factors such as the environmental conditions where the structure is located, and the microclimate affecting particular stones in the buildings (Rives and Talegón, 2006).

The first investigation of Umm el-Jimal considered the **microclimate**, such as temperature, relative humidity and pollution, which are significant factors within the stonework, and have a major influence on the patterns of salt movement. Subsequently, the type and severity of salt-induced decay, which means chances for salt to deliquesce, crystallize, hydrate or dehydrate on porous building materials when interacting with microclimate regimes, are not easy to control and harder to reverse (Smith et al., 2008; Hoyos et al., 1998).

5.1. Temperature and Relative Humidity Readings

Tinytag logger Pluse 2 (TGP / 4500) was placed at certain sites in the buildings, and measured automatically. The device provided continuous recordings of the temperature and relative humidity over two periods of time. The first period was in winter and lasted from December, 2015 to March, 2016, while the second period took place for a shorter span of time during the summer season.

Data retrieved from the first duration of temperature recordings show a maximum value of 24.4 °C, while the minimum value was 2.6 °C, and reached an average of 12.5 °C. The relative humidity recorded during the period varied from 23.8 %, to 76.3 %.

For the majority of the duration of monitoring, relative humidity was recorded at rates above 52.5 %. The next table and graph summarize the most important data regarding the readings.

Table 1. Important data regarding readings at Umm el-Jimal.

Property	Temperature	Relative Humidity
Type	TGP-4500	TGP-4500
Logging started	December1, 2015 12:10 PM	December1, 2015 12:10 PM
Logging ended	February 29, 2016 5:50 PM	February 29, 2016 5:50 PM
Logging duration	92 days 5 hours 39 minutes	92 days 5 hours 39 minutes
Interval between readings	10 minutes	10 minutes
Number of readings	16307	16307
Minimum readings	2.6 °C	23.8 % RH
Maximum readings	24.4 °C	76.3 %RH
Average readings	12.5 °C	52.5 % RH

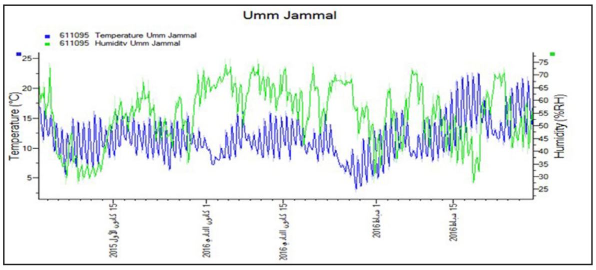

Figure 4. Peculiarities of temperature and relative humidity at Umm el-Jimal took place in winter.

The results of temperatures and relative humidity recordings from various readings logged for three individual durations are shown in Figures 4, 5, and 6.

1. During the first period of monitoring (December 1, 2015 to December 31, 2015) temperature reached a maximum of 17.5 °C and a minimum of 5.1 °C, with an average reading at about 11.5 °C.

During this period, temperature readings varied greatly, which gave a large difference between the maximum and minimum temperatures recorded. Relative humidity fluctuated greatly and was unstable ranging between humid and very dry. The maximum reading of relative humidity was 74.7 % and the minimum reading was 26.6 %, with an average reading of 49.1%

2. The second duration of monitoring at the site took place from (January 1, 2016 to January 31, 2016). The maximum temperature reading decreased to 16.6 °C. The minimum reading in all the periods of monitoring was recorded at 2.6 °C, so the average reading of temperature also decreased to be around 10.1 °C. As the temperature decreased, the relative humidity increased. The maximum reading of relative humidity was recorded at 76.3 %, and the minimum reading was 27.3 %, with an average of 60.8 %.

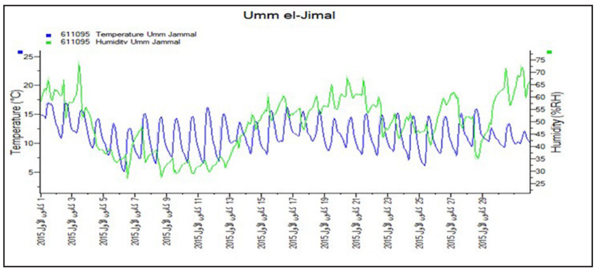

Figure 5. Temperature and relative humidity readings from data logger for the first duration of monitoring at Umm el-Jimal.

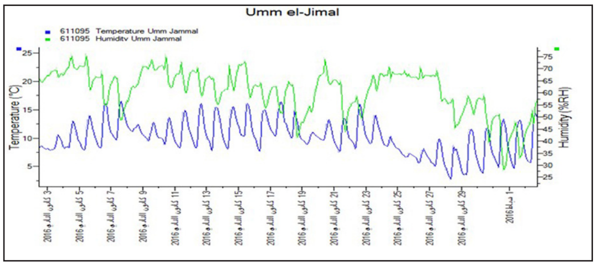

Figure 6. Temperature and relative humidity readings from data logger for the second duration of monitoring at Umm el-Jimal.

3. The third duration of monitoring at the site lasted from (February 1, 2016 to February 29, 2016). The maximum temperature was 24.4 °C, and the minimum reading was 6.2 °C, so the average reading of temperature was around 15.2 °C. The maximum recorded rate of relative humidity was 73.1 % and the minimum reading was 23.8 %, with an average of 48.2 %; humidity fluctuated greatly and was unstable ranging between humid and very dry.

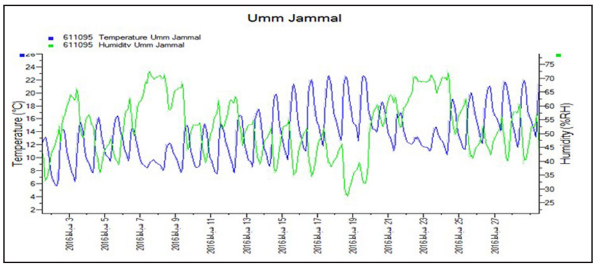

Figure 7. Temperature and relative humidity readings from data logger for third duration of monitoring at Umm el-Jimal.

After exhibiting the results of the readings from the logged research, a day was chosen to discuss the behavior of two parameters of microclimates. The day chosen was in winter on December 1st, 2016, as shown in the next table:

Table 2. Temperature and relative humidity readings and behavior during one day (December 1, 2016).

Parameters	Duration	from	to	Dec/inc
Temperature	(12:00 - 08:00) AM	6.0 °C	3.8 °C	Decrease
	08:10 AM- 03:00 PM	4.1 °C	11.8 °C	Increase
	(03:10 – 11:50) PM	11.1 °C	6.08 °C	Decrease
Relative Humidity	(12:00 - 09:00) AM	57.4 %	59.6 %	Increase
	(09:10 - 10:00)AM	59.1 %	59.6 %	Increase
	(10:10 – 05:00) PM	59.1 %	38.5%	Decrease
	(05:10 – 11:50) PM	38.3 %	49.4%	Increase

After monitoring temperature and relative humidity for one day, the researches showed the variations of these two parameters over the period of a whole week starting on February 14, 2016 until February 20, 2016 (figure 7, a and b). A maximum temperature of 22.7 °C and a minimum reading of 8.6 °C were recorded. Therefore, the average temperature was approximately 16.3 °C. The maximum relative humidity reached 61.4 % and the minimum recorded reading was 27.1 %, with an average rate of relative humidity at 44.3 %.

The following graph shows the daily variations that occurred over the period of one week as an individual unit.

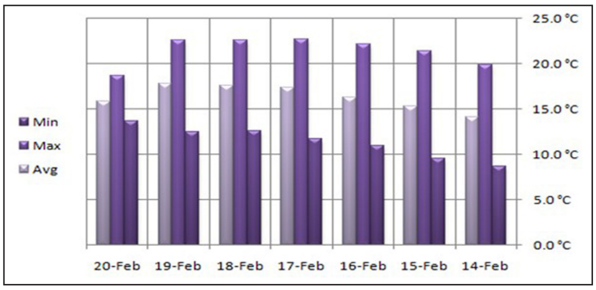

Figure 8a. Maximum, minimum, and average temperature readings from (February 14-20, 2016).

4. The Fourth duration: Data retrieved from the second duration of monitoring were for a shorter period of time during summer lasting only from June to July of 2016. Temperature records show a maximum value of 37.9 °C, while the minimum value was 19.9 °C, and reached an average of 29.1°C. The relative humidity recorded during the period varies from 33.3 % as the minimum value, to 58.4 % as the maximum value. For the majority of duration, the relative humidity recorded was above 18.0 %. The next table and graph summarize the most important data regarding the readings.

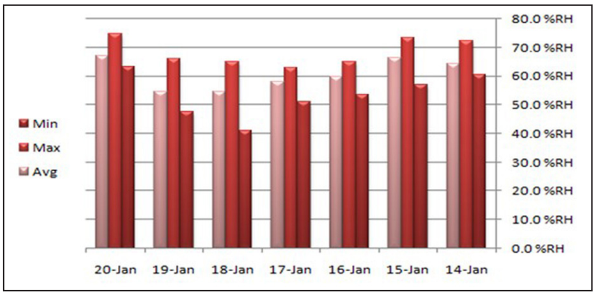

Figure 8b. Maximum, minimum, and average relative humidity readings from (February 14-20, 2016).

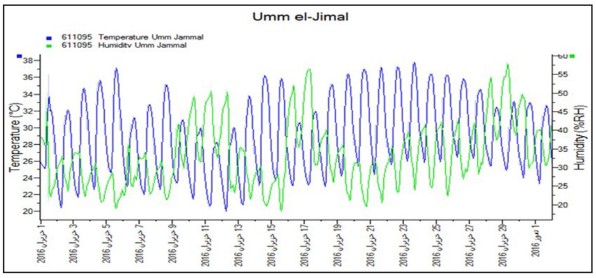

Figure 9. Maximum, minimum, and average relative humidity readings from (February 14-20, 2016).

As an example of the weekly behavior of microclimate during summer at Umm el-Jimal, the researchers chose to exhibit the recordings for one week, that is from June 6, 2016 to June 12, 2016. During this week, the maximum temperature reading was 35.2 °C. The minimum temperature in all the periods of monitoring was recorded at 19.9 °C, and the average reading of temperature was around 26.8 °C. As the temperature increased, relative humidity decreased. The maximum reading of relative humidity was recorded at 50.9 %, and the minimum reading was at 21.2 %, while the average reading was 33.8 %.

Table 3. Important data regarding the readings at Umm el-Jimal in summer.

Interval	10 minutes	10 minutes
Number of Readings	6639	6639
Statistics Start Time	1 June 2016	1 June 2016
Statistics End Time	1 July 2016	1 July 2016
Minimum Reading	19.9 °C	18.0 %RH
Maximum Reading	37.9 °C	58.4 %RH
Average Reading	29.1 °C	33.3 %RH

Table 4. Maximum, minimum, and average temperature and relative humidity readings from (June 6-12, 2016).

Date	**Temperature**			**Relative Humidity**		
	Min	Max	Avg	Min	Max	Avg
6/June/2016	22.9 °C	31.3 °C	27.2 °C	22.2%	38.3 %	28.5 %
7/June/2016	21.8 °C	32.8 °C	27.7 °C	22.5 %	34.2 %	28.5 %
8/June/2016	22.5 °C	35.2 °C	29.0 °C	21.1 %	31.9 %	26.7 %
9/June/2016	23.3 °C	30.9 °C	27.1 °C	28.0 %	43.6 %	35.1 %
10/June/2016	21.4 °C	30.0 °C	26.0 °C	31.4 %	49.4 %	41.2 %
11/June/2016	20.5 °C	28.3 °C	24.9 °C	32.1 %	50.7 %	41.7 %
12/June/2016	19.9 °C	30.1 °C	25.6 °C	23.1 %	50.9 %	35.3 %

5.2. Carbon Dioxide (CO_2)

The data on carbon dioxide were collected using TGE-0011 Tinytag CO_2 Logger. The reason behind the choice of this type of logger is that it records a range of 0 to 5,000ppm, and can be used in more specialized applications. TGE-0011 Tinytag CO_2 Logger is capable of working in a temperature range of -20°C to +60°. In addition, the device is distinct in its self-calibrating system. The logger uses a self-calibrating NDIR sensor. This uses an infrared source to accurately measure the carbon dioxide concentrations. Over time, the properties of the infrared source will change, so the sensor uses a second infrared source, which is only powered up occasionally, to calibrate the first. The patented measurement technique allows for excellent long-term accuracy and stability. Moreover, the logger has a discreet case housed in a small, neutral colored, low profile case. The logger can be wall-mounted for unobtrusive use in an office or workplace applications (Gemini Data Loggers, 2015).

TGE-0011 Tinytag CO_2 Logger was placed at certain sites in the buildings, and measured automatically. The device provided continuous recordings of CO_2 levels. The period of measurement took place from December 1, 2015 to June 30, 2016. The CO_2 recorded during this period varied from 0 ppm as the minimum value, to 910 ppm as the maximum value with an average reading at about 640 ppm. The next table and graph summarize the most important data regarding the readings.

The researcher separated the readings of the data logged during the monitoring behaviors for one day, one week, and monthly. This results in notably more accurate readings due to an increase in the variation in the data available. A discussion of the level of CO_2 for the duration of one day is given bellow:

The researchers picked up the device on May 5, 2016 and noted the changes that have occurred regarding CO_2 levels during one day. The CO_2 readings have not varied during this day, which gave a similar approximation in the change between the maximum and minimum CO_2 levels that were recorded. The maximum CO_2 reading was 630 ppm, and the minimum reading was 580 ppm, while the average reading of CO_2 was about 600 ppm.

Table 4. Maximum, minimum, and average temperature and relative humidity readings from (June 6-12, 2016).

Property	**CO_2 Concentration**
Logging Started	December 1, 2015
Logging Ended	June 30, 2016
Logging Duration	215 days 11 hours 29 minutes
Interval	10 minutes
Number of Readings	32614
Minimum Reading	0 ppm
Maximum Reading	910 ppm
Average Reading	640 ppm

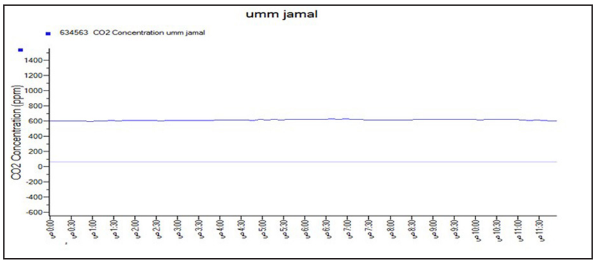

Figure 10. Levels of CO_2 at Umm el-Jimal for 215 days.

Weekly levels of CO_2 can be very different from one day to another as shown in the next graph. During the two days, the maximum CO_2 level for this week reached 640 ppm, while the minimum level was around 550 ppm. These two readings are not much different from one another, so the average CO_2 level was around 580.

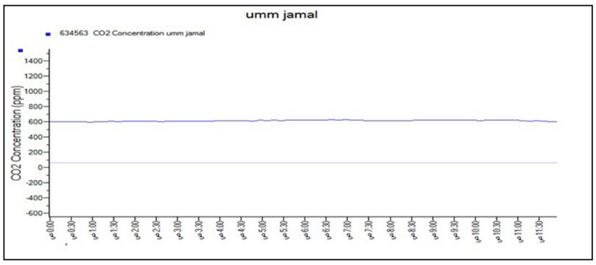

Figure 11. Diagram combining CO_2 readings from the data logger for one day.

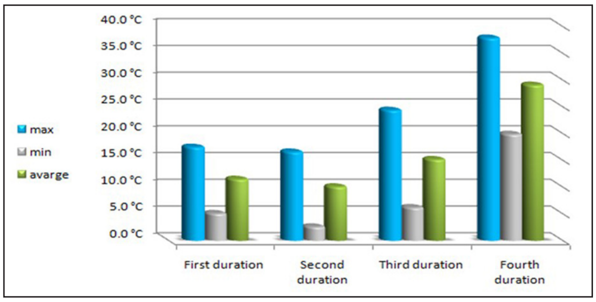

Figure 12. Maximum, minimum, and average CO_2 readings for the period (April 20-26, 2016).

5.3. Summary of Umm el-Jimal Microclimate Condition

The changes monitored at Umm el-Jimal can be identified as microclimate conditions and behavior (temperature, relative humidity and CO_2). It is knwon that humidity is inversely proportional to temperature. This means that an increase in one factor leads to a decrease in the other. During the four months of the monitoring, temperature and relative humidity showed differences between the lowest values and the highest values that were very irregular for the same month. The observed rates during one month differed from humid to dry. Afterwards, when data were compared for different months, they showed rates of convergence.

At Umm el-Jimal, December displayed a microclimate with low temperatures and high humidity that exceeded the average rate of 50 %. In the following month of January, the relative humidity rates amounted to about 60 %, with temperatures declining to an average of 10 °C. The microclimate can be described as humid with moderate temperatures, while the last month of the winter period showed a steady rise in temperature, reaching 20 C. Throughout the monitored period, the researchers observed a decrease in relative humidity to less than 48 %. The microclimate can be described as humid with moderate heat.

The following two figures (23 and 24) illustrate the differences and fluctuations of maximum, minimum, and average observed data of temperature and relative humidity at Umm el-Jimal.

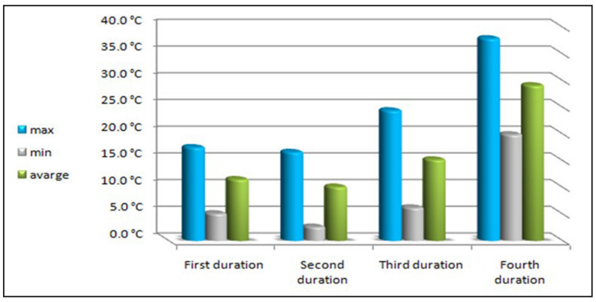

Figure 13. Maximum, minimum, and average temperature readings for four months of monitoring.

During the last month of the summer period, temperatures were very high, reaching about 38 C. This in turn led to a very low relative humidity, reaching a very dry rate of 18 % during that month. The rates were moderate reaching almost 33%.

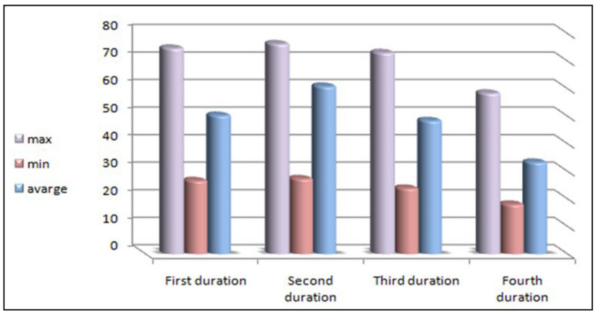

Figure 14. Maximum, minimum, and average relative humidity readings for four months of monitoring.

From the results of the measurements of the CO_2 concentration over the period of seven months, it can concluded that CO_2 levels were consistently high during this period. As seen in the next figure, the maximum and minimum levels of carbon dioxide varied for each month. The maximum levels of CO_2 measured in Umm el-Jimal (910 ppm) were reached during February. The minimum values were (551 ppm) and were recorded during June. It is important to note that the zero values were excluded as this device may have been removed from its power outages during these periods. Therefore, the CO_2 concentration rate is very high, usually around 640 ppm.

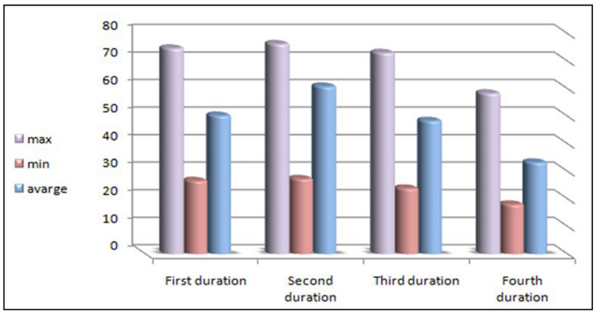

Figure 15. Maximum, minimum, and average CO_2 readings during seven months of monitoring.

The fluctuations in temperature, relative humidity, and CO_2 rates caused the basalt stone buildings of Umm el-Jimal to suffer. The microclimate changes affected the stability of the historic buildings at this site. These changes affected both the internal structures through the movement of salts through the pores, and the external ones through the accumulation of pollutants on the surface which resulted in changes in colors and shape.

6. Stone Decay at Umm el-Jimal

After investigation of the structures at Umm el-Jimal discussed earlier, the most important causes of the decay of stones are displayed following Smith's classification system. It becomes evident that a simpler and a more convenient system is needed in order to facilitate the assessment of the risks to some of the structures in Umm el-Jimal, and find a simpler way to represent these decay patterns in the form of photographic images.

A flow chart is shown as a way to distinguish between the types of stone decay. Each major type of decay is represented in a rectangle that carries a specific color. In addition, the following branches of the decay types hold a character key to follow the chart more easily. The following images have rectangles of colors that correspond to those in the flow chart. Those rectangles are enlarged so that the details are seen more easily.

Table 5. Classification of stone decay editied by the researchers.

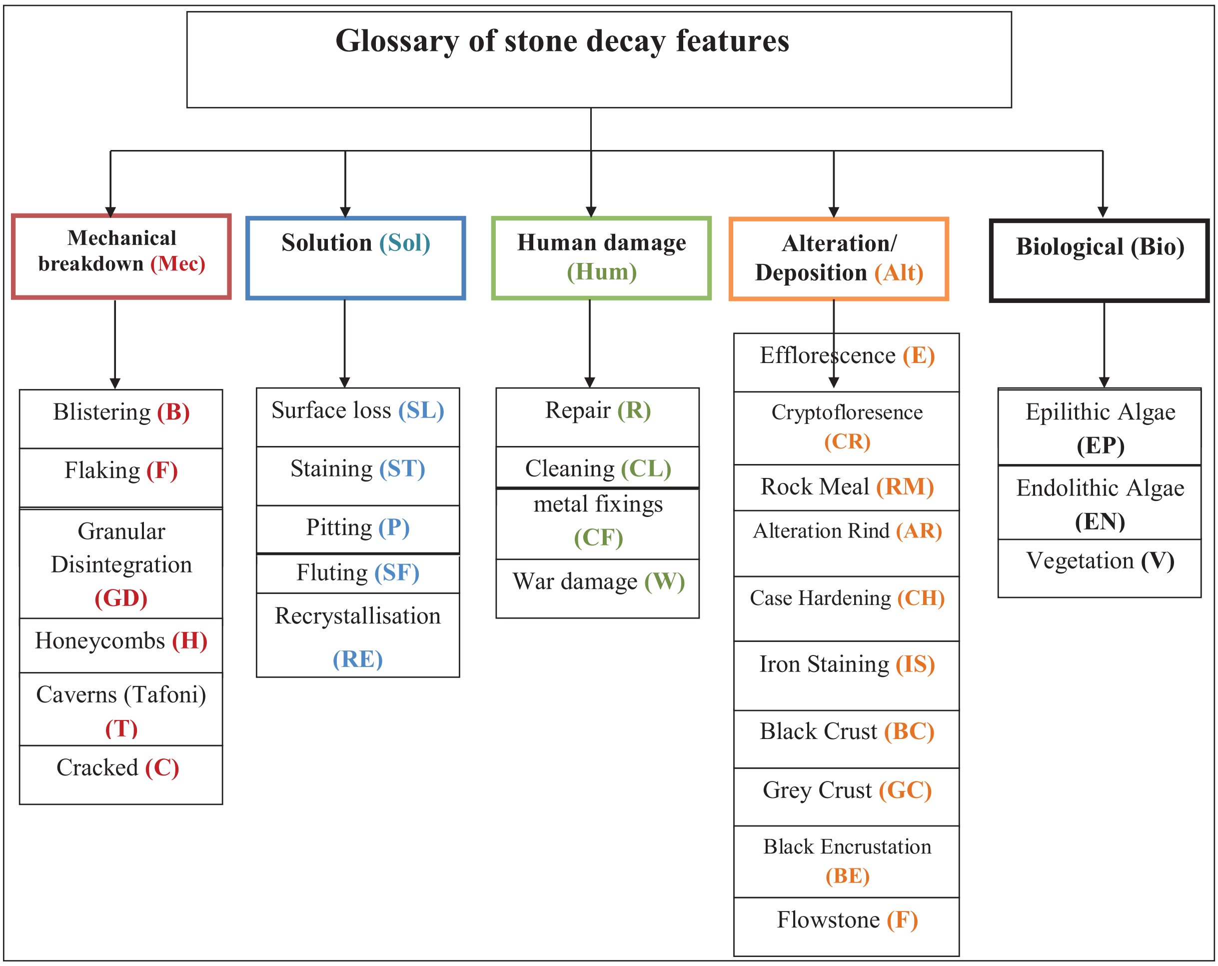

Table 6. Stone decay feature of front façade Praetorium, Umm el-Jimal.

<table>
<tr><th colspan="3">Types of stone decay of front façade of Praetorium</th></tr>
<tr><td colspan="3"></td></tr>
<tr><td></td><td></td><td></td></tr>
<tr><td>Human Damage? (HU)
Repair (R)
Scale (1-5): 2</td><td>Mechanical breakdown (MB)
Scaling (S)
Scale (1-5): 3</td><td>Biological (Bio)
Vegetation (V)
Scale (1-5): 2</td></tr>
<tr><td colspan="3">Photo taken by Researcher, 2016</td></tr>
</table>

Table 7. Stone decay feature of other façade of Praetorium, Umm el-Jimal.

Types of stone decay inside of Praetorium		
		
		
Alteration (Alt) Efflorescence (E) Scale (1-5): 2	Alteration (Alt) Efflorescence (E) Scale (1-5): 2	Alteration (Alt) Black crust (BC) Scale (1-5): 3
Photo taken by Researcher, 2016		

Table 8. Stone decay feature inside of Praetorium, Umm el-Jimal.

<table>
<tr><th colspan="3">Types of stone decay inside of Praetorium</th></tr>
<tr><td colspan="3"></td></tr>
<tr><td></td><td></td><td></td></tr>
<tr><td>Alteration (Alt)
Black Encrustation (BE)
Scale (1-5): 1</td><td>Solution (Sol)
Pitting (P)
Scale (1-5): 2</td><td>Solution (Sol)
Pitting (P)
Scale (1-5): 2</td></tr>
<tr><td colspan="3">Photo taken by Researcher, 2016</td></tr>
</table>

6. Conclusions

The researchers of this study took part in several fieldwork assignments after installing devices at Umm el-Jimal. The results of monitoring over a period of seven months allowed the researchers to determine the factors that threaten the survival of Umm el-Jimal archaeological heritage site. These factors can greatly influence the site structure and damage it permanently.

The temperature at Umm el-Jimal affects the stones of the site in two ways. Fluctuations in temperature during one day or one month may cause an acceleration of fatigue in susceptible materials, which results in a frequent expansion and contraction of the stones. In order to collect evidence on the expansion and contraction of the stones in Umm el-Jimal, the researchers observed the readings of the loggers; In winter, the maximum temperature reached 24.4 °C, and the minimum was around 2.6 °C. This shows a large difference in temperature. Regarding evidence on the changes occurring during one day, the maximum temperature reached 35.9 °C, while the minimum reading was 23.5 °C –

which indicates an unstable temperature. This fluctuation is relevant to the structural stability of the buildings bevause it induces a number of weathering mechanisms, particularly speaking, cracks and scaling. Furthermore, this may affect the structures significantly, and cause a collapse in the bonds between particles and or between layers.

The increasing temperatures and the rotting, increased the biological growth of micro-organisms. Usually, their growth increases at temperatures ranging from 20 °C to 35 °C; this range is generally favorable to the micro-organisms' metabolic activity (Camffuo, 1998). Such conditions were present at Umm el-Jimal. During June, the recorded temperature in Umm el-Jimal was no less than 20 °C. In winter, the logger recorded many readings around 20 °C. These temperatures led to a notable growth of micro-organisms across a wide area on the surface of the structures. Several micro-organisms such as the special lichen cover the surface of materials, which enhances the deposition of airborne particulate matters.

Changes in relative humidity during the day and seasonally were also considered in this study. The standard rates of relative humidity are between 30-40 %, but a greater proportion of relative humidity had been recorded at Umm el-Jimal reaching an average of 52 % during the first three months of monitoring. The maximum relative humidity recorded reached 76.3%. On average, relative humidity was recorded at 33.3 %. During June, it was recorded at 18% - which is less than that of the international standards. Thus, the results demonstrate high and fluctuating levels of relative humidity which can have an effect on dissolving crystallized salts, movement, and change contributing to the formation of decay. The changes also played a role in the increase of decay features at the site which usually include pitting, staining, surface loss, case hardening, and efflorescence.

In reference to pollutants, the researchers monitored the level of CO_2 as an important factor which contributes to the contamination at Umm el-Jimal. The site witnesseed a high level of CO_2 during the seven months of monitoring reaching up to 550 ppm while the standard limit of CO_2 in the atmosphere is 450 ppm. The level is remarkable on the surface, with the emergence of black and grey crust in many blocks of stone at the site. The reasons behind the high levels of CO_2 may be attributed to the location of Umm el-Jimal in al Mafraq semi-industrial region which houses plenty of factories in addition to the fact that Umm el-Jimal is located near a highway with heavy traffic. Furthermore, the high CO_2 levels are generated also by the behavior of local communities in the area who build outdoor campfires, which is, another factor that influences the degeneration of the structure of the wall.

References

Abo Ali, Y. (2012). Development and Marketing Umm Al-Jamal archaeological site. Master thesis. Moath Uinversity. Karak – Jordan. (In Arabic).

Al-kurdi, N. (2014). Hard building marital and suitable architecture: The case of Umm el Jimal – Jordan. Architecture and Modern information Technologies, 26: 1-8.

Alonso, F., Carrizo, C., Gibeaux, S., Schneider, C., Vazquez, P. (2015). Influence of surface finish and composition on the deterioration of building stones exposed to acid atmospheres. Construction and Building Materials, 392-403.

Brown, R. (2009). The Druze experience at Umm al-Jimal: Remarks on the history and archaeology of the early 20th century settlement. SHAJ, 10: 377-389.

De Vries, B. (1981). The Umm el-jimal project, 1972-1977. ADAJ, 14: 97-115.

De Vries, B. (1985). Urbanization in the Basalt region of North Jordan in late Antiquity: the case study of Umm el-Jimal. SHAJ, 14: 249-257.

De Vries, B. (1990). Umm el-Jimal 'Gem of the black desert', a brief guide to the antiquities. AI Kutba, Jordan.

De Vries, B. (1993). The Umm el-jimal project, 1981-1992. ADAJ, 27: 433-460.

De Vries, B. (1995). The umm el-jimal project, 1933 and 1994 field seasons. ADAJ, 29: 421-435.

Gemini Data Loggers. (2015). Tinytag Gemini Data Loggers. Accessed online 2015. Available at https://www.geminidataloggers.com/

Giesen, M., Mazel, A., Graham, D., Warke, P. (2011). Care and Management of Ancient Stone Monuments during Environmental Change. International Journal of heritage and Sustainable Development, 2: 60-71.

Kennedy, D. (2013). Settlement and soldiers in the Roman Near East, Ashgate, USA.

Haddad, D. (1991). The churches of Umm Al Jammal: A comparative study with some selected location from the north east area from Jordan. Master thesis: Yarmouk university: Irbid- Jordan. (In Arabic).

Horsfield, G. (1937). Umm el-jamal Antiquity. The University of York, 11: 456-460.

Hoyos, M., Soler, V., Can˜averas, C., Moral, S., Rubio, E. (1998). Microclimatic characterization of a karstic cave: human impact on microenvironmental parameters of a prehistoric rock art cave (Candamo Cave, northern Spain). Environmental Geology, 33: 231-242.

Littman, E. (1914). Semitic inscription. The Princeton archaeological expeditions to Syria, Leyden.

Obidat, D. (2002). The cultural features of the city of Umm Al-Jamal in the cultural and civilizational monuments in Jordan through the ages. Ministry of Cultural Publication. P97-151. (In Arabic).

Rives, V., and Talegón, J. (2006). Decay and Conservation of Building stones on Cultural Heritage Monuments. Materials Science Forum, 514-516: 1689-1694.

Salvatore, M., Mustard, F., Head, W., Wyatt, B., Marchant, D., Cooper, R. (2013). Development of alteration rinds by oxidation weathering processes in Beacon Valley. Antractica, and implication for mars, 112: 137-161.

Smith, B., Heras, M., Srinivasan, S. (2008). Experimental studies of near-surface temperature cycling and surface wetting of stone and its implications for salt weathering. SWBSS- Salt Weathering on Buildings and Stone Sculptures, 65-78.

Whitcomb, D. (1996). Urbanism in Arabia. Arabian archaeology and epigraphy, 7: 38-51.

المملكة الأردنية الهاشمية
صندوق دعم البحث العلمي
الجامعة الهاشمية

المجلة الأردنية
لعلوم الأرض والبيئة

JJEES

مجلة علمية عالمية محكمة

المجلد (١٠) العدد (١)

http:// jjees.hu.edu.jo/

ISSN 1995-6681

المجلة الأردنية لعلوم الأرض والبيئة

مجلة علمية عالمية محكمة

المجلة الأردنية لعلوم الأرض والبيئة : مجلة علمية عالمية محكمة ومفهرسة ومصنفة، تصدر عن عمادة البحث العلمي في الجامعة الهاشمية وبدعم من صندوق البحث العلمي - وزارة التعليم العالي والبحث العلمي، الأردن.

ترسل البحوث إلكترونيا إلى البريد الإلكتروني التالي:

رئيس تحرير المجلة الأردنية لعلوم الأرض والبيئة

jjees@hu.edu.jo

لمزيد من المعلومات والأعداد السابقة يرجى زيارة موقع المجلة على شبكة الانترنت على الرابط التالي:

www.jjees.hu.edu.jo

المملكة الأردنية الهاشمية صندوق دعم البحث العلمي الجامعة الهاشمية

JJEES

المجلة الأردنية لعلوم الأرض والبيئة

المجلد (١٠) العدد (١)

مجلة علمية عالمية محكمة تصدر بدعم من صندوق دعم البحث العلمي

ISSN 1995-6681 jjees.hu.edu.jo آذار ٢٠١٩